CVAP-TR-78-011
JUNE 1978

CODE VERIFICATION AND APPLICATIONS PROGRAM

PREDICTION OF KWU PKL EXPERIMENTS K5A AND K7A USING RELAP4/MOD6

BY

W. S. HAIGH

NRC Research and Technical Assistance Report

EG&G Idaho, Inc.

IDAHO NATIONAL ENGINEERING LABORATORY

DEPARTMENT OF ENERGY

IDAHO OPERATIONS OFFICE UNDER CONTRACT EY-76-C-07-1570

ABSTRACT

The RELAP4/MOD6 transient thermal-hydraulic code was used for prediction of two West German PKL reflood experiments. The calculations were part of a broader study for independent verification of the code in blowdown and reflood applications. The reported test predictions were made to evaluate the adequacy of the codes in representing reflood systems thermal-hydraulics. The calculated results indicate a strong code capability for analytical representation of the experimental reflood phenomena. Code-data comparisons of significant core thermal behavior and system hydraulic response were made. These identified code predictive strong points as well as correctable deficiencies. Special studies categorized and assessed the most significant deficiencies.

ACKNOWLEDGEMENT

The test prediction calculations for the PKL experiments were made by Dr. Y. S. Chen of EG&G Idaho, Inc. Dr. Chen also did much of the code input preparation for the predictions and made the additional study calculations described in this report.

SUMMARY

Test predictions of two KWU PKL[(a)] reflood systems experiments, K5A and K7A, were made using the RELAP4/MOD6 transient thermal-hydraulic code. These predictions were part of a larger and broader independent verification study evaluating use of the code in analysis of reactor loss-of-coolant accidents. Although the calculations were made after the experiments were completed, the predictions were considered "double blind", because no access to the data had been allowed the verifiers and no prior modeling application of the RELAP4/MOD6 code had ever been made to the PKL facility.

Independent verification techniques require the application of recommended user input and modeling guidelines. This provides a consistent analytical representation of experimental or prototypical system behavior for a wide and varied calculation spectrum. The specific objective of the PKL test-prediction study was the assessment of code capability to predict the thermal-hydraulic behavior of a simulated reactor vessel under gravity-feed reflood conditions. Of particular interest was the adequacy of liquid entrainment and dispersed flow heat-transfer models. The PKL facility is a 1:134-scale simulation of a West German pressurized water reactor that uses an electrically-heated core (1.45MW maximum power) to represent the nuclear fuel rod assemblies. Experiments were conducted with the system initially filled with saturated steam at 0.42 MPa and the core heater rods at maximum power. Decays in pressure and power were programmed as functions of testing time.

Modeling applications and resultant code-data comparisons are presented in this report. Preliminary test-prediction results had been transmitted to the NRC under separate cover prior to data release for code evaluation purposes. Data comparisons show that the code predicted maximum clad temperature to within 3% for Test K5A and 5% for Test K7A. Deviations were greater in lower and upper core regions. At higher elevations in all three radially-defined core energy zones, quench occurred earlier in the experiments than in the calculations. The

(a) KWU: Kraftwerk Union, Erlangen, West Germany; "PKL" stands for "primary coolant loop".

hydraulic modeling of the experimental system generally simulated the experimental loop flow histories. However, some core oscillation amplitudes were over-predicted, and a calculational sensitivity to steam-generator gas vaporization dynamics was identified.

Areas where a need exists for further code development and improvement are identified in the report. The most significant are in core liquid entrainment and dispersed-flow heat-transfer modeling. The requirement for improved modeling of upper plenum de-entrainment and fallback, of ECC injection-point mixing, and of steam-generator primary-side thermodynamic processes is emphasized.

CONTENTS

FIGURES

TABLES

CVAP-TR-78-011
JUNE 1978

PREDICTION OF KWU PKL EXPERIMENTS K5A AND K7A USING RELAP4/MOD6

By

W. S. Haigh

REVIEWED BY:

T. R. Charlton, Acting Manager
Code Verification Branch

APPROVED BY:

J. A. Dearien, Manager
Code Verification and
Applications Program

L. J. Ybarrondo, Director
Water Reactor Research

I. INTRODUCTION

This report presents the results of code-data comparisons made to evaluate RELAP4/MOD6 Transient Analysis Code[1] application to "blind" predictions of the KWU PKL systems reflood experiment behavior. The code is a development of an earlier version, RELAP4/MOD5[2], and has capability for calculation of the reflood phase of a postulated loss-of-coolant accident (LOCA). Update 3(b), evaluated in this study, was released for internal use at the Idaho National Engineering Laboratory (INEL) in November, 1977. A subsequent version, Update 4, was released to the Argonne Code Center in January, 1978, for public use.

The conduct of blind test predictions assures objectivity in the assessment of a code and supports the integrity of the verification process. The term "blind" infers that the code calculation has been made without reference to experimental data obtained from the experiment being analyzed. The treatment here is of what may be considered "double-blind" predictions; i.e., the calculations represent the initial application of the code to the modeling of the experimental facility.

This study represents a portion of a broader-scoped effort to apply independent verification techniques. Independent Code Verification[3] is a new field of study currently being developed into a structured process. Therefore, the objectives of this study were twofold:

(1) To explore and develop optimum techniques, rules, and guidelines for performing independent verification of codes.

(2) To apply the preceding techniques, rules, and guidelines to the RELAP4/MOD6, Update 3 code to gain insight into what constitutes a successful (or unsuccessful) independent verification and to gain further knowledge about the quality of the subject code.

(b) RELAP4/MOD6, Update 3 Configuration Control Number C00100005. Associated steam tables are controlled in File H00201 IB.

At the time this effort was initiated, RELAP4/MOD6 had not been released to the Argonne Code Center; therefore, the studies must be considered pre-release verification. However, the analyses were treated in the structured manner of the independent verification process. One of the first steps in this process was to develop a matrix (Table I) identifying the complete scope of effort. As shown in Table I, that scope included analyses of component, of system and integral blowdown, and of reflood phenomena. The studies described in this report are included in Subtasks 8 and 18 in Table I and specifically address system reflood heat-transfer and hydraulic effects models.

The approach taken in each base run was to formulate a firm set of ground rules prior to all analysis. These ground rules covered modeling techniques, code option selection, and code user input values and were based on the best published information from all previous developmental verification. They consist of the user recommendations identified in Section III.3 of Reference 1 except as superseded by the user guidelines of Reference 4. The use of a fixed set of ground rules was necessary to avoid criticism of code "tuning" during the base runs, and to provide consistency between the several blowdown and reflood, gravity and forced-feed studies. Where further diagnostic analyses were performed to clarify prior results, these analyses are clearly identified as Additional Studies.

The results of this study are important because:

(1) They provide insight to steps required for the successful independent verification of a code

(2) They identify some of the capabilities and deficiencies of the RELAP4/MOD6, Update 3 code within the framework of independent verification

(3) They advance the state-of-the-art of the code input selection process on which the success of PWR-event prediction depends.

Table I

MATRIX FOR INDEPENDENT VERIFICATION OF RELAP4 - MOD6, FY 1978

	EXPERIMENTS SELECTED	FEATURES EVALUATED								
		BLOWDOWN HEAT TRANS. & HYDRAULICS	REFLOOD HEAT TRANS. AND HYDRAULICS	FUEL BEHAVIOR	SCALING EFFECTS	DIFFERENT SYSTEMS	TEST PREDIC-TION	COMPONENT EFFECTS	SYSTEMS EFFECTS	INTEGRAL EFFECTS
1. SEMISCALE, THTF CORE BLOWDOWN	SEMISCALE S-06-5, THTF 105	X				X		X		
2. SEMISCALE, LOFT PRESSURIZER BLOWDOWN	SEMISCALE S-04-4, S-06-5, LOFT L1-4				X	X		X		
3. SEMISCALE, LOFT STEAM GENERATOR BLOWDOWN	SEMISCALE S-01-4A, S-06-5, LOFT L1-4				X	X		X		
4. STANDARD PROB. 7 LOFT L1-4	LOFT L1-4						X		X	
5. SEMISCALE, LOFT ISOTHERMAL COMP.	SEMISCALE S-01-4A, LOFT L1-4				X	X			X	
6. SEMISCALE, FLECHT CORE REFLOOD	SEMISCALE S-03-0, FLECHT LFR 4019, 11003		X			X		X		
7. SEMISCALE, FLECHT-SET, PKL COMP.	SEMISCALE S-03-5 FLECHT-SET 27148 PKL K5A		X		X	X			X	
8. PKL PREDICTION	PKL K5A		X				X		X	
9. SEMISCALE INTEGRAL EXPERIMENTS (6)	SEMISCALE S-04-5, S-04-6, S-06-1, S-06-2, S-06-5, S-04-5	X	X						X	X
10. MARVIKEN CRITICAL FLOW TESTS	TBD				X			X		
11. SEMISCALE MOD-3 BLOWDOWN	TBD	X				X	X		X	
12. SEMISCALE MOD-3 REFLOOD	TBD		X			X	X		X	
13. SEMISCALE MOD-3 INTEGRAL	TBD	X	X			X	X		X	X
14. PBF LOCA SERIES	LOC-11, LOC-3	X		X				X		
15. ADDITIONAL THTF TEST (Extension to Subtask 1	TBD	X					X	X		
16. LOFT L1-5 PREDIC-TION	LOFT L1-5						X		X	
17. ADDITIONAL SEMI-SCALE, FLECHT CORE REFLOOD (Extension to Subtask 6)	SEMISCALE S-03-A FLECHT LFR 2414, 13404, 13609		X			X		X		
18. ADDITIONAL SYSTEM REFLOOD TESTS (Extension to Subtask 7)	SEMISCALE S-03-8, FLECHT-SET 22138 PKL K7A		X		X	X			X	

The specific purpose of this report is to provide a comparison of test predictions with the experimental data obtained for two KWU PKL Bundle I reflood tests, K5A and K7A. Although the calculations were made after the actual testing, the experimental results were held in controlled custody by the NRC until after the calculations were completed and the calculated results were transmitted. The transmittals are included in this report as Appendix A (K5A) and Appendix B (K7A).

Material presented includes description of the experimental facility, with discussion of the basis for test selection, of the facility configuration, and of the location, type, and adequacy of measurements. The test-prediction modeling for code calculation is detailed through definition of nodalization, model option selection, and boundary-condition application. The code-data comparisons for significant thermal-hydraulic parameters are presented and the results are analyzed. Additional studies required in development of the modeling format are discussed in detail and their impact on usage options and recommendations is identified.

The experiments forming the data base for this study were conducted in March and May, 1977. Initial modeling of the experiments was accomplished at the INEL before the end of FY 1977 and the calculations were completed in March, 1978. Calculated results have been stored on the following computer tapes:

Calculation	Tapes	Configuration Control Nos.
K5A Base Case	T9R133, T9S582, T9V752	H00328IB
K5A Alternate Case	T9Y692, T9Y705	H00328IB
K7A Base Case	T9N478, T9V204, T9W766	H00327IB

II. EXPERIMENTAL FACILITY

1. TEST SELECTION

1.1 Test Conditions for the Bundle I Program.

The PKL Bundle I experiments were designed to simulate hot- and cold-leg break reflood transients hypothetically occurring for a representative West German pressurized water reactor (PWR). Break geometry considered was a 200% offset piping shear in one of the coolant loops. Part 1 of the first test series was devoted to hot-leg break simulation with pump flow resistance and steam generator secondary conditions being the main parametric variables. Part 2 consisted of cold-leg-break experiments, for which emergency core coolant (ECC) injection location and rates were changed from test to test. The significant as-planned test conditions for both parts of the first series are identified in Table II.

It was originally intended that two radial power profiles would be evaluated during the cold-leg break experiments (Part 2) and that the more peaked of the two would be used if a significant effect of the peaking could be identified experimentally. The radial power distribution given in Table II is the flatter of the two candidates, the one actually used in the experimental series.

Plans called for top and bottom flooding in both hot- and cold-leg-break experimental series. Top flooding was to be accomplished by injection into the hot-leg nozzles (at the upper plenum); bottom flooding, by injection into the upper annulus and/or the system cold legs. Possible simulation was of eight (8) prototype PWR injection lines, four for the hot-legs and four for the cold-legs. The experimental application is defined by the number of prototype lines simulated and the location of the injection. For example, 5 lines on the cold side means that in the experiment, a scaled amount of injectant, representing 5 of the 8

TABLE II

PLANNED EXPERIMENTAL TEST CONDITIONS

	Part 1	Part 2
Pressure downstream of break (KPa):	489.5 to 317.2	489.5 to 317.2
ECC temperature (K):	307	307
Total rod bundle power (MW):	1.45	1.45
Power decay function:	1.2 x ANS std	1.2 x ANS std
Axial power peak factor:	1.19	1.19
Radial power distribution (hot/average/cool):	1.31/1.0/0.85	1.16/1.0/0.9
Initial maximum rod temperature (K):	873	833
Pump simulation resistance factor:		
Broken loop	0,20	20
Intact loops	0,20	0
Steam generator secondary :		
Initial pressure (KPA)	2227, 5600	5600
Initial temperature (K)	491, 544	544
Water level (m)	--	7.5
Liquid inventory in system (Kg):	0	0
No. of ECC injection lines simulated:		
Hot side	2	0, 3, 4
Cold side	3	2 - 7

possible line capacities, was injected into the "cold side" of the experimental facility. Actual injection points for this condition were as follows:

No. of Prototype Lines	Location in Experiment
2	Double-intact-loop cold leg
1	Single-intact-loop cold leg
2	Upper annulus
Total 5	

1.2 Tentative Test Selection.

Part 2 of the first PKL test series featured a group of cold-leg-break tests designed for bottom flooding (cold-leg injection). Of these, Test K7A simulated prototype ECC injection from two lines, and Test K5A, ECC injection from five lines. The former was selected for test prediction because it was most representative of United States PWR conditions, and the latter was held as second choice. This order of preference was subsequently reversed when the as-tested boundary conditions for Test K5A were transmitted to the NRC first, allowing modeling of the experiment to be initiated with minimal delay. Test K5A had a total injection rate averaging about 500 Kg/m^2-s, a magnitude typical of that for a United States PWR. Test K7A, for which boundary conditions were received later, had a substantially lower injection rate, but represented only cold-leg injection in the German prototype. Eventually, both experiments were modeled, and a test prediction calculation was made for each.

2. FACILITY DESCRIPTION

2.1 Design Concept.

The PKL facility was conceived and designed to represent the four-loop West German 1300 MW B1BL1S-B PWR in reduced scale. The prototype

volume-to-power ratio was maintained in the 340-rod experimental design. Consequently, the nominal scaling factor of 1:134 is the ratio of the number of heater rods in the experimental core to the corresponding number in the prototype.

Principal simulation features are as follows:

(1) Relative heights of system components were maintained the same as in the prototype.

(2) Coolant loop total volume was in exact scale (1:134) with the prototype, although each individual component volume was not necessarily held in this proportion.

(3) Steady-state pressure loss coefficients for the equivalent loop sections were the same as in the prototype.

(4) The steam-generator secondary side heat capacity was maintained in scale and the fluid pressure and temperature were representative of the prototype.

Areas where scaling requirements were maintained to the best reasonable approximation were:

(1) The ratio of component structure surface area to flow area.

(2) Lower plenum height-to-diameter ratio.

(3) Loop flow areas and piping lengths.

The four primary coolant loops of the prototype were simulated in the experiment using three loops: two intact, and one containing a break simulation. One of the intact loops was representative of two of the prototype loops. The three-loop arrangement is illustrated schematically in Figure 1. Each of the loops contained an operating steam

generator and a simulated pump volume with variable resistance. Figure 2 shows the loop and vessel simulation concepts and indicate the main ECC injection ports in the hot and cold legs. Also indicated is the method used for simulating the vessel downcomer: a separate U-tube concept with a simulated upper annulus volume. Figures 1 and 2 were obtained from facility description literature.

The experimental start-up sequence is unique in that all liquid is initially removed from the system and the testing starts with the lower plenum filled only with gas. The procedure is essentually as follows:

(1) The containment steam supply is heated and fed through the experimental system for purposes of preheat to saturation. Condensate is drained.

(2) The steam-generator secondary is heated to initial conditions by a slow warm up, several days in advance of the testing.

(3) Low power is applied to the rod bundle, heating at a slow rate and manually setting maximum temperatures in the three core power zones to prescribed values.

(4) ECC injection feed pump is started and full injection flow, diverted to the bypass system, is established.

(5) A change is made to a process computer and the ECC valves are switched to the injection point flow condition. At the same time, the specified test power sequence is initiated, maintaining 1.45MW until the prescribed power decay simulation curve is intersected and followed.

2.2 Design Details.

The 340-rod experimental vessel core matched the prototype in heated length (3.9 m), had a total available power of 1.45 MW, and was

divided radially into three power regions. These are the inner (hot channel), the middle (average channel), and the outer (cool channel). The three power zones are shown, with the number of rods in each, in Figure 3. Only heated rods were used; "dead" rods, such as control-rod thimbles, were not modeled. The rods each had a stepped simulation of a cosine axial power distribution with a 1.19 peaking factor. The radial power distribution for the three zones (Table II) was controlled as an experimental input.

The reactor vessel contained internals (Figure 4) in the upper plenum to simulate control-rod guide sleeves, and structural internals in the lower plenum that doubled as power input dividers. An annular downcomer channel outside the core housing was sealed off for these experiments, replaced by an external U-tube downcomer with a cylindrical upper annulus volume simulator. A steam bypass pipe linked the lower plenum and the upper annulus to allow for counterflow of steam during the initial downcomer penetration period (Figure 5).

Provision was made in the facility to inject ECC at six locations, as indicated in the schematic of Figure 2. For the experiments discussed in this report, only lines 4, 6, and 7 were used. The ECC injection control system was designed so that prior to testing, water was bypassed to a recirculation reservoir. At test initiation command, simultaneous control of two valves in each line directed the ECC to the appropriate injection points.

The three steam generators reflect the essential features of prototype components. Actual tube geometry was used in bundles of 30 tubes for each of the single loops and of 60 tubes for the double intact loop. No simulation was provided for the regions above the top of the bundles because the main mode of heat transfer was anticipated to be from the secondary to the primary side of each component.

Simulation of the piping break in the single broken loop was accomplished by removal of a piping spool in the hot or cold legs and replacement by elbows that exhausted both sides of the "break" into a

manifold. This manifold was linked through centrifugal phase separators to a simulated containment that functioned both as a system pressure control tank and as a reservoir for the system supplementary steam supply. Figure 6, showing the broken loop components and elevation, is also representative of the two intact loops of the system in general arrangement.

2.3 Instrumentation Details.

Principal instrumentation in the 340-rod core were 80-92 cladding-installed thermocouples. These were located as shown in Figure 7, welded in longitudinal grooves in the outside surface of ten to twelve selected rods. In addition, fluid thermocouples were installed in core flow channels at axially spaced stations and on core spacer grids. Core housing temperatures were measured in axial distributions, 90 degrees apart.

Table III lists some of the main flow, pressure, and temperature instrumentation locations in the three coolant loops and the break exhaust system. These are described in a general sense; for more specific information, facility measurement documentation may be consulted.

The three steam generators were instrumented at multiple axial stations for the measurement of primary and secondary fluid temperature and of tube wall temperatures.

Discussion of instrumentation and measurements pertinent to comparison of code calculations with experimental data will be expanded as necessary to the analysis of the individual comparisons made subsequently in this report.

3. MEASUREMENTS AND ACCURACY

Principal thermal measurements are well placed in the core and the steam generator. The three energy zones in the core each have three to

TABLE II

PRINCIPAL INSTRUMENTATION OF THE PKL
LOOPS AND LOOP COMPONENTS

Measuremement Type	Location
Absolute Pressure:	Upper Plenum
	Broken Loop Cold-Leg Inj. Pt.
	Break Manifold
	Hot Leg Upstream of S.G. (all loops)
	S.G. Secondary, Top, Broken Loop
	Containment
Differential Pressure:	Upper Plenum to Containment
	Across S.G. (all loops)
	Cold-Leg Nozzle to S.G., Broken Loop
	Upper Plenum to Upper Annulus
ΔP Head:	S.G. (all loops)
	Loop-Seal Riser to Pump (all loops)
	Upper Plenum to Lower Plenum
	Lower Plenum to Top of Core
	Across Height of Upper Plenum
	Across Height of Containment
	Across Height of Phase Separator
Fluid Temperature:	S.G. Outlets (all loops)
	Hot Leg (all loops)
	Injection Points (all loops)
	Top and Bottom of Containment

TABLE III (cont.)

Fluid Temperature (cont.)	Separation System, 5 Places
	Exhaust Piping to Containment
	Top and Bottom of Core
	Upper Plenum
	Upper Annulus
	Bottom Of Downcomer
Wall Temperature:	Bottom of Downcomer
	Bottom of Loop Seal (all loops)
	Separator Tanks
	Core Boundaries
	Steam Generator Secondary
	Hot-Leg Piping (all loops)
Mass Flow and Velocity	Cold Legs Between Steam Generators and Pumps, each loop
	Downcomer Inlet to the Lower Plenum
	Containment Inlet and Outlet

five instrumented heater rods with adequate axial thermocouple distribution. Although some exceptions are evident in the data presented, agreement in data obtained from widely dispersed rods at corresponding axial and heater zone locations is generally very good. Because no instrumentation accuracy data were provided in data and facility reports, much reliance is placed on the adequacy of agreement in corresponding instrumentation.

The experimental data presented for cladding temperature show measurements taken at distributed radial locations for the same core height. In the hot and average channels, measurements obtained for Test K5A agreed within 20K in the lower and middle core regions. There was more scatter at higher elevations, with the range of agreement increased slightly to 30K. The data presented for the cool channel had considerably more scatter, for deviations were as great as 75K.

The core temperature measurements for Test K7A were noticeably better than for K5A. Agreements at all elevations for hot and average channels were 20K or better. The cool channel measurements had about the same amount of scatter as for the other experiment.

The observed scatter in the experimental data is indicative of location effects as well as of instrumentation accuracy. However, the implication is that the overall experimental measurement data band is substantially smaller than 30K ($\cong$ 3%) in width over the height of the core. Code-data comparisions presented in this report for cladding temperature may be evaluated with reference to this increment.

Flow measurements are indicators of hydraulic performance, allowing comparisons of hydraulic response in experiment and code. The three cold-leg orifice flow measurements are suitable for analytical use primarily because the flow measured is superheated steam and the measurement for a single-phase fluid is a perfected state-of-the-art technique. The turbine measurements at the inlet to the lower plenum from the downcomer are subject to error of location. They fail to indicate core

inlet flooding rate because of the presence of the steam bypass line, a potential path for a recirculating flow. Consequently, reliance is placed on these measurements for qualitative purposes only.

Pressure measurement coverage is satisfactory, particularly with respect to liquid inventory determination in the vessel and other components. Pressure differential and liquid head measurements provide a valuable diagnostic adjunct. In this diagnostic sense, lack of accuracy analysis is not an insurmountable handicap.

III. BASE - CASE MODELS

1. NODALIZATION

Code representation of the cold-leg break reflood experiments was accomplished using 37 control volumes and 40 junctions. As shown in Figure 8, each of the three coolant loops was modeled with its separate steam generator and simulated pump. The reason for not "lumping" the intact loops was that variation in loop piping length could conceivably have an effect on propagation of local disturbances. The broken loop hot leg was modeled as two volumes instead of one to facilitate changeover to a hot-leg break configuration.

The simulated break was analytically modeled to resemble the experimental configuration, with elbows exhausting into a "break manifold". Each steam generator required three volumes to represent the primary side and one to simulate the secondary. The three volumes were arbitrarily sized and located to accomodate the anticipated liquid evaporation in a volume of relatively small size on the inlet side. This reduced the effect of equilibruim gas generation, a potential source of system dynamics.

The core was divided into three control volumes, matched in size to the three power zones of the heater-rod bundle. The axial power distribution was simulated using 12 heat slabs in each channel (see Figure 9). Heat slabs were also used with each primary volume of the steam generators and in the upper annulus and downcomer. Four slabs were used in the latter to provide distributed gas generation consistent with the use of a complete-separation bubble-rise model. Complete phase separation was also modeled in the upper annulus and the lower plenum. Vertical slip between phases was allowed in the junction between the upper annulus and the downcomer.

ECC was injected into the upper annulus volume through a fill junction. System pressure was maintained by programming pressure vs. time in the containment to match experimental boundary conditions.

2. CODE OPTIONS

2.1 Modeling Options.

Selection of special applicable analytical modeling options was made on the basis of specific experimental facility requirements and was subject to design review before incorporation. Principal modeling selections and conditions were as follows:

(1) All three core channels were partitioned using the moving-mesh technique(c). This technique incorporated the bubble-rise model with recommended[4] fine and medium mesh size and extent. The explicit core superheat model was used in conjunction with the moving-mesh technique.

(2) The Wilson bubble-rise model was used in the vessel upper plenum to allow the build-up of liquid inventory while providing liquid carryover into the loop hot legs. Neither fallback nor de-entrainment models for the upper plenum were used. These two models had not been checked out in code developmental verification studies and for that reason were not recommended for use.

(3) ECC injection was accomplished using a single fill junction into the upper annulus volume. The injection matched the experimental boundary condition for total flow rate, but ramped liquid enthalpy from saturati to that corresponding to 307 K over the initial 20 seconds. Upper annulus injection was used because of difficulty in getting satisfactory code operation for the condition of cold-leg injection.

(c) This and other specified reflood models are described in Reference 1.

(4) Heat slabs were not used at the core or upper plenum boundaries because these boundaries were thermally thin and were surrounded by a fluid jacket.

(5) The core liquid entrainment above the quench front was calculated using the Steen-Wallis implicit model. Input parameters initially selected were based on developmental verification guidelines[4]: EN2 = 0.30, HC1 = 10^6, HC2 = 3×10^{-6}. Other values of EN2 used are discussed in Section 2.2.

(6) Heat transfer in the transition and dispersed-flow region was calculated using the sum of the Hsu and Bromley correlations. The Hsu exponent was calculated by the code using an internal subroutine.

(7) The partitioning of the dispersed-flow heat transfer was calculated by the program. The values of the liquid and vapor factors, N and M, were determined from the guidelines[4] to be 11.0 and 1.0, respectively.

(8) Rough pipe wall friction was used in the piping volumes.

(9) Natural-convection heat transfer was used with a bubble-rise model on the secondary side of each steam generator.

2.2 Input Options.

The parameters N (heat-transfer weighting factor) and EN2 (maximum liquid entrainment ratio) were selected initially using guidelines provided through developmental verification[4]. The data base used in guideline development, however, was restricted to a series of FLECHT[5] forced-feed reflood experiments. The guidelines defined the parameters as functions of system pressure, peak rod power, ECC subcooling, and core inlet flooding rate. The latter two variables were only available for gravity-feed experiments through calculational iteration. Moreover, there was considerable doubt that the guidelines, even when iterated, would have valid application under dynamic gravity-feed conditions.

Initial parameter values derived, N = 11 and EN2 = 0.3, were used objectively in the initial calculation of the K5A "Base Case". Because this usage resulted in extended system dynamics and delayed turnaround and quench, an alternate selection was made on the basis of code default values[1] and the calculation was repeated. For the calculation of Test K7A, similar default values were used. These were:

Test	N	EN2
K5A	30	0.665
K7A	30	0.60

Further discussion of the use of these parameters is given in Sections IV and V.

Time-step sizing was initially based on recommended guidelines[4]. However, as computation progressed, parameter gradients became severe, with the occurrence of dynamics at the core inlet and in the broken cold leg; this necessitated program restarts with revised time-step increments. These changes were made, in accordance with need, several times in the progress of each computation.

3. BOUNDARY CONDITIONS

Program boundary conditions of power vs time, injectant flow vs. time, and containment pressure vs time were obtained from test control data. Otherwise, only test initialization parameters were used in the calculation. No experimental results were available to influence calculations. The boundary conditions as received from KWU are presented, in the form used in the calculations, in Appendixes A and B.

IV. TEST-PREDICTION RESULTS

1. CODE-DATA COMPARISONS

The primary performance indicator used in the code-data comparisons of this study is the behavior of heater-rod surface temperature. Figure 10 presents the relationships in the core between the axial power distribution representation by core heat slabs and the location of the experimental thermocouple measurements. Use of this figure and Figure 7 as reference will aid in interpreting the data comparison plots that reference thermocouple locations and reflect the rod axial power profile.

Code-data comparisons are presented in Figures 11-37 for Test K5A and Figures 38-63 for Test K7A. Calculations for both the base case and the alternate input options are shown in most of the K5A plots; these will be discussed in parallel analysis with reference to each other. Computing time requirements for the calculations were: Test K5A base case, 36 CPU seconds/second[(d)]; Test K5A alternate calculation, 16 CPU seconds/second; Test K7A, 24 CPU seconds/second.

1.1 Test K5A Comparisons.

1.1.1 Clad Surface Thermal Behavior. Figure 11 shows that the base-case prediction for midplane cladding temperature falls outside the envelope for the measured thermocouple data, with the calculation high by 5 to 15%. Calculated turnaround and quench were slightly overpredicted. The corresponding comparison for the alternate calculation is shown in Figure 12, using the same experimental data. Here, the maximum temperature is predicted only about 3% high (30 K), and turnaround and quench are in close agreement.

(d) CPU seconds/second represents the number of computer control processing unit seconds required for each second of calculated transient time.

Figures 13, 14, and 15 present comparisons of maximum temperatures as functions of axial location on the heater rods for the hot, average, and cool channels, respectively. Figure 13 (hot channel) shows that the highest experimental temperature occurred at the 2.25-meter location, slightly above midplane. Here, the code overpredicted the temperature in the base-case calculation and underpredicted it for the alternate calculation. Code overprediction generally was greater in lower and upper regions than at midplane. Near midplane, the calculations for the alternate case lay within the experimental variation band. It is of interest that the shapes of the calculation curves and of the experimental data distribution clearly reflect the step function of the heater-rod axial-power distribution (Figure 10). For the average channel (Figure 14), the relationships are very similar to those for the hot channel, except that the overall temperature levels are lower as would be expected. Corresponding trends are evident for the cool channel comparison. However, at these lower temperatures, the calculations lay within the data scatter band below and through midplane and lay above the scatter band above midplane. In each figure, the alternate calculation predicted substantially lower temperatures above midplane than did the base-case calculation. Of interest is the evident data scatter for the cool channel as contrasted with excellent agreement within the experimental data at each station for the hot and average channels.

Figures 16, 17, and 18 present the maximum clad temperature comparison in a form that indicates the general predictability of this parameter. Again, the lack of data scatter for the hot and average channels is evident in the local clustering of plotted points. The deviation at high core elevations for the base-case is apparent at high predicted temperature levels in each figure. The presentations use the same information as given in Figures 13-15; the format yields a general picture of data agreement, one emphasizing temperature magnitude rather than location along the heater rods.

Code calculations of time to turnaround[e] are compared to experimental turnaround times in Figures 19-21. Both base-case and alternate calculations agree well with data in the lower regions of the core. Near midplane, a divergence in the calculated results occurs, with the base case predicting excessively long times to turnaround for the core upper regions. Despite some scatter, agreement for the alternate case is reasonably good except in the regions above the maximum power step (above 2.6 m). In the upper region so defined, turnaround occurs much earlier in the experiment than in either calculation.

Figures 22-24 allow comparison of the quench-time predictions to the data for the three channels. In all three, the base-case overpredicts the time at and above midplane, whereas the alternate calculation predicts quench time well through midplane. The tendency for early quench in the upper regions of the core, as shown in the data, is predicted by neither calculation.

Figure 25 is a presentation of general interest. It represents the predicted and the measured local hot-channel temperature at selected transient times. At 100 sec, the alternate calculation indicates occurrence of peak clad temperature; at 200 sec, the base-case calculation has a corresponding indication at a temperature level substantially higher than that of the alternate. The figure shows the progression of the quench front at these two reference times for both calculation and experiment. Both calculations show quenching to occur at a lower core height than shown in the data at 100 sec; an indeterminate difference is indicated at 200 sec. Of interest is the increase in the base-case calculated maximum temperature with time (from 1060 K to 1100 K). This increase does not occur either in the alternate calculation or in the experimental data. Random quench in the data at and above 2.9 m is not reflected in either calculation.

---

[e] Turnaround time is that point in the transient when the core temperature rise trend is reversed and maximum temperature occurs.

1.1.2 Diagnostic Comparison for K5A.

(1) Liquid Inventory Analysis. Liquid inventory data for the downcomer and upper annulus, the upper plenum, and the core are shown in Figure 26. The curves shown represent the effective collapsed liquid level as determined from differential pressure measurements. Some of the significant comparisons of these data with calculations can be made with reference to Figures 27-29. Figure 27 indicates a mass inventory maximum of about 6 kg for the base-case and about 0.6 for most of the alternate calculation. This compares to a measured maximum 0.2 m or approximately 15 kg. For an upper plenum capacity of more than 150 kg, indication of an inventory accumulation of less than 10% for both calculations and for the experiment represents good agreement, justifying the uses of the Wilson bubble-use model. Use of this model in the calculations is additionally justified in that the level swell in the upper plenum provides early onset of liquid carryover to the hot legs that compares well with the early detection in the experiment of entrained liquid at the steam generator inlets.

The mixture level rise in the upper annulus (Figure 28) is similar to the experimental behavior with one exception. For both calculations, there is an initial inventory build-up that releases liquid to the downcomer in a rapid deluge before final inventory level rise to the top of the volume at about 60-65 sec. The time to fill is about the same in the calculations and the experiment, but the initial build-up occurs only in the calculation. In the experiment, the volume fills to the cold-leg centerline at 60 seconds and to the top of the volume at 150 seconds. This represents a deficiency in modeling that is not of large significance in overall effect.

The collapsed liquid level history in the core hot channel is shown for both calculations in Figure 29[(f)]. Reflood of the core is shown to

---

[(f)] The experimental mixture level does not differentiate among power zones. Accordingly, the hot-channel levels are presented as representative of all core channels.

start at about 28 seconds in that figure, a time very close to that indicated in Figure 25. The calculations show an initial large-amplitude oscillation having a period of approximately 3 seconds. This oscillation damps when the upper annulus fills. In the experiment, the oscillations are of only slightly less amplitude, of similar period, and damp at approximately the same time. After the initial damping, the oscillation characteristics differ in the two calculations, and the calculations, from the experiment. Both calculations show that the liquid level oscillates across the core inlet until initial damping occurs; not only does the flow reverse periodically, but it removes all liquid from the core as it does. Not so in the experiment, where the flow reverses but the liquid level remains in the core.

The oscillations in the core are initially driven by core gas generation, supplemented by a condensation driving function in the upper annulus. When the upper annulus fills, the availability of steam from the containment is reduced, the condensation driving function is diminished, and the oscillations are damped. After the initial damping, each of the calculations shows a different dynamic history; neither resembles the experiment in detail. The base-case calculation continues the oscillations with reduced amplitude and increased period. The alternate calculation shows full damping. The difference between the dynamic behavior of the base-case and the alternate calculations lies in the entrainment and dispersed-flow heat-transfer calculation. The base-case has a moderate entrainment factor, but a low relative heat flux to the liquid entrained. As a result, the carryover to the upper plenum and to the hot leg is high. The alternate calculation has a high liquid entrainment, but a very high heat flux to the liquid, reducing the carryover. The consequence is that the vapor generation dynamics in the steam generator differ for the two calculations, allowing one to permit full core damping and the other, to enhance system oscillation. In effect, the calculated behavior for the two cases brackets the experimental behavior. A further damping characteristic is observed in the experimental data as the oscillations change in nature at about 125 seconds. It is of interest that this change appears to coincide with the over-fill of the upper annulus to a level above the steam bypass pipe upper vent.

Comparison of the indicated mixture levels of Figures 26 and 29 shows the base-case mean comparing well with experimental data, but that the alternate calculations results in a level 20% or more higher. The higher level is attributed to the reduced liquid head above the core in the vessel and to potentially reduced loop steam binding.

(2) Flow and Pressure Analyses. Experimental flows in the coolant loops are shown in Figure 30. The dominant indication is that of reverse flow in the broken loop. This reversal occurs until the upper annulus fills to the cold-leg centerlines, when the flow becomes positive and compares well with that in the single intact loop. Both base-case and alternate calculations indicate this same tendency (Figure 31). In the intact loops (Figures 32 and 33), the calculated and experimental loop flows also show generally good agreement in magnitudes and characteristics except in the amplitude of flow oscillations.

Figure 34 shows the pressure histories measured in the upper annulus and upper plenum. The calculated values of upper plenum pressure (Figure 35) show close agreement with the experimental. This is also true for the loop pressure difference, upper plenum to upper annulus, shown for the experiment in Figure 36 and for the calculations in Figure 37. The difference in the calculated differential pressure in the latter figure is significant only after 200 seconds, implying that steam binding effects in the loop are probably not as significant as liquid inventory above the core prior to that time in controlling rate of core mixture-level advance. After 200 seconds, the calculated presssure differential for the alternate case is about 15% less than in the experiment, implying a reduced loop steam binding and an influence in causing an increased rate of calculated core flooding.

1.2 Test K7A Comparisons.

1.2.1 Clad Surface Thermal Behavior. Figure 38 presents a comparison of heater rod surface temperature history near core midplane. The code-calculated curves for Slabs 6 and 7 (see Figure 10) should

bracket the experimental data. Comparison shows that the code overpredicts maximum temperature by approximately 50K, but that times to turnaround and quench are well represented by the calculation. Figures 39-41 present distributions of maximum temperature over the heater rod length for all three core channels. The general tendency for the code to predict high is shown in each figure. For the hot and average channels, the differential is consistent over rod length except at the highest elevations, where the increment increases. For the cool channel, (Figure 41) data scatter is evident, although the mean differential between the data points and the code calculation corresponds well to the increments indicated in Figures 39 and 40.

The maximum clad temperatures, predicted and measured, are related in Figures 42-44. In Figures 42 and 43, the clustering of data points indicates minimal data scatter and good rod-to-rod measurement relationships. It is evident that optimum agreement between predicted and measured temperatures occurs near maximum temperature locations, i.e., the rod "hot spot". For the cool channel rods, the data scatter is shown in Figure 44 to be worse (as in Figure 41), but the minimizing of the differential near the hot spot is also evident.

Comparisons of code-calculated turnaround times with experimental results for the three channels are shown in Figures 45-47. The agreement is good for hot and average channels at and below midplane and poor nearer the top of the core. The deviation occurs at lower levels for the cool channel. Generally, the rod-to-rod experimental data consistency is excellent.

Figures 48-50 show comparisons relating the rod quenching time to core heated length. For all three channels, the agreement is good below and through midplane; deviations above midplane become substantial. Experimental data scatter in quenching time is relatively large above midplane, but not sufficient to obscure the general level of code-data differences.

The temperature distributions along the hot channel heater rods at 115 seconds (calculated time of peak clad temperature) and at 175 seconds are presented in Figure 51. The calculated quench front at 115 seconds is shown to be in good agreement with the experimental. At 175 seconds, it lags the experimental by 0.2 m or more. It is of interest that in the experiment, the centerline rod L 11 at 175 seconds is quenched at high elevations whereas hot channel peripheral rods are not. This is also shown in Figure 46, although less dramatically. Overall, the experimental high-elevation quench appears to be random.

1.2.2 Diagnostic Comparisons for K7A.

(1) Liquid Inventory Analysis. Figure 52 presents experimentally-measured liquid mixture-level data for the vessel and downcomer-upper annulus. These data indicate that the lower plenum refills and reflooding starts between 40 and 45 seconds. Subsequently, an inventory build-up starts in the upper plenum, reaching a maximum head of approximately 0.25 m, or 19 Kg. Oscillations occur in the system, damping at approximately 225 seconds, when the upper annulus fills.

The mass inventory history calculated for the upper plenum is shown in Figure 53. After an initial surge during a period of large core oscillations, the calculations show a relatively unchanging inventory level of about 0.5 Kg. This is more than an order of magnitude lower than that indicated in the experiment, but both calculated and experimental magnitudes represent only a very small percentage of upper plenum liquid capacity. At the time the large calculated oscillations terminate, the mixture level in the upper plenum stabilizes at the elevation of the hot legs, although initial carryover of liquid to the steam generators occurs with the start of reflood for both calculation and experiment.

The mixture level calculated for the upper annulus is shown in Figure 54 to reach the elevation of the cold-leg nozzles in about 225 seconds. This agrees with the experiment. At that time, the system oscillations, with a period of 2-4 seconds, damp in the experiment. Similar oscillations that appear in the calculations (Figure 55) damp at

just over 80 seconds, even though longer-period oscillations continue until the upper annulus fills. As for Test K5A, the calculated core oscillations that are shown just after the start of reflood alternately fill and evacuate the core channels. When these oscillations cease, reflood progresses at a mixture-level rise rate substantially greater than observed in the experiment. The calculation showed that during the initial oscillations the liquid carried over to the steam generators was not all evaporated in the steam generator inlet volumes (35-37 in Figures 8). After 80 seconds, it was.

(2) Flow and Pressure Analyses. The experimental mass-flow rates in the coolant-loop cold legs are shown in Figure 56. A flow reversal similar to that observed for Test K5A occurs in the broken loop during the period 0-50 seconds. This is reflected in the calculated flow history of Figure 57. Similarly, the flow characteristics calculated for the intact loops (Figures 58 and 59) are in close agreement with the experimental data.

The experimental pressure-time histories for the upper plenum and upper annulus volume are shown in Figure 60. The initial condensation depressurization is evident in the period 0 to 50 seconds. This same depressurization is shown in Figure 61. The main difference is in the calculated amplitude of pressure variation during the period of large-amplitude core oscillations (50-80 seconds). A noticable difference is shown in the pressure difference across the loops, the experimental difference being the larger by nearly 15% (Figures 62 and 63). This implies that the difference in progression of the core mixture level is related to a difference in loop steam binding.

2. CODE CAPABILITIES AND DEFICIENCIES

The discussion of the code-data comparisons has defined several areas of good code capabilities as well as some deficiencies. One main deficiency lies in the inadequacy of the developed modeling and input

guidelines of Reference 4. For example, the guideline-derived dispersed-flow weighting factor and the liquid entrainment factor used in the base-case calculation for Test K5A resulted in what was considered to be unrealistic system behavior. This occasioned the alternate calculation for that experiment. Another deficiency lay in the unproven applicability of code de-entrainment and fallback models. Substitution of the Wilson bubble-rise model for the former resulted in adequate system hydraulic response, so the impact of the deficiency has not been shown great. Similarly, there is little evidence that not using a fallback model was detrimental to the calculation.

The code handling of system oscillations is a computational deficiency. During the period of initial reflood when the oscillations are induced by forcing functions above the core and in the ECC injection region, the amplitudes were consistently overpredicted. However, damping criteria were similar to a great extent in both calculation and experiment. The extent to which the steam-generator gas generation is responsible for forcing or damping calculated oscillations is not understood. However, it is clear that some sensitivity to steam-generator nodalization does exist. This sensitivity occurs in the homogeneous equilibrium nature of the steam-generator volumes. Carried-over liquid is forced by the equilibrium assumption to be vaporized instantly, where sufficient heat flux exists. This makes the resultant pressurization sensitive to the size of the steam-generator volumes. A method of calculation that uses a partitioning system similar to that in the core could result in substantial improvement. In a similar concept, the equilibrium nature of the code has a strong influence on the condensation depressurization in the region of ECC injection. The lack of a rate limitation allows overprediction of condensation effects.

The guidelines for use of the dispersed-flow weighting factor N and the entrainment factor EN2 were derived from consideration of forced-feed reflood experiments[5]. It was recognized that application to dynamic gravity-feed systems reflood was not necessarily appropriate. One principal reason for this is that during the reverse flow of liquid in the core, entrainment of liquid from the core collapsed liquid level

surface is discontinued. Because of the explicit stepping of the calculation procedure through the partitioned core volumes, the dispersed liquid is effectively nonexistent for approximately half of the time of the calculation. Thus, even during the "damped" period after 80 seconds in Figure 55, the inlet flow is fluctuating and reversing direction. The effect of this "loss-of-dispersed-flow memory" is that substantially larger values of the factors N and EN2 are required for a oscillating system than for a forced-feed system. Accordingly, both the K5A alternate calculation and the base-case K7A calculation used such substantially increased values.

Despite the indicated code deficiencies, a high predictive capability has been demonstrated. The principal performance indicator, maximum cladding temperature, was generally well predicted in the code. Correspondingly, calculated and measured rod turnaround times, quench times, and temperature distributions showed very good agreement. Moreover, the hydraulic characteristics in the core and the coolant loops were predicted very well by the code when default levels of heat transfer and entrainment parameters were used. Some of the special studies that were made to enhance the code predictive capability are described in the succeeding section of this report.

V. ADDITIONAL STUDIES

Several preliminary, preparatory studies were made to establish modeling and input criteria for the test-prediction calculations Some of these consisted of brief analyses made to determine the best approaches to localized modeling of conditions or behavior peculiar to the PKL facility. Others considered modeling or input problems of a more generic nature. Specific problems peculiar to the facility are identified in this section with minimal discussion; the more generally applicable problems are analyzed in greater detail.

1. FACILITY MODELING PROBLEMS

1.1 Phase-Separation Modeling.

Early in the planning stage, a decision was reached not to use code fallback or de-entrainment models because of the lack of developmental verification check-out of these features. Candidates for modeling phase structure in the upper plenum were (1) assumption of a homogeneous fluid with and without vertical phase slip between plenum and core, (2) use of a complete-separation bubble-rise model in the plenum without slip, and (3) incorporation of the Wilson bubble-rise model without slip.

Calculations were made using preliminary code versions to establish the effect of these alternatives. A summary of the results is as follows:

(1) Homogeneous model without slip: Large-amplitude core inlet flow oscillations that damp quickly 20 seconds after start of reflood.

(2) Homogeneous model with slip: Core-inlet flow oscillations of relatively small amplitude that damp within 20 seconds after start of reflood.

(3) Complete separation model: Large-amplitude core-inlet flow oscillations that damp about 5 seconds after start of reflood. This model effectively prevented carryover to the hot-legs until the plenum filled with liquid to the level of the hot-leg nozzle centerline.

(4) Wilson bubble-rise model: Moderate-to-large amplitude oscillations that damped at about 45 seconds after the start of reflood.

The progression of the core collapsed liquid level was sensitive to the selection of the model concepts. Reflood progressed most quickly using the complete-separation model, mainly because of the lack of liquid carryover. The homogeneous modeling resulted in an intermediate progression of the liquid front. The Wilson model, allowing early carryover and a distributed buildup of liquid inventory, provided the lowest liquid-level rate (maximum carryover). Because it was concluded that this latter model provided the best simulation of the anticipated experimental phase structure, it was incorporated in the test-prediction modeling.

1.2 ECC Injection Modeling.

The experimental facility provided ECC injection into two intact cold-legs and into the upper annulus simulation volume. The cold-leg injection was close to the upper annulus volume and was angled toward it. Modeling of the cold-leg injection in the code resulted in back flow and severe oscillation. This condition was alleviated by assuming that the angled injection in the experiment effectively constituted injection into the upper annulus volume and modeling it accordingly. To represent the probable elevation of the liquid temperature to near saturation at the upper annulus inlet, an enthalpy-time ramp was used for the injectant; i.e., the enthalpy of the liquid was initially set at

saturation and was allowed to ramp to its design subcooled level during the period of lower-plenum refill. A sensitivity calculation was made, demonstrating that there was no appreciable effect on the calculation of core reflood events because of this ramp. The only influence was that it prevented code failure at the start of the calculation.

2. NODALIZATION AND INPUT STUDIES

2.1 Steam-Generator Nodalization Study.

Prior to code release for internal laboratory use in independent verification study, a preliminary code version was used to evaluate the effect of subdividing the primary volume on the inlet side of the steam generator. The initial nodalization concept was to model the primary using two control volumes, dividing the steam-generator tubes at the midpoint. It was observed that carryover of a moderate amount of liquid into the steam generator from the hot leg in an oscillating flow system had a unique result. In a given time step, a homogeneous mixture at some quality greater than zero entered the steam-generator primary volume. The heat-transfer mode adjusted to add heat to the mixture, an amount sufficient to flash the liquid to steam and then superheat the [illegible] gas. This provided a localized steam explosion that imposed a pressure pulse on the system and tended to drive the inlet flow back in a reverse direction. This had the potential to enhance the fundamental system flow dynamics.

It was determined, by subdividing the inlet primary volume, that some of the entering liquid would not be vaporized in the first subdivision if the available heat flux from the secondary side was inadequate. The liquid that was not vaporized was carried over to the next volume, where vaporization was completed. This had the effect of relieving the intensity of the generated pressure disturbance and, in the example studied, of allowing damping of the system oscillations for

an appreciable period of time. Figures 64 and 65 illustrate this effect. For the mixture level calculation shown in Figure 64, the system nodalization was as presented in Figure 8 except that Volumes 10, 17, and 23 were enlarged to include Volumes 35, 36, and 37, respectively. For the mixture level calculation shown in Figure 65, the nodalization of Figure 8 was used.

The effectiveness of the nodalization change depends on the relative amount of liquid carryover to the steam generators. However, with sufficient carryover, the volume subdivision represents an improved simulation of actual steam generator behavior. This potential for improved simulation was incorporated into the nodalization for the K5A and K7A test predictions and was effective (Section IV 1.2.2.(1)).

2.2 Dispersed-Flow and Entrainment Study.

As discussed in Section IV.2, guidelines for selection of the dispersed-flow liquid weighting factor N and the maximum entrainment fraction EN2 were developed from a limited data base. This data base consisted of the results of forced-feed reflood experiments. Consequently, it was recognized that the guidelines might not apply for dynamic gravity-feed analysis.

Several calculations were made to evaluate the sensitivity of the code to selection of values of the parameters N and EN2 for use in gravity-feed reflood analysis. The study was made using the K5A model. The effects of parameter variation on maximum clad temperature and turnaround time are shown in Figures 66 and 67, respectively. One evident observation from both figures is that the guideline selections for the base case, N=11 and EN2=0.3, lie in a region of strong sensitivity. For values of EN2 of about 0.1 and greater, calculation of both maximum temperature and turnaround time vary severely for $N < 30$. Correspondingly, for $N \geq 30$, the performance parameters are relatively insensitive to changes in EN2. These behavior patterns do not in themselves provide sufficient information to justify values of EN2 and N for use in the K5A test prediction. However, when analysis of the

results of the K5A base-case calculation indicated that an alternate selection was warranted, and in view of the implied need to increase the magnitude of the N and EN2 parameters over the guideline values, new values outside the sensitive areas were selected. These values, N = 30 and EN2 = 0.665, were essentially the same as the code default magnitudes incorporated when Update 4 was released to the Argonne Code Center in January, 1978.

The information in Figures 66 and 67 has been replotted in Figure 68 for the peak clad temperatures measured in Tests K5A and K7A and for hot-spot turnaround for those tests. Additionally, the calculated data base for Figures 66 and 67 was reviewed to estimate the boundary between the regions of damped and undamped calculational oscillations. This boundary is shown to cross the K5A and K7A curves in Figure 68. One implication to be derived from this figure is that if a guideline pair of values for N and EN2 defines a point in the undamped zone, these values will be inadequate for calculation of the given test behavior. For example, the guideline values N = 11 and EN2 = 0.3, as used in the base case for K5A, lie to the left of the damped zone boundary. For the alternate case, and for the K7A calculation, the values of N and EN2 are well to the right fo the boundary, beyond the curves representative of the experimental conditions. Hindsight indicates that N = 20, EN2 = 0.3 would have been better values for both calculations. The specific combinations of numbers is arbitrary, the objective of the selection being to locate a point in the map close to the damping boundary, but to the right of it.

The question remains as to the reason for the inadequacy of the Reference 4 guidelines for N and EN2 in the region of Figure 68 to the left of (or near) the damping boundary. It was stated in Section III.2.2 that calculational iteration on ECC subcooling and core-inlet flooding rate was necessary to define N and EN2 for gravity-feed experiments. This need for iteration has been examined further.

Inspection of the shape of the experimental clad histories of Figure 11 indicates that during the period of large-amplitude oscillation

just after the start of reflood (30-65 seconds), the clad cooling is relatively large. This is evident in the occurrence of a negative slope in the data curves, with a subsequent recovery after the severe oscillations are damped. The code calculation shows a decreased slope, but a continuously positive one. In Figure 12, the alternate calculation is also shown to have a positive slope, but at 65 seconds this slope is substantially greater than for the base-case curves. This infers that the code is not indicating nearly as high a heat-transfer rate as is evident in the test data, although the alternate calculation is an improvement over the base case during the time period of the large oscillations. It is also clear that after the alternate calculation shows system damping (after 65 seconds), it overpredicts the heat transfer from rods to fluid. This compensation is reasonably successful, for it results in overal good code-data comparison.

Consider the code treatment of the entrainment and heat transfer during the period of large-amplitude oscillation. Figure 29 shows that the calculated mixture level moves down and out of the bottom of the core. When the inlet fluid velocity is positive (as the mixture level rises), there is core liquid entrainment; when the inlet velocity is negative, entrainment is shut off and liquid in the core above the mixture level simply disappears from the computation. Thus, there is heat transfer from the rods to the entrained liquid only when the mixture level is rising, and the factor N has significance only during this period. For this condition, the core pressure is substantially lower than average (core pressure is a driving function for the oscillations). At the same time, the entering fluid is initially saturated steam, if the lower plenum is represented by a bubble-rise model. Entrainment will not occur until the liquid level reenters the core. Thus, in a symmetrical oscillation cycle, entrainment only occurs for 25% of the time period. Even then, the entering liquid is at saturation conditions, for it has reached equilibrium with saturated steam while the liquid level was in the lower plenum. If the lower plenum had been modeled as a homogeneous fluid volume, liquid level rise in the core would have been initiated at the time the inlet flow became positive, although entrainment would have started only when the level reached the heated region of the core.

It follows that the occurrence of dispersed flow and the integrated magnitude of heat transfer to liquid in the core above the collapsed liquid level depends on the fluid modeling in the lower plenum and on the distance between the bottom of the core volume and the bottom of the rod heated length. This sensitivity justifies the use of values of the factor N, for the K5A alternate calculation and for the K7A test prediction, that are substantially higher than those selected on the basis of forced-feed reflood guidelines. A structured procedure for selection of a numerical value for N cannot be defined on the basis of the foregoing review. Nevertheless, the need is justified for iteration on pressure and subcooling to establish the effects of initial reflood dynamics that alternately empty and reflood the core volume, and for formulation of a guideline, such as that of Figure 68, to aid in selection of an appropriate value of the liquid weighting factor.

VI. CONCLUSIONS AND RECOMMENDATIONS

Evaluation of RELAP4/MOD6, Update 3 has shown the code to have significant capabilities in PKL reflood analysis application. The best demonstrated of these capabilities are as follows:

(1) Prediction of maximum cladding temperature in the midplane regions of the core for all three experimental energy zones was within 3% and 5% for the alternate calculation of Test K5A and the base-case calculation of Test K7A, respectively. For each, the calculated temperatures were higher than the experimental (Sections IV-1.1.1 and -1.2.1). Turnaround and quench times for the K5A alternate calculation were predicted within 10 seconds at and below midplane; for Test K7A, the predictions were within 20 seconds for the same region.

(2) The damping of the system fluid oscillations occurred at the same time in the code calculations as in the experiments (Sections IV-1.1.2 and -1.2.2). The influence of upper annulus filling on damping was also the same in the calculations as in the experiments.

(3) Calculation capability for determination of loop fluid flows and pressure balances was demonstrated (Sections IV-1.1.2(2) and -1.2.2(2)). The calculated initial flow reversal in the broken loop was the same as in the experiments, both in magnitude and duration. Loop pressure drop calculations matched the time characteristics of the experimental results, although the experimental steam binding was 15% less than calculated.

Several code deficiencies were identified in this study (Section IV-2). One principal deficiency was the inadequacy of developmental verification guidelines for definition of appropriate code-input values of dispersed-flow heat-transfer and entrainment parameters. Another deficiency lay

in the inadequacy of available modeling of upper-plenum phase separation and fallback to the core. This led to uncertainty in the calculation of liquid carryover from the vessel. The calculation of system dynamics was another area where the code showed some inadequacy: core oscillation amplitude was consistently overpredicted, and the progression of the reflood liquid front upwards into the core was not representative of the experiment during the large-amplitude oscillation period. Driving functions for system fluid oscillations in the steam generator and at the cold-leg injection location were not well reproduced by the code.

Recommendations for improvement in code predictive capability derived from the results of this study are as follows:

(1) An improvement in the method of calculation of entrainment and of dispersed-flow heat transfer is mandatory. The calculation of fluid conditions and heat transfer above the core collapsed liquid level should be modified to continue entrainment during reverse core inlet flow and to improve definition of rod-to-fluid heat transfer in the upper core region. New guidelines for code input should then be derived through developmental verification based on a broad experimental data base.

(2) Further study is also required in the development and verification of upper-plenum phase-separation models.

(3) The problem induced by equilibrium vaporization in the steam generator primary volumes could be reduced by the development of a marching partition approach similar to that used in the reflood core modeling. This would provide a more realistic phase distribution and a smoothed dynamics-forcing function in the steam generators.

(4) An ECC mixing model usable for analysis of cold-leg injection conditions should be developed. This would allow direct modeling of the injection process.

(5) The guidelines for selection of the dispersed-flow input parameter N, developed in code developmental verification from forced-feed reflood data, should not be used in gravity-feed reflood analysis. Instead a minimum value 20 as implied in Section V-2.2 of this report should be used. Should the magnitude of N determined using Reference 4 techniques be greater than 20, the larger value should be used. Pending the development of an improved entrainment model, the existing guidelines from Reference 4 should be used to determine the parameter EN2.

VII. REFERENCES

1. RELAP4/MOD6, A Computer Program for Transient Thermal-Hydraulic Analysis of Nuclear Reactors and Related Systems, EG&G Idaho, Inc. Report CDAP TR 003 (January, 1978)

2. RELAP4/MOD5, A Computer Program for Transient Thermal-Hydraulic Analysis of Nuclear Reactors and Related Systems, Volume I, RELAP4/MOD5 Description, Aerojet Nuclear Co. Report ANCR-NUREG-135, (September, 1976).

3. S. Fabic Ltr, "Independent Verification of Codes," transmitted to attendees of November 18, 1977 meeting on independent verification in Denver, November 28, 1977.

4. C. D. Fletcher and G. E. Wilson, Developmental Verification of RELAP4/MOD6, Update 1, with FLECHT LFR Cosine Test Data Base, EG&G Idaho, Inc. Report PG-R-77-24, (July, 1977).

5. E. R. Rosal et al, FLECHT Low Flooding Rate Cosine Test Series Data Report, Westinghouse Electric Corp. Report No. WCAP-8651 (December, 1975).

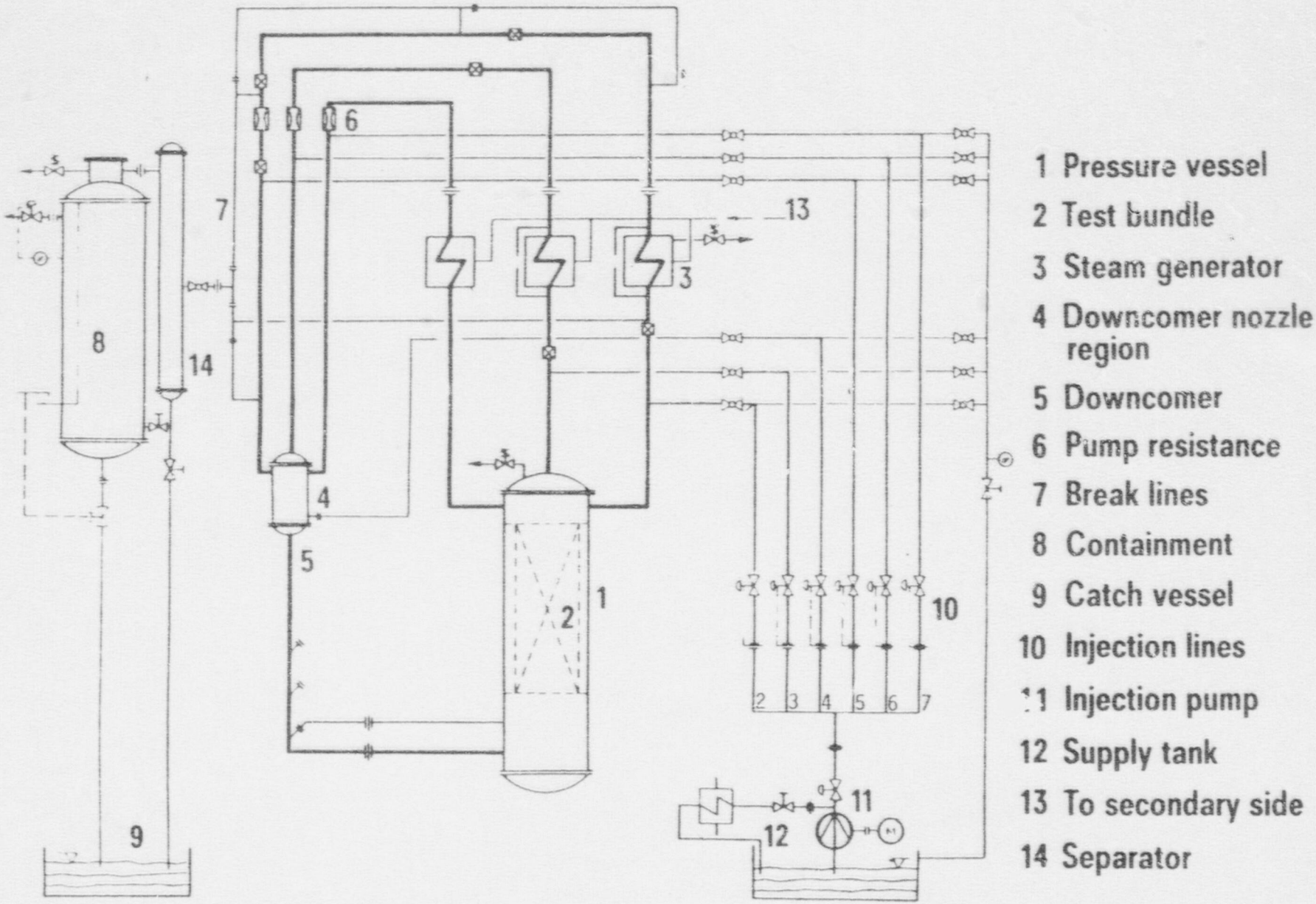

Fig. 1 Schematic of the PKL test facility.

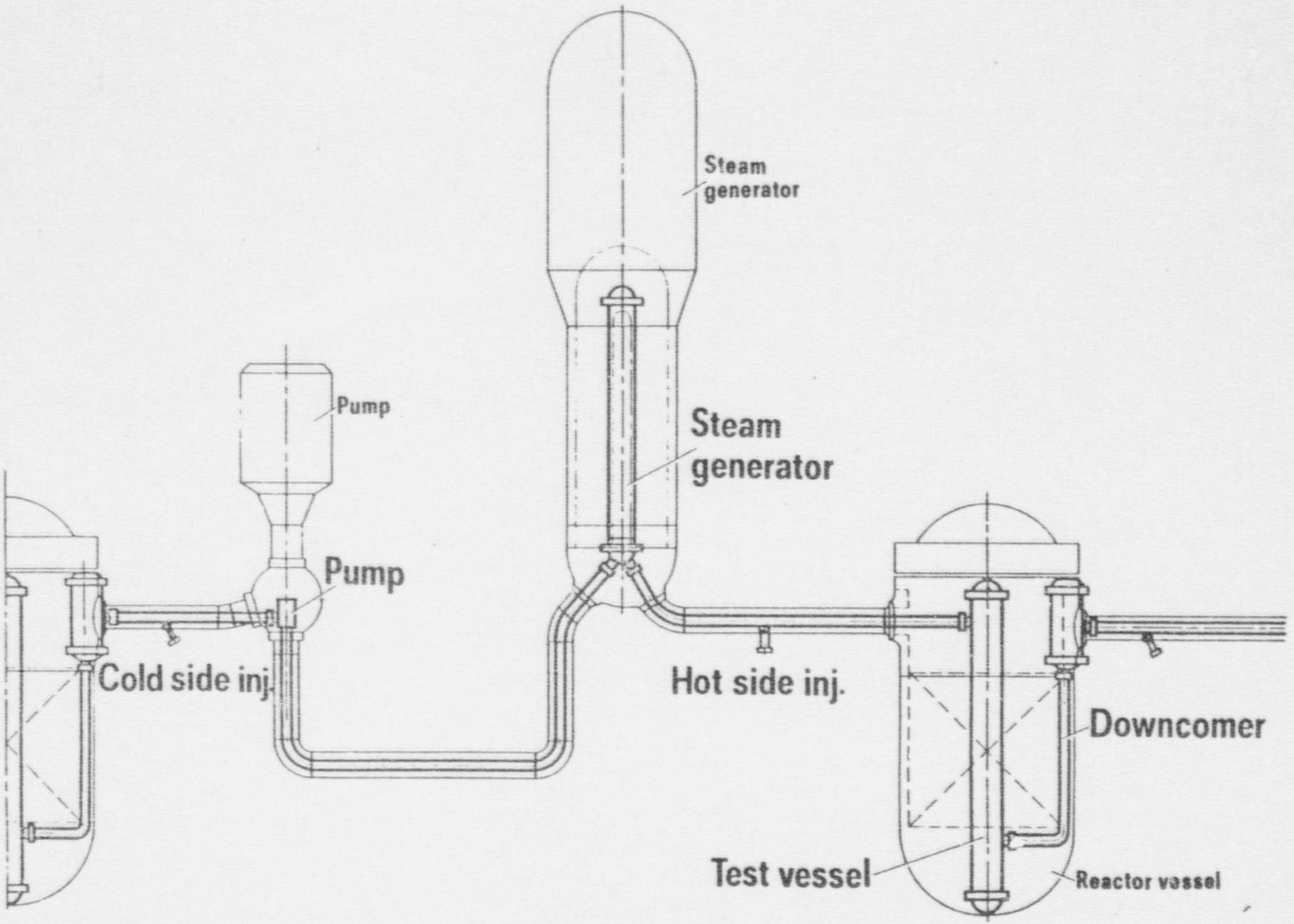

Fig. 2 Simulation concept for the PKL vessel and loops.

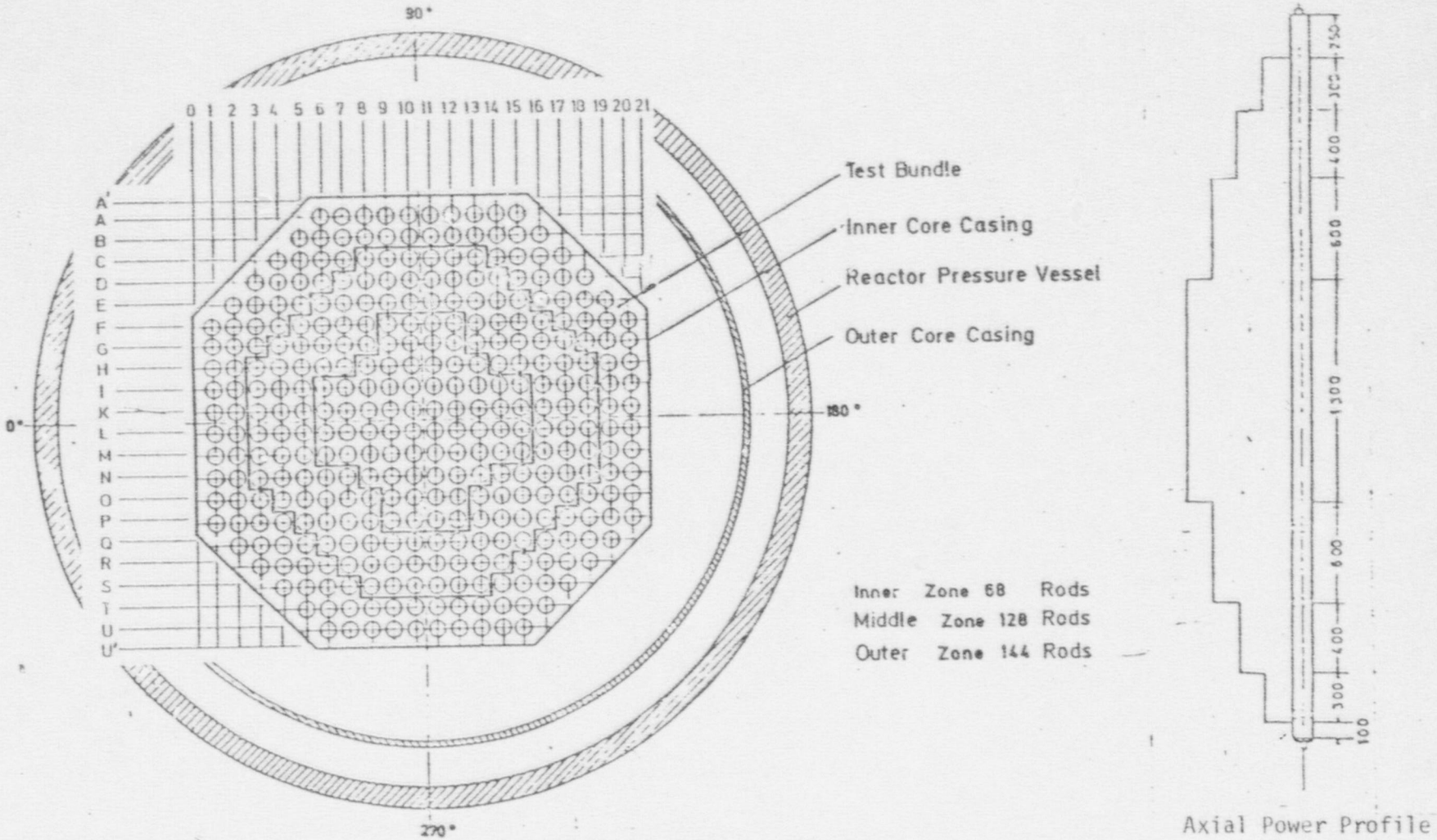

Core Cross Section

Axial Power Profile

Fig. 3 Core rod array cross section and power distribution.

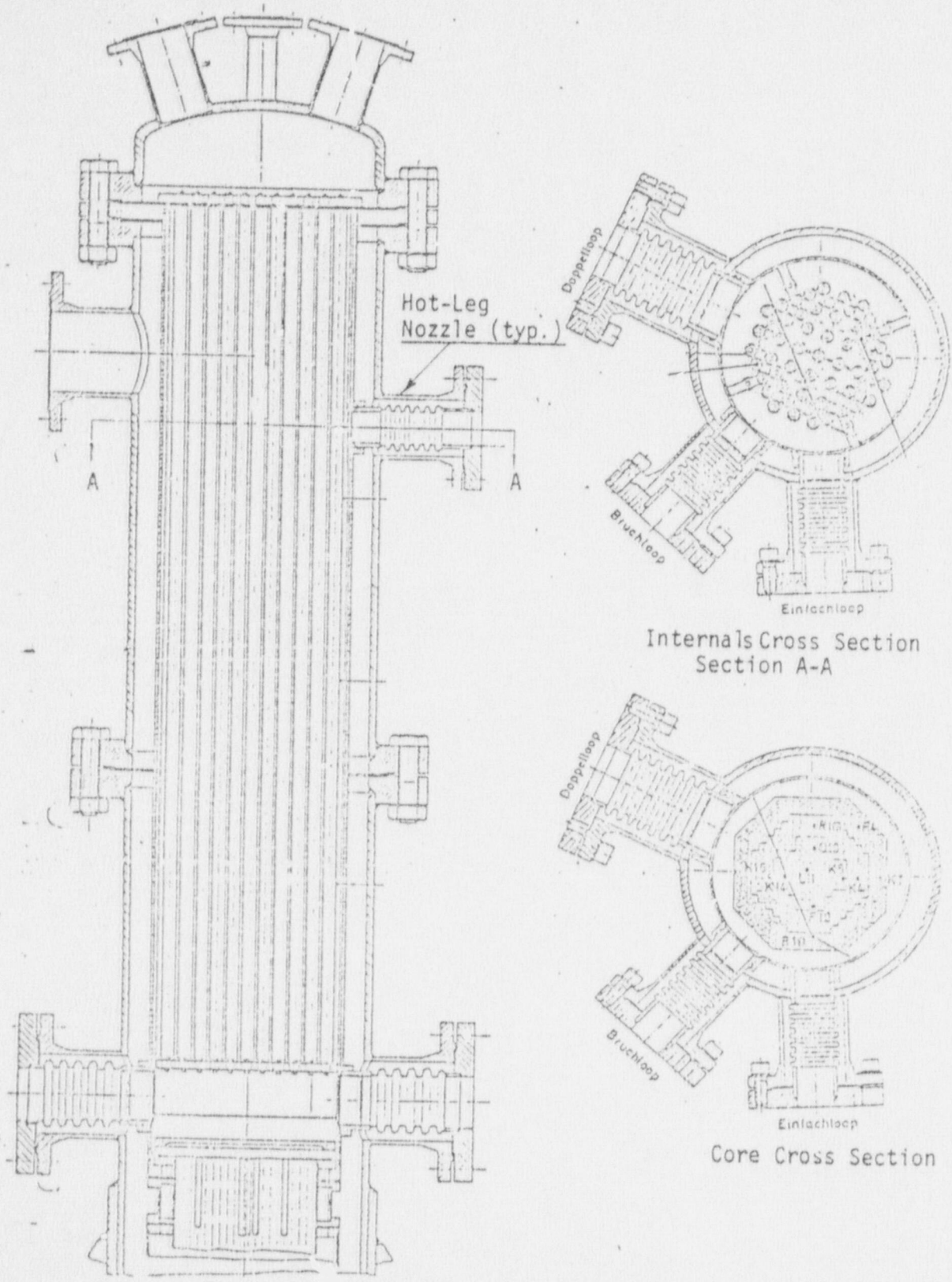

Fig. 4 Vessel upper plenum internals simulation.

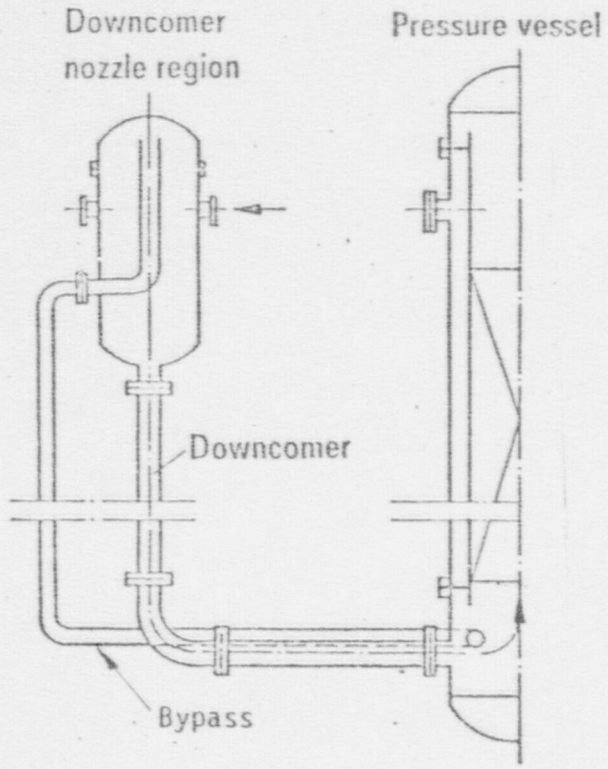

Fig. 5 Installation of downcomer steam bypass.

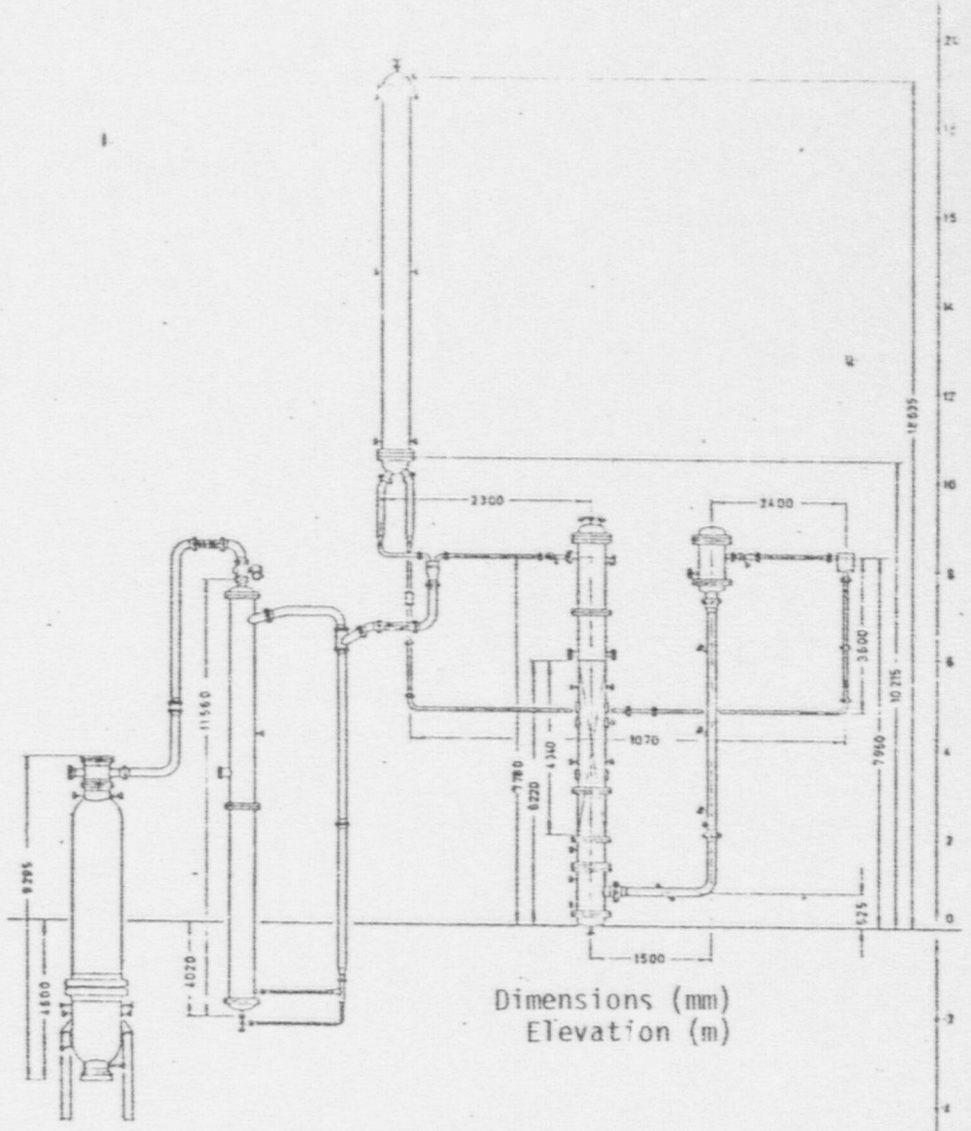

Fig. 6 Elevation details for the PKL broken loop.

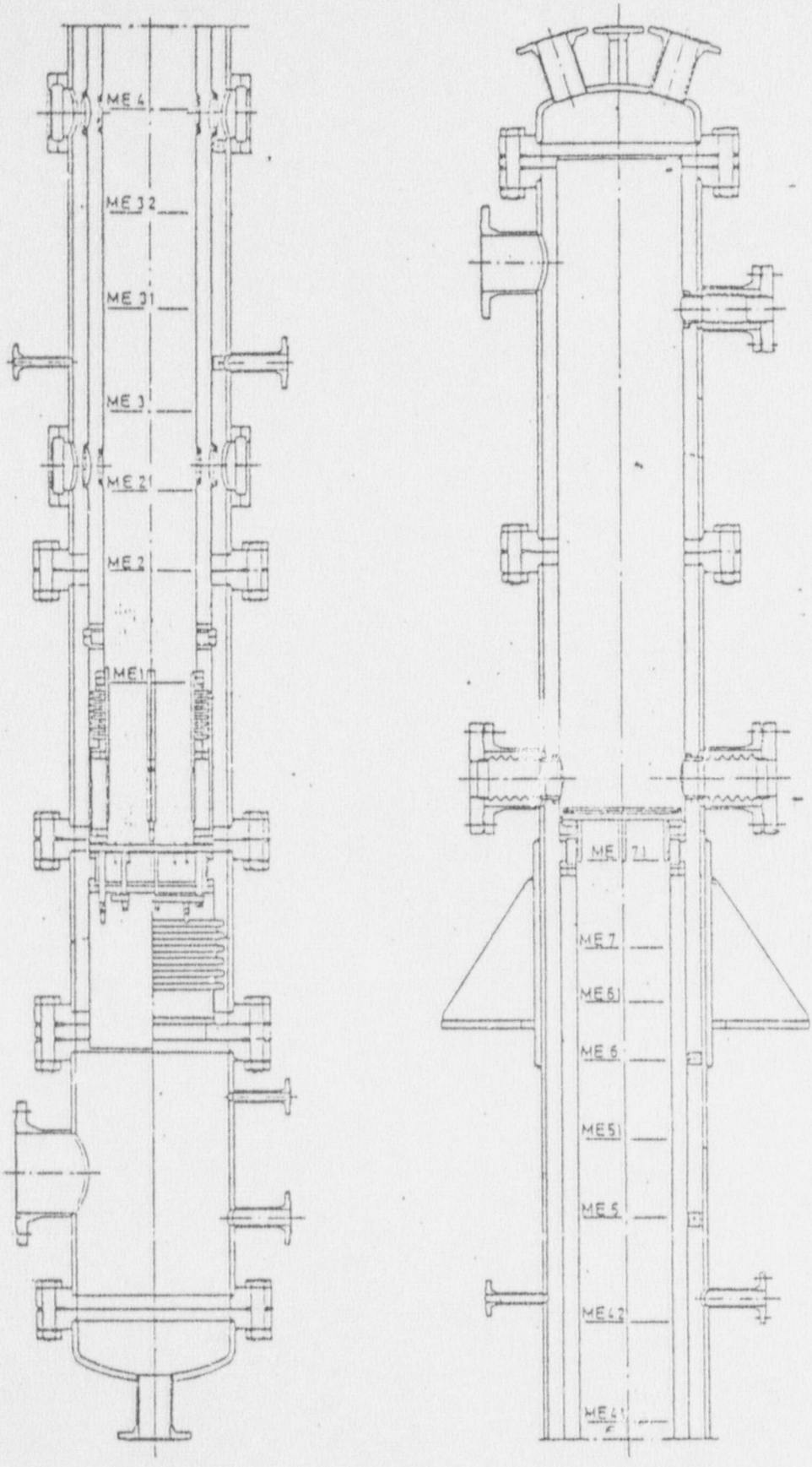

Fig. 7 Vessel layout showing core cladding thermocouple locations

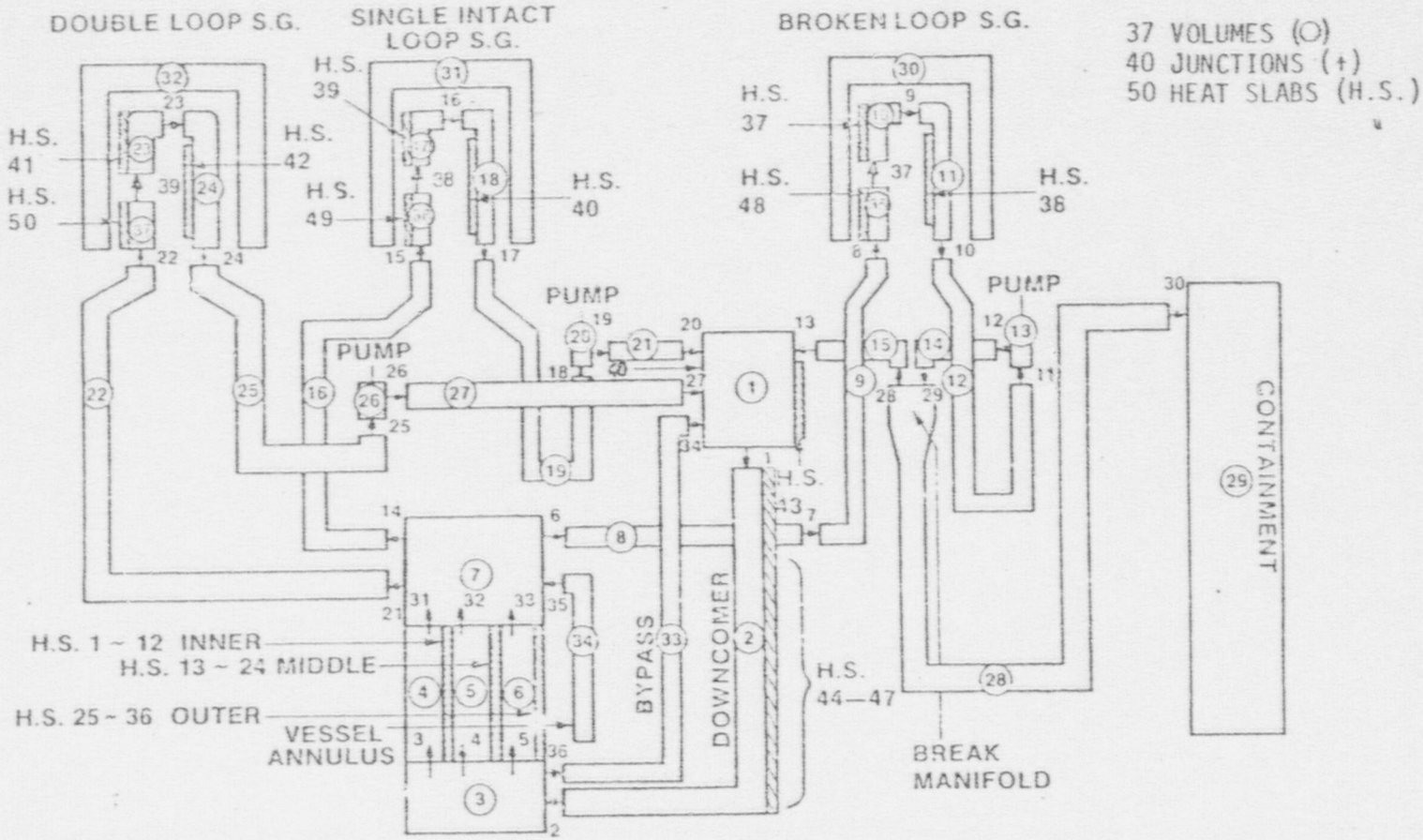

Fig. 8 KWU PKL three-loop RELAP4/MOD6 nodalization.

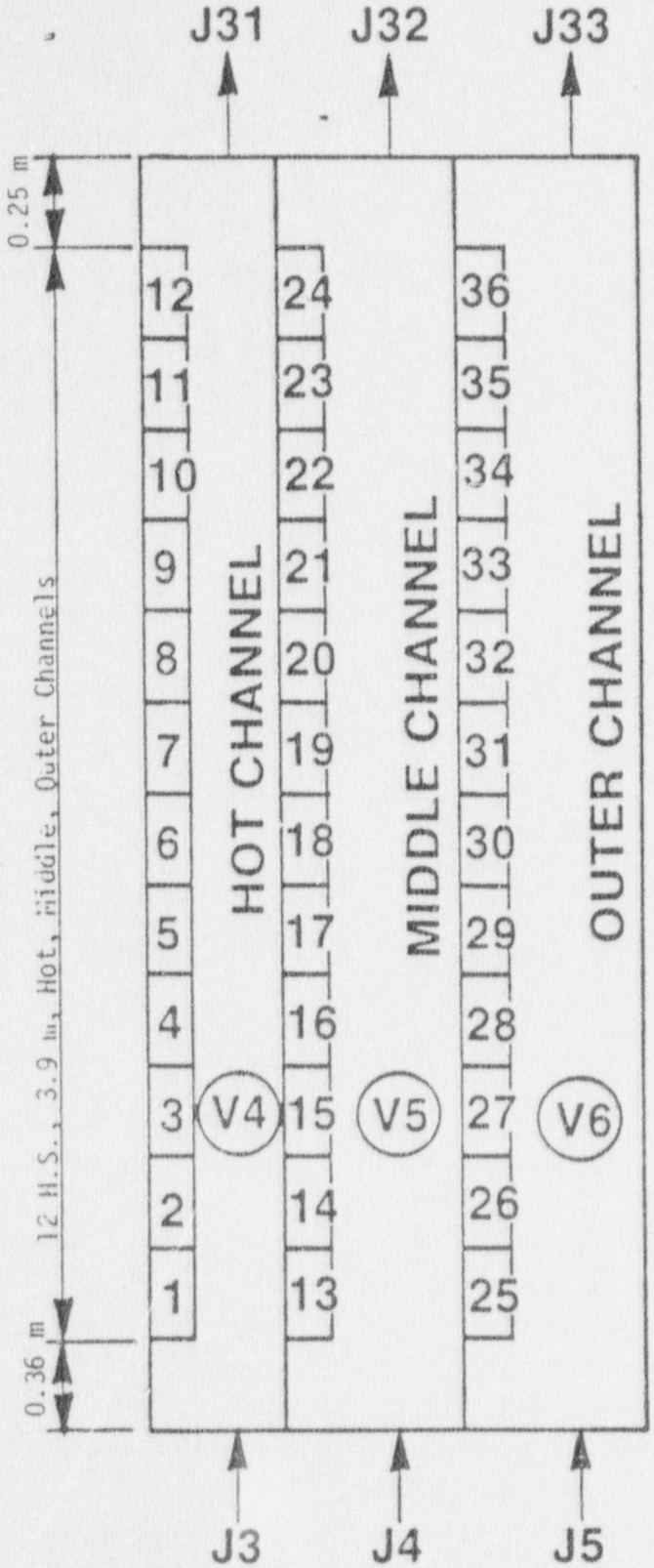

Fig. 9 Core heat-slab structure.

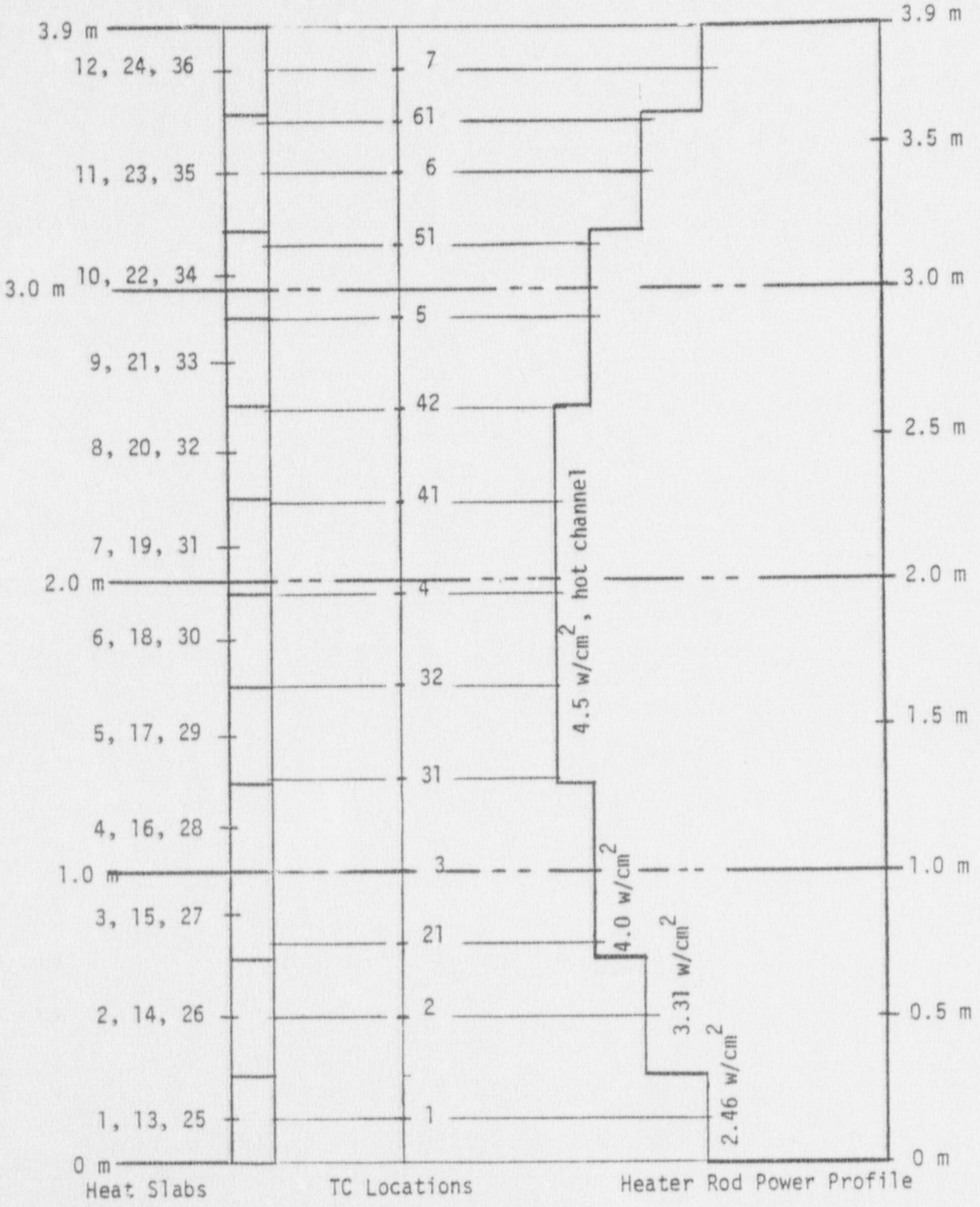

Fig. 10 Relationship of heat-slab centers to rod thermocouple locations.

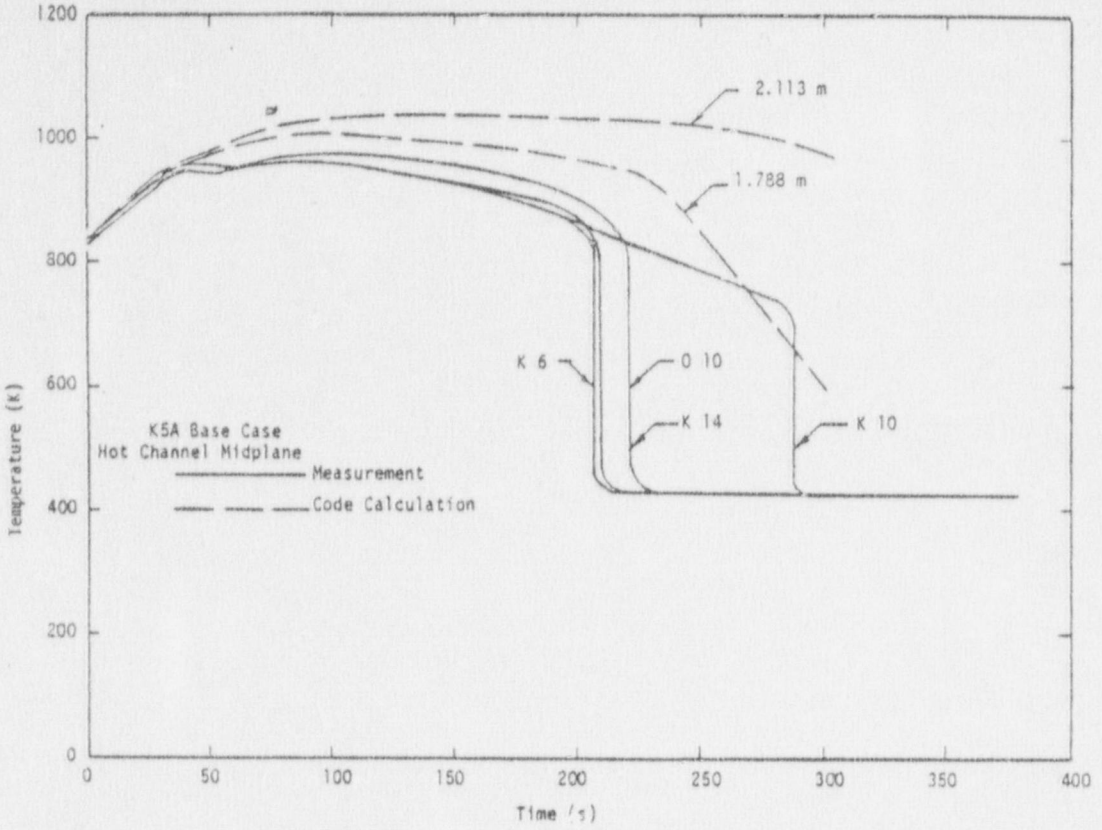

Fig. 11 Comparison of cladding temperature history at the midplane, Test K5A base case.

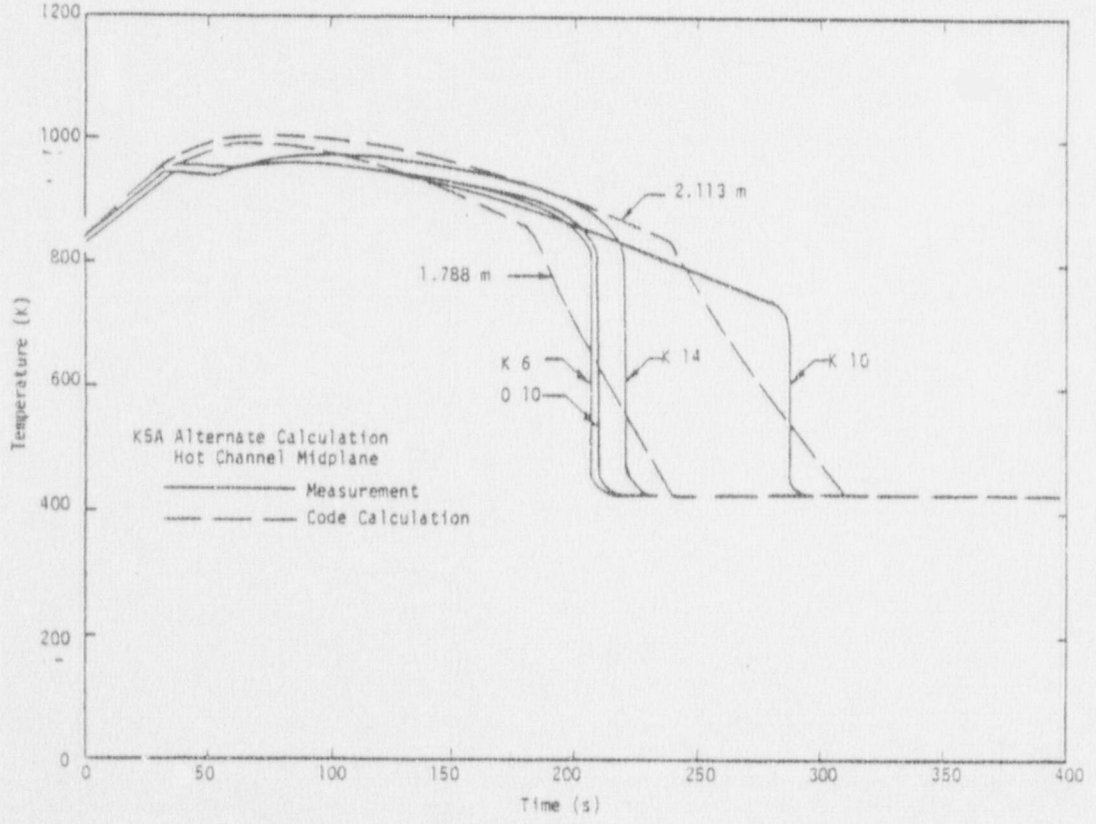

Fig. 12 Comparison of cladding temperature history at the midplane, Test K5A alternate case.

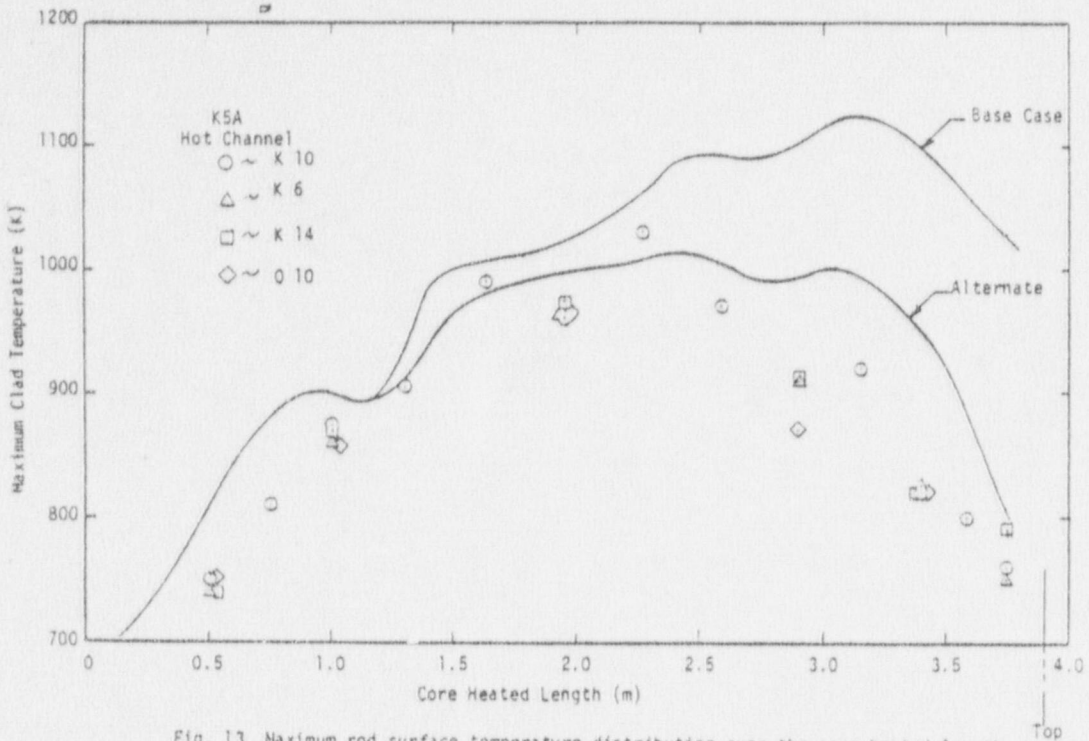

Fig. 13 Maximum rod surface temperature distribution over the core heated length, K5A hot channel.

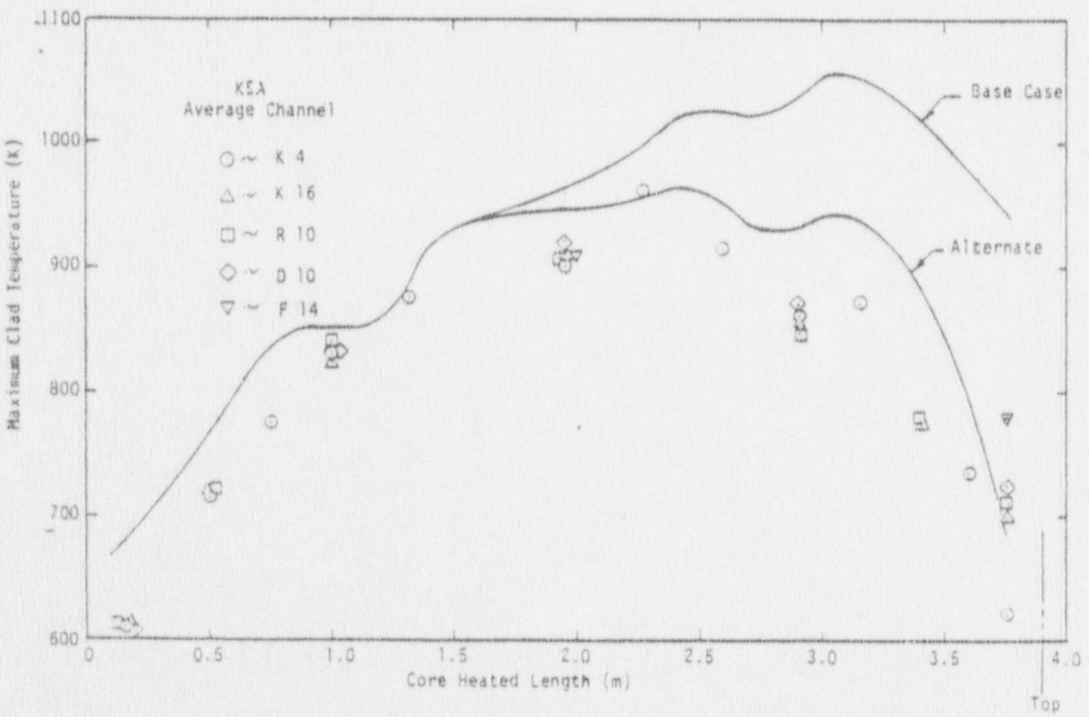

Fig. 14 Maximum rod surface temperature distribution over the core heated length, K5A average channel.

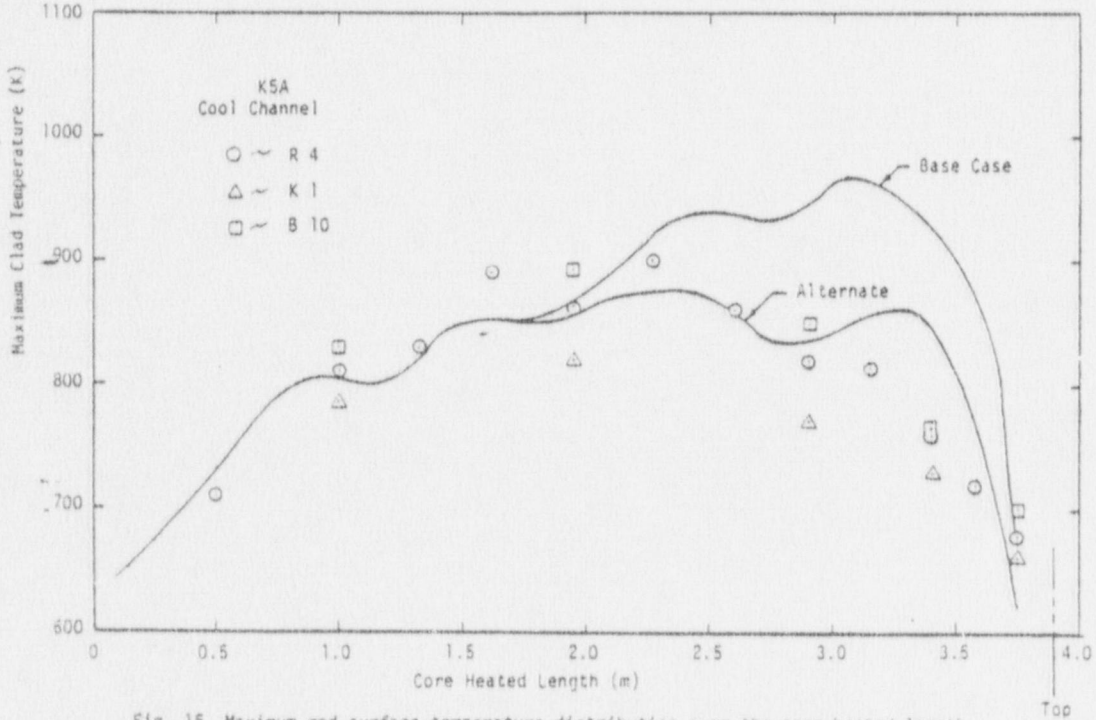

Fig. 15 Maximum rod surface temperature distribution over the core heated length, K5A cool channel.

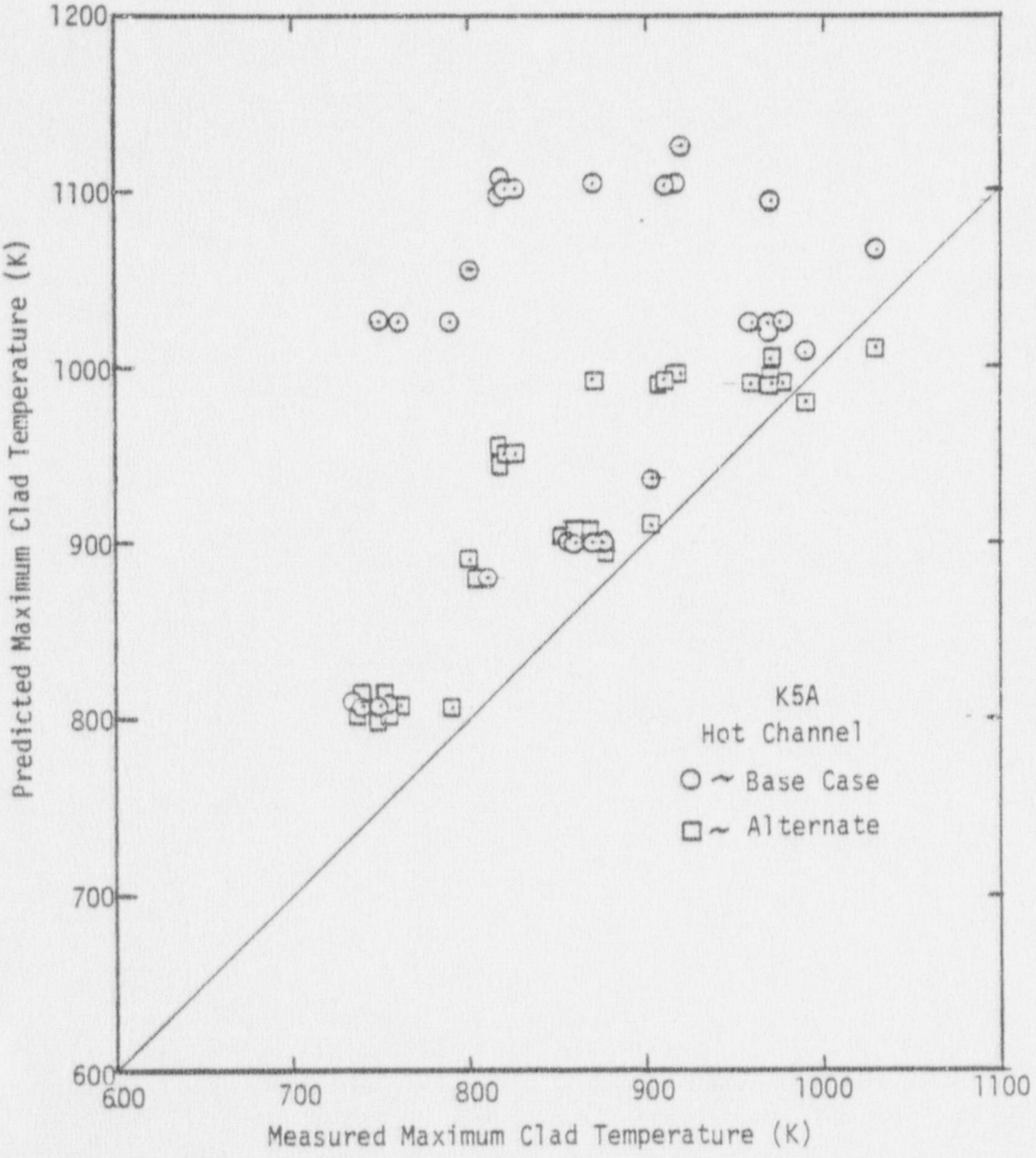

Fig. 16 Predicted vs. measured rod surface temperature, K5A hot channel.

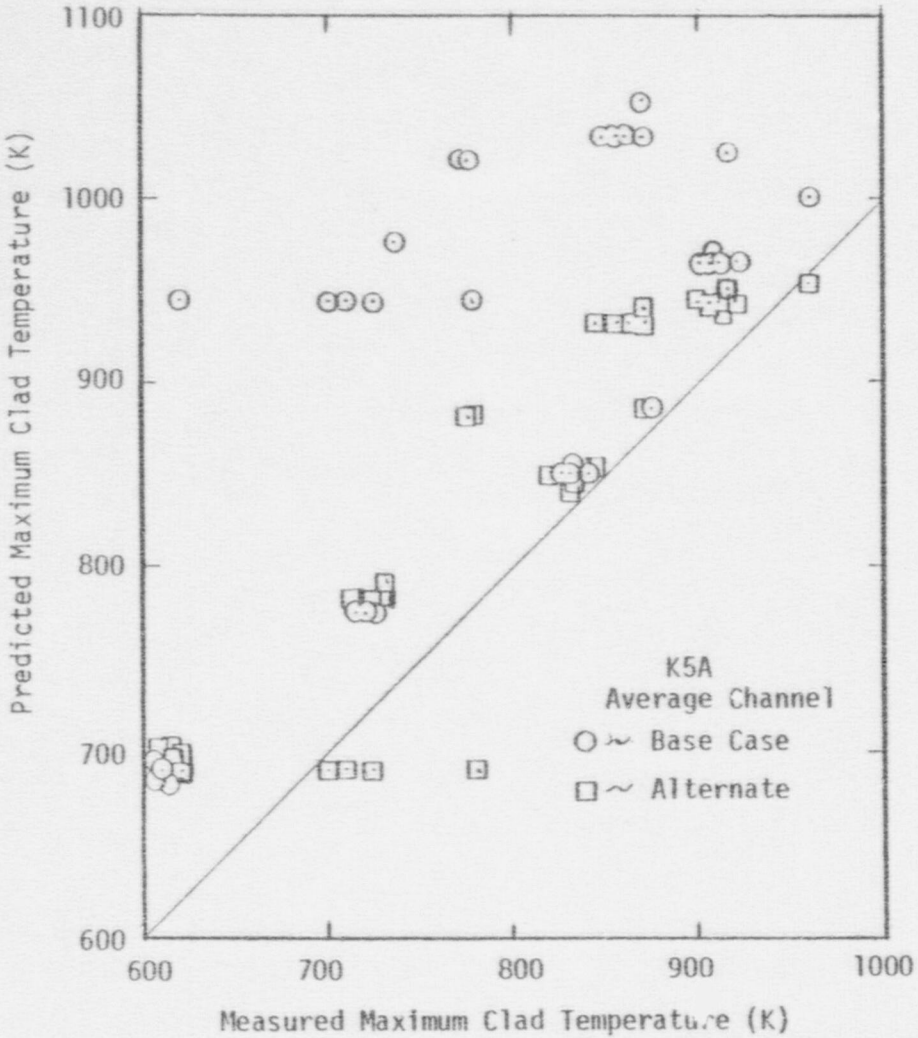

Fig. 17 Predicted vs. measured rod surface temperature, K5A average channel.

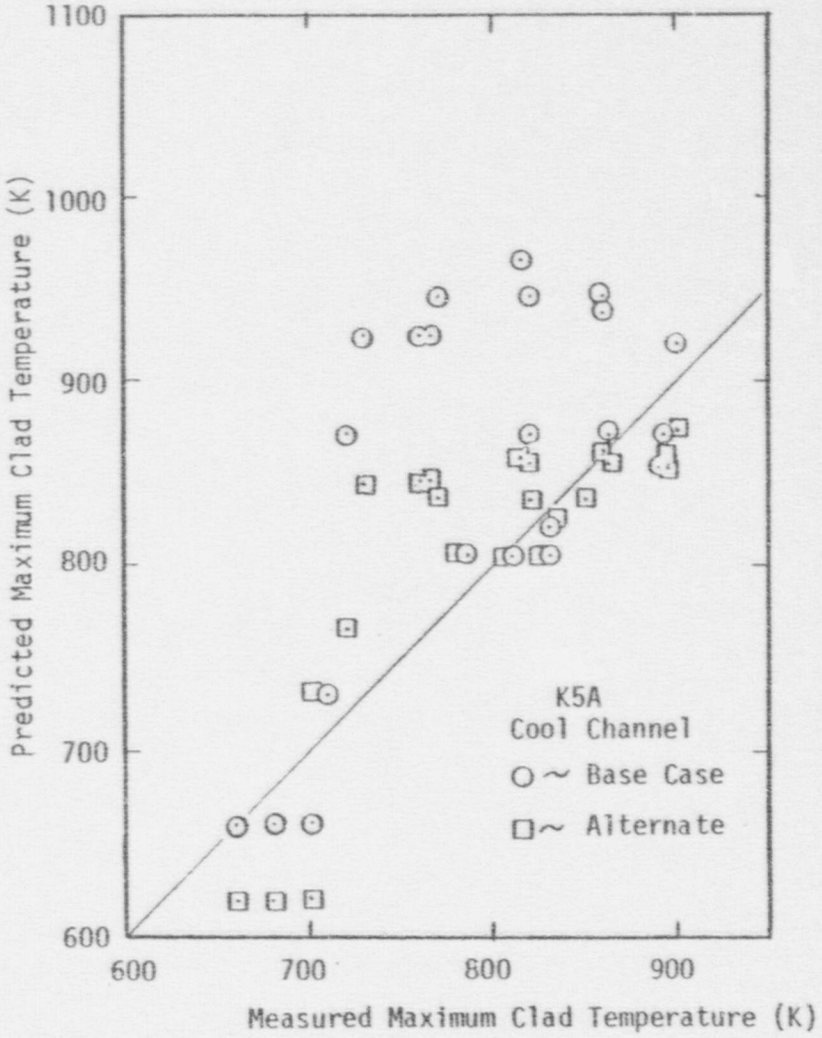

Fig. 18 Predicted vs. measured rod surface temperature, K5A cool channel.

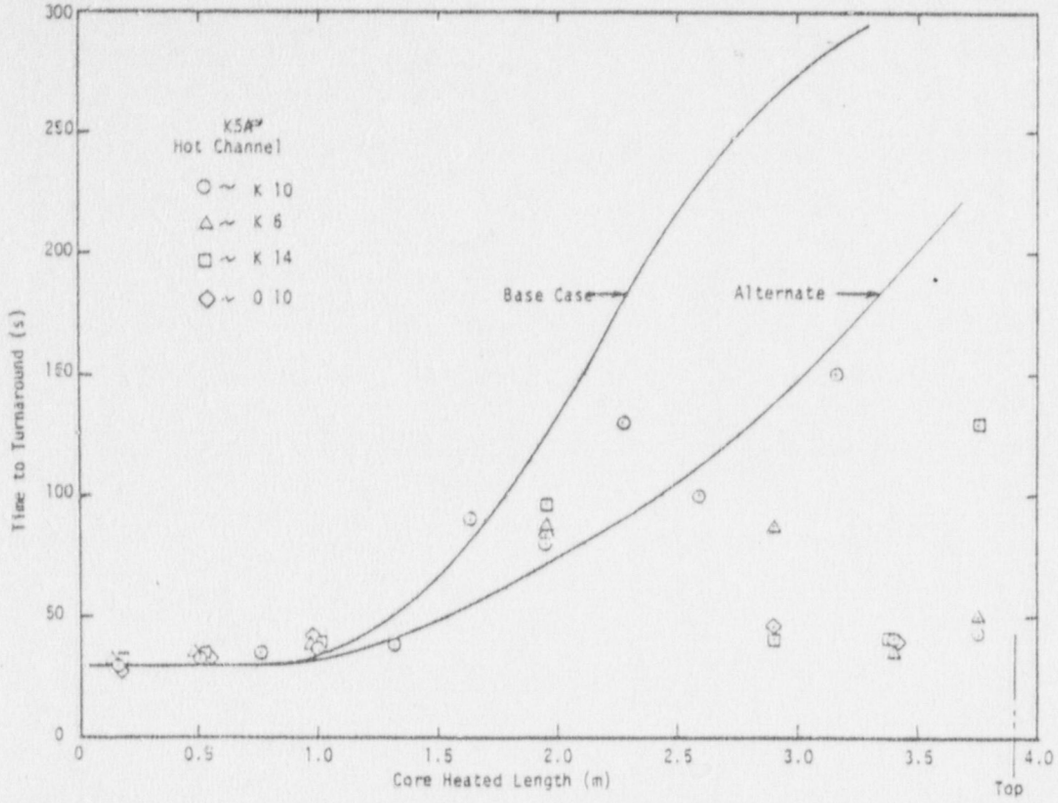

Fig. 19 Time to turnaround vs. core heated length, K5A hot channel.

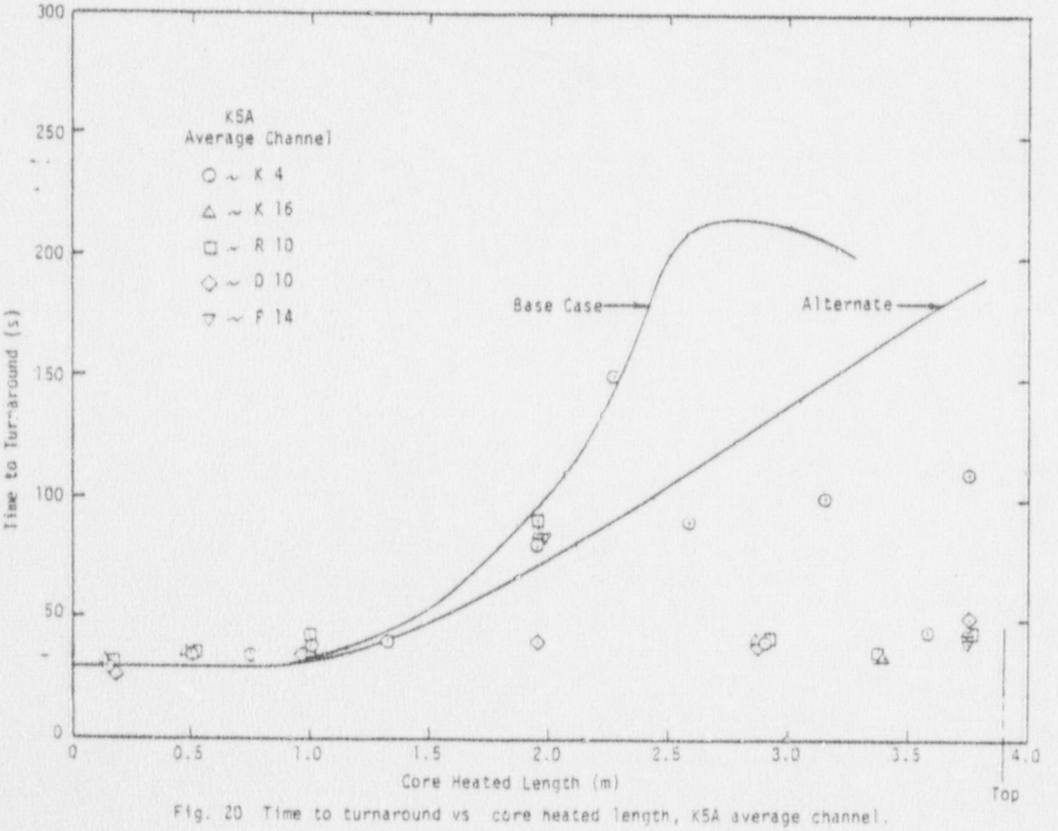

Fig. 20 Time to turnaround vs core heated length, K5A average channel.

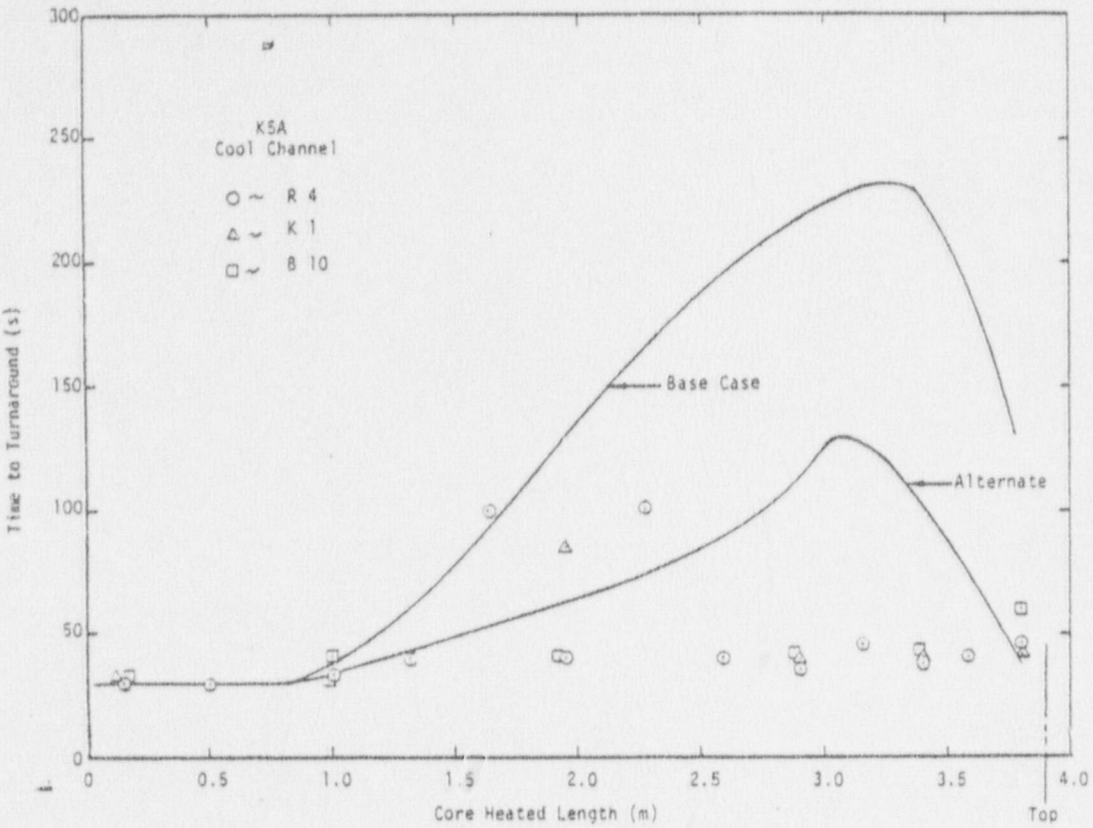

Fig. 21 Time to turnaround vs. core heated length, K5a cool channel.

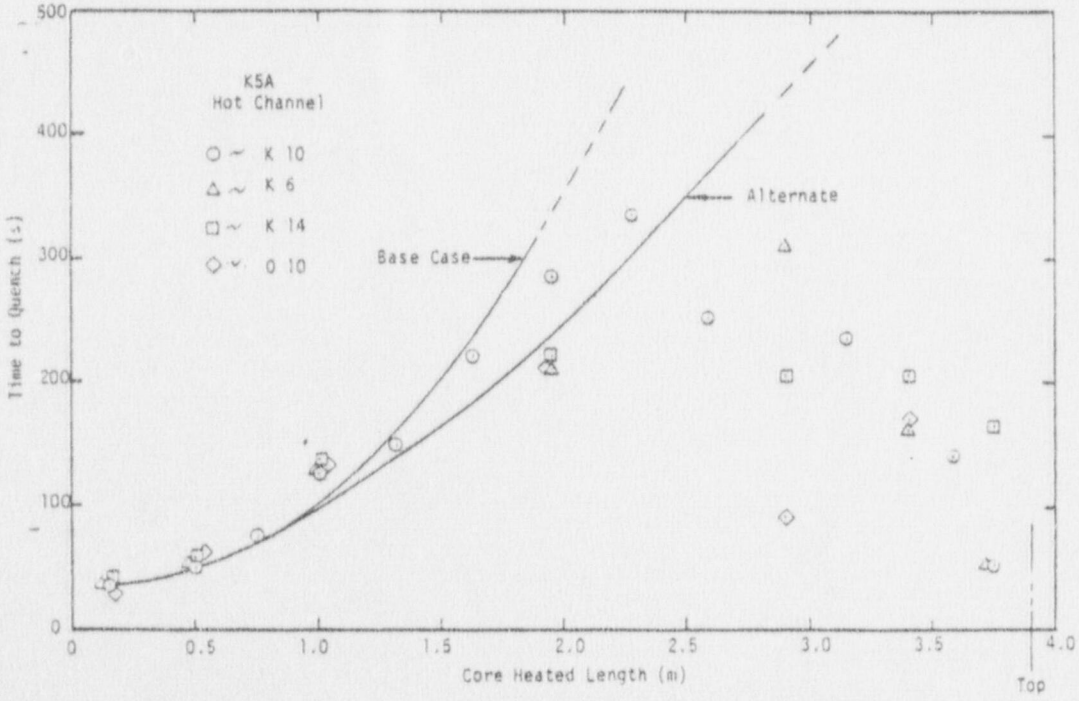

Fig. 22 Time to quench vs. core heated length, K5A hot channel.

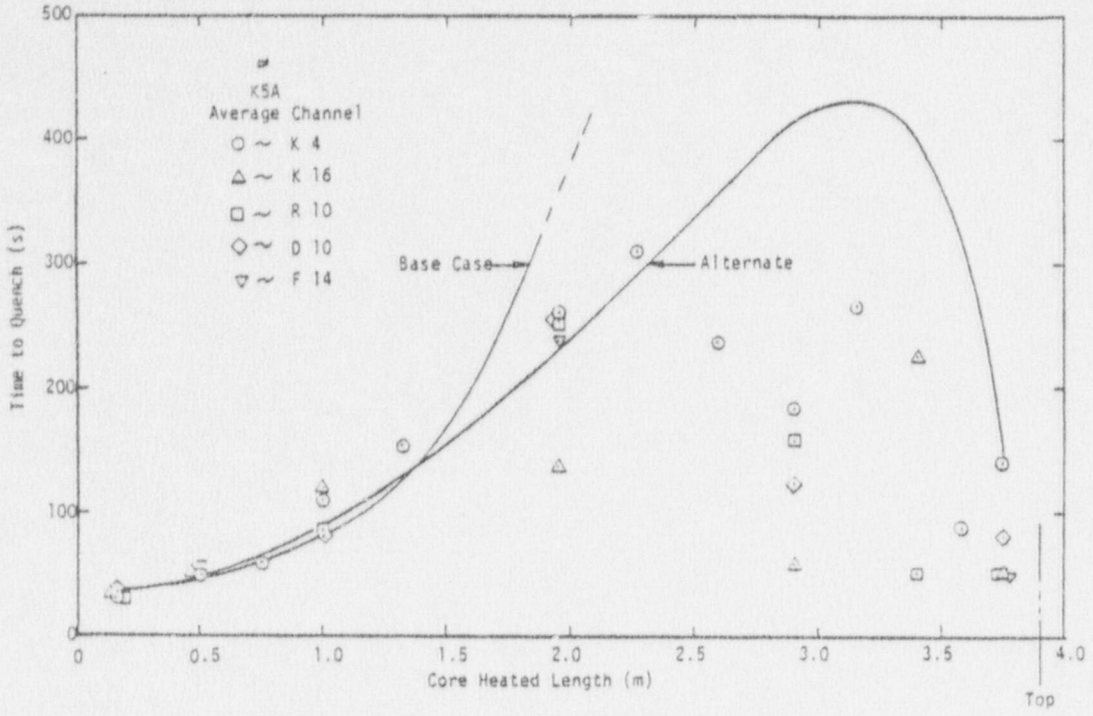

Fig. 23 Time to quench vs core heated length, K5A average channel.

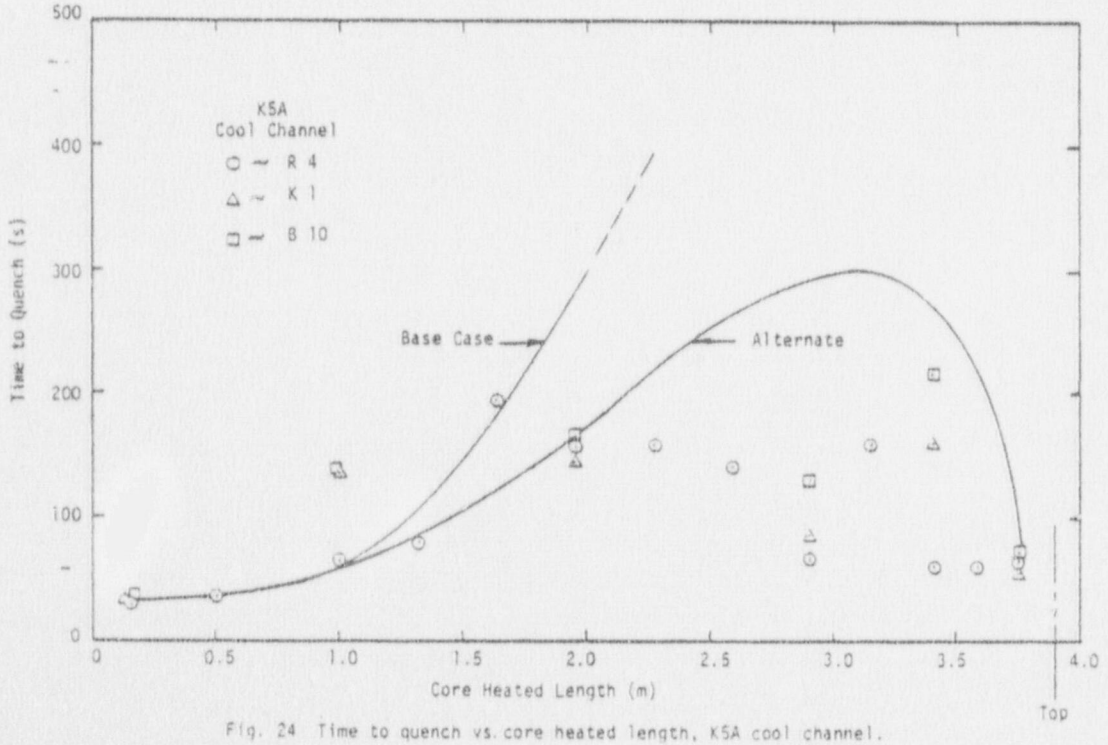

Fig. 24 Time to quench vs core heated length, K5A cool channel.

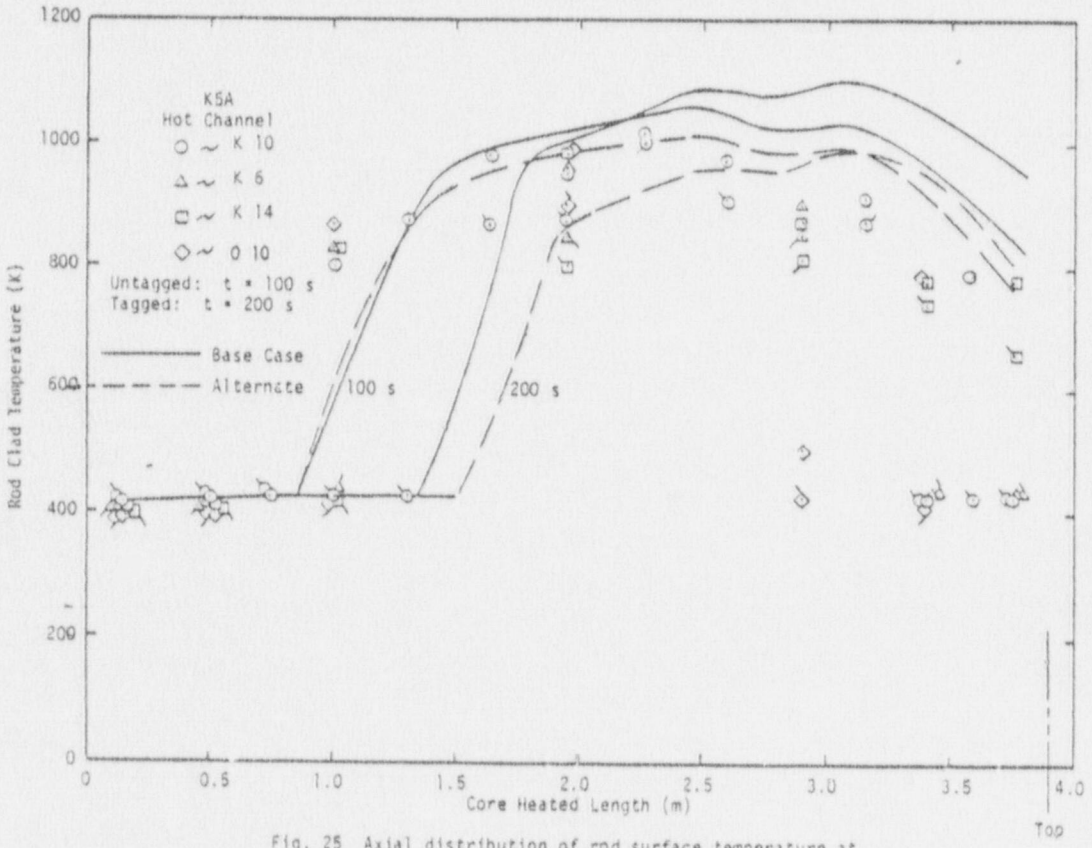

Fig. 25 Axial distribution of rod surface temperature at 100 s and 200 s, K5A hot channel.

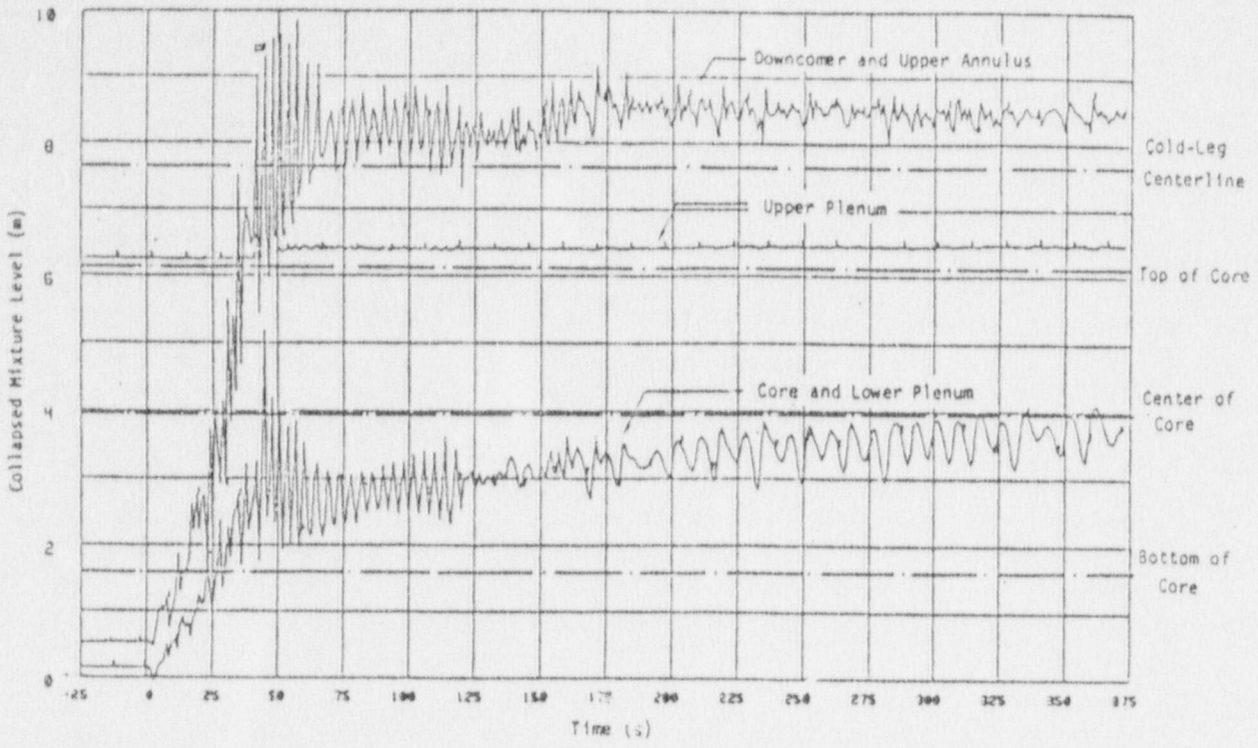

Fig. 26 Mixture level history in the vessel and downcomer for Test K5A.

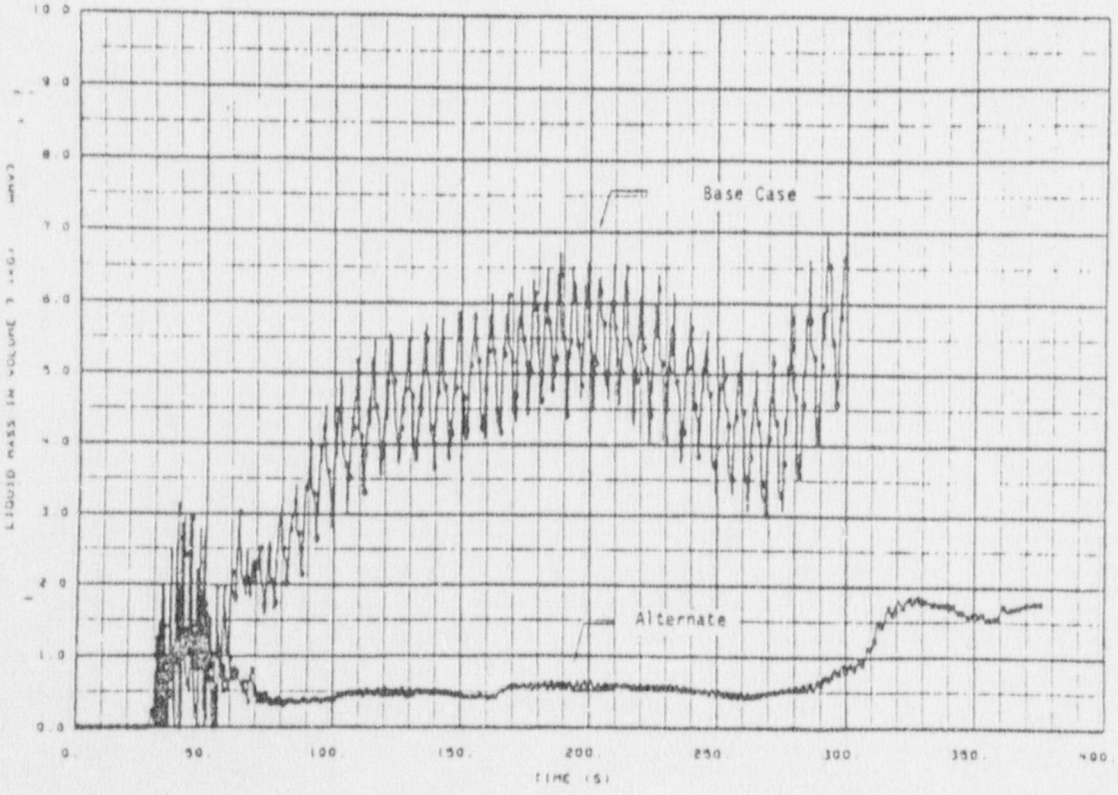

Fig. 27 Total mass in the upper plenum as calculated by RELAP4/MOD6 (3) for Test K5A.

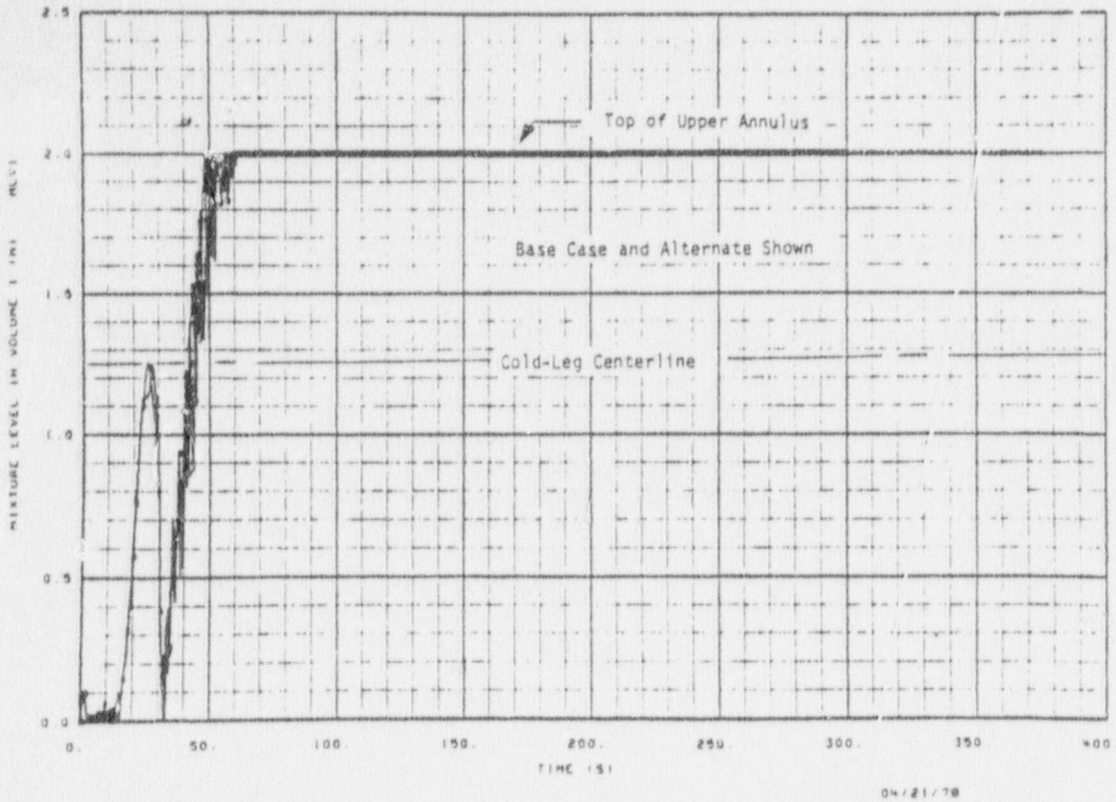

Fig. 28 Mixture level history in the upper annulus as calculated by RELAP4/MOD6 (3) for Test K5A.

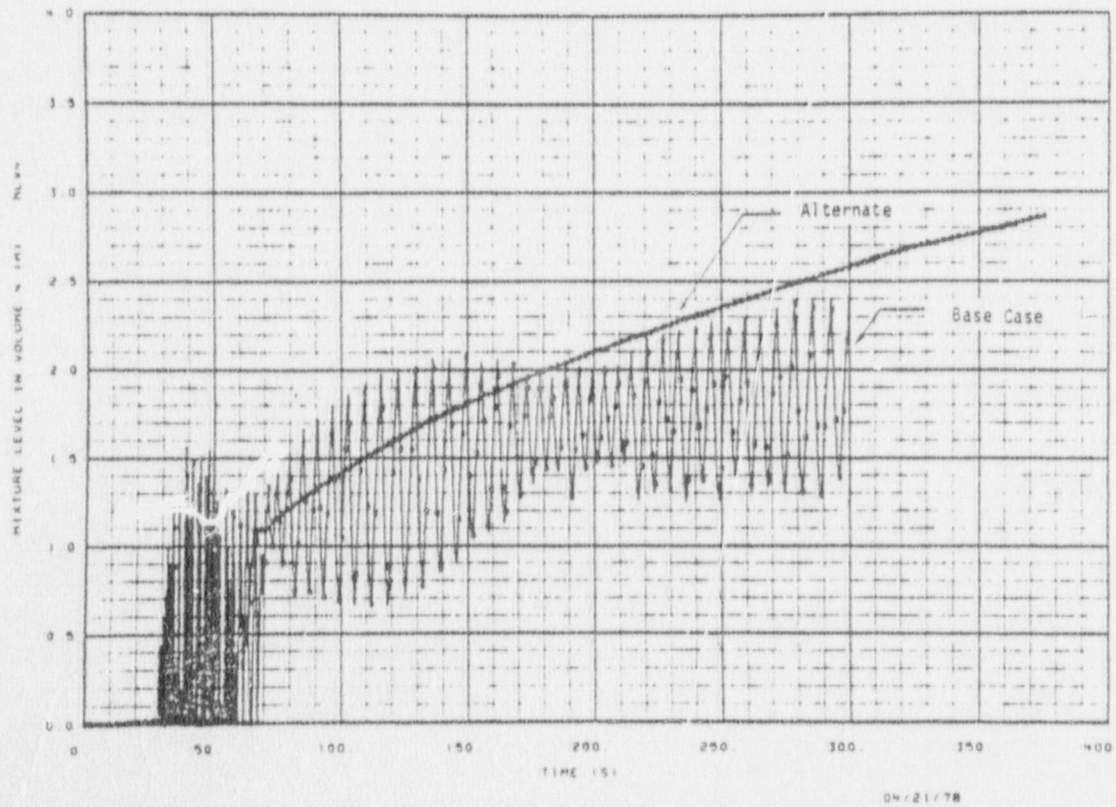

Fig. 29 Mixture level history in the core hot channel as calculated by RELAP4/MOD6 (3) for Test K5A.

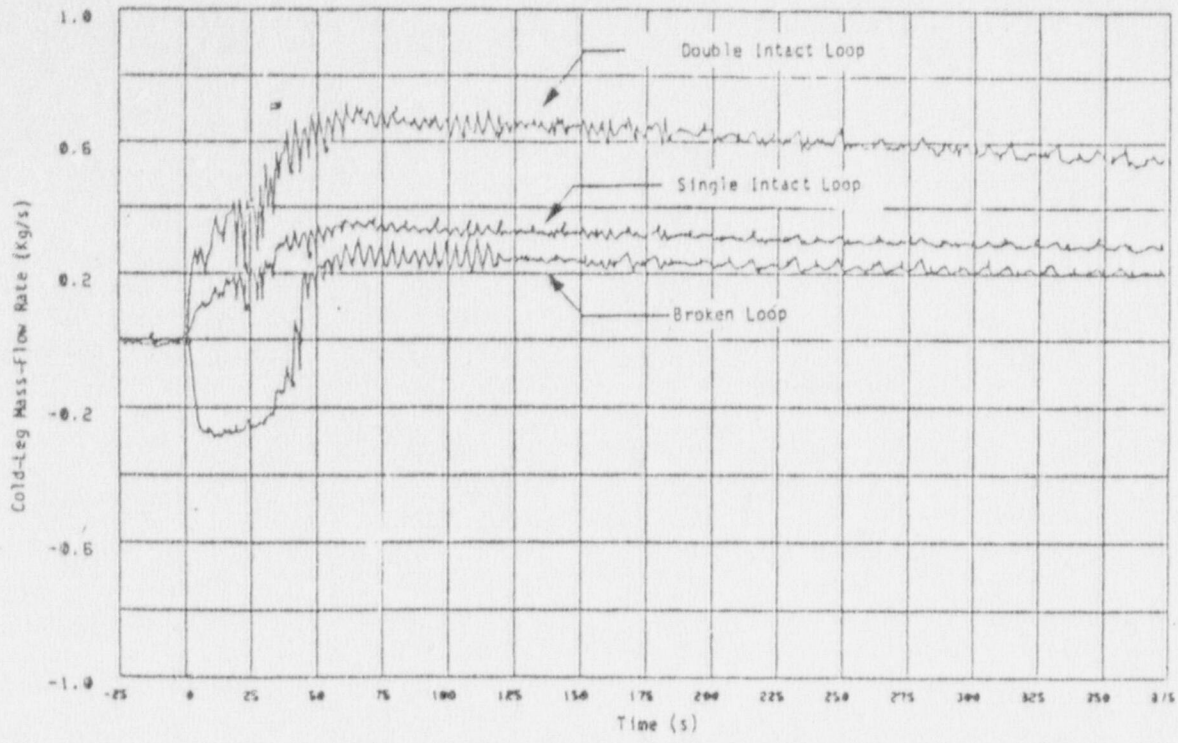

Fig. 30 Experimental cold-leg mass-flow-rate histories for Test K5A.

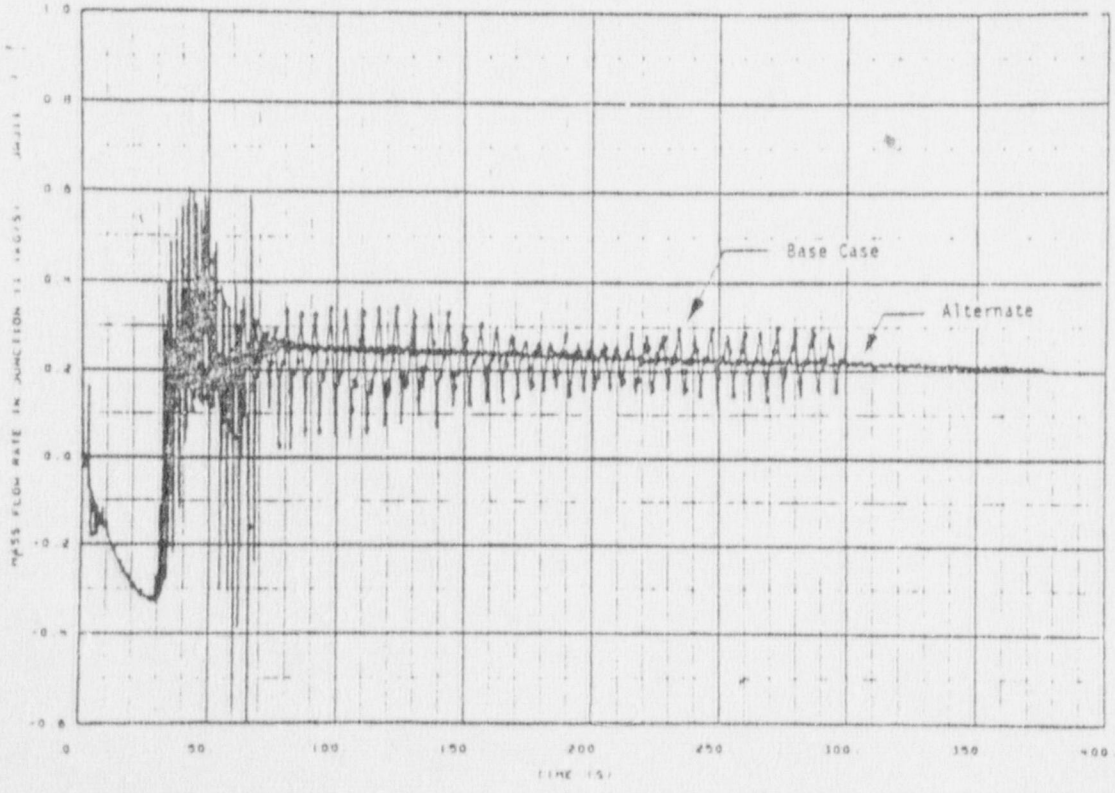

Fig. 31 Broken-loop cold-leg mass-flow-rate history as calculated by RELAP4/MOD6 (3) for Test K5A.

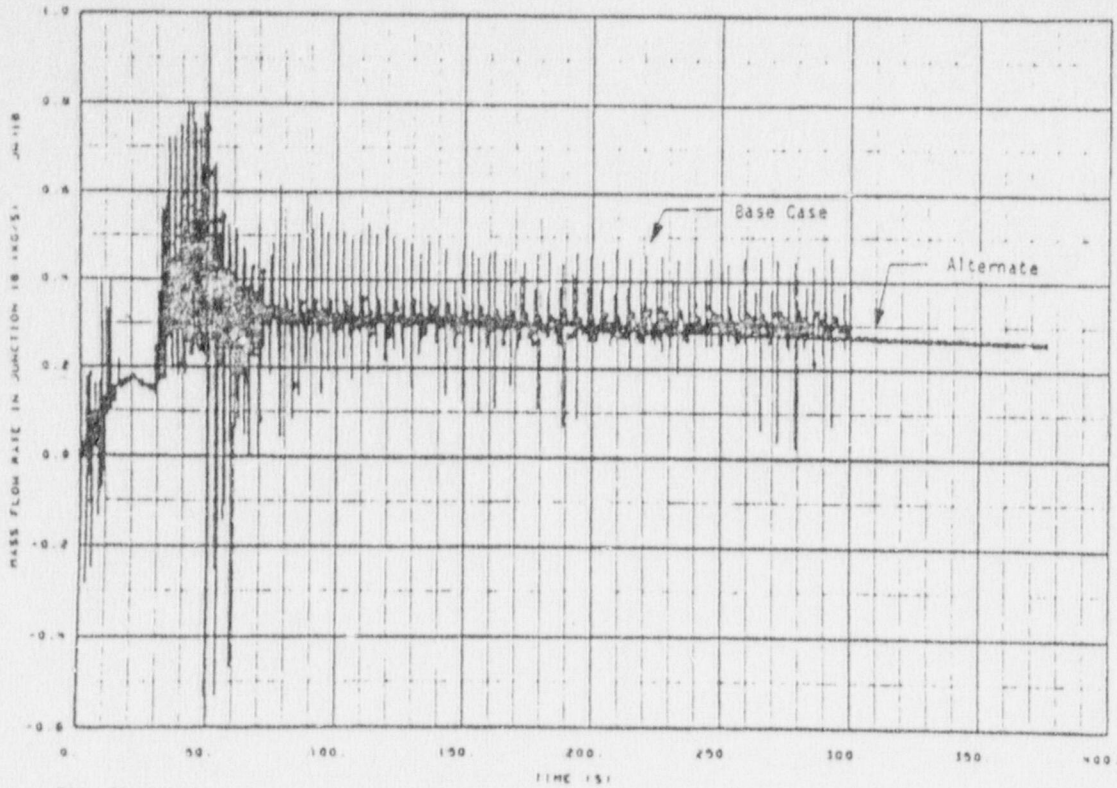

Fig. 32 Single-intact-loop cold-leg mass-flow-rate history as calculated by RELAP4/MOD6 (3) for Test K5A.

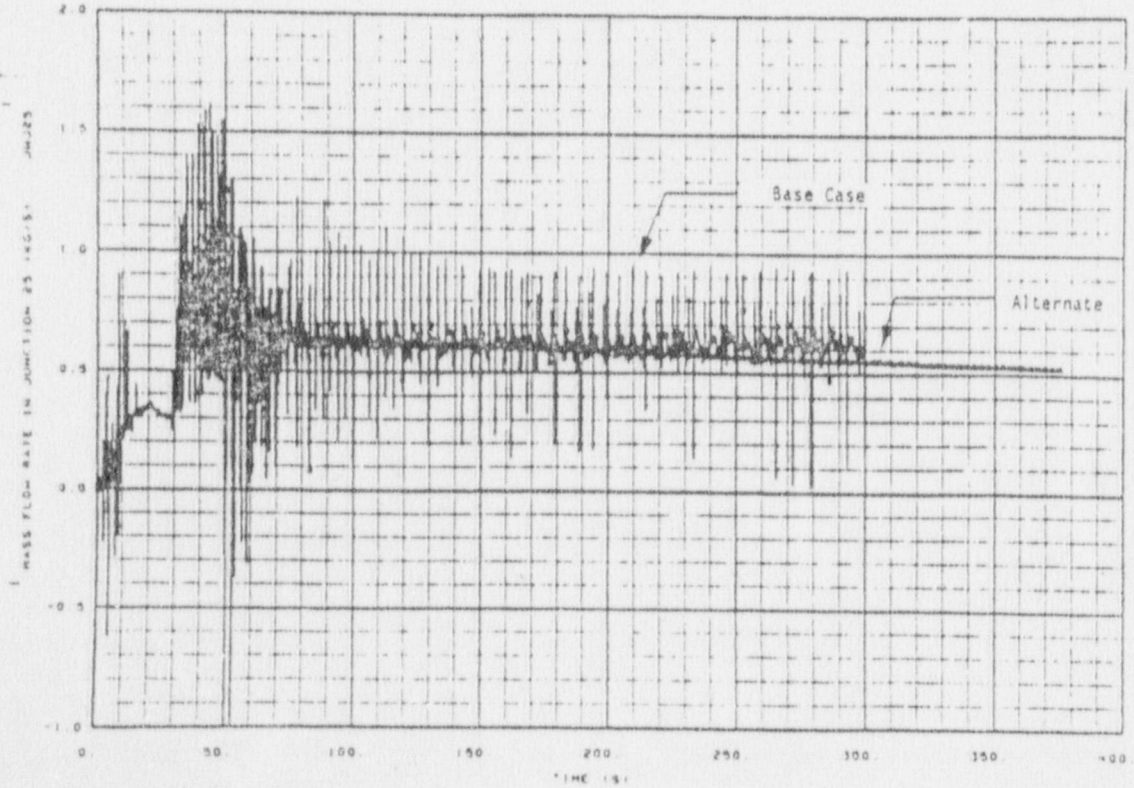

Fig. 33 Double-intact-loop cold-leg mass-flow-rate history as calculated by RELAP4/MOD6 (3) for Test K5A.

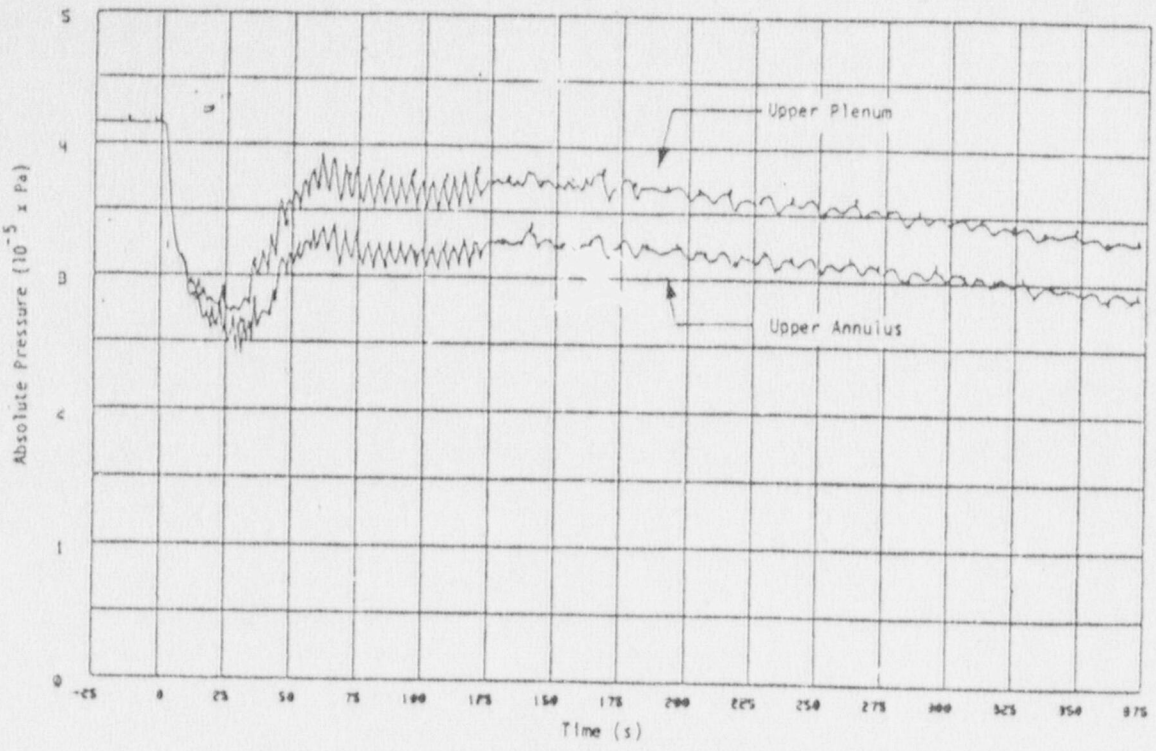

Fig. 34 Upper plenum and upper annulus experimental absolute pressure history for Test K5A.

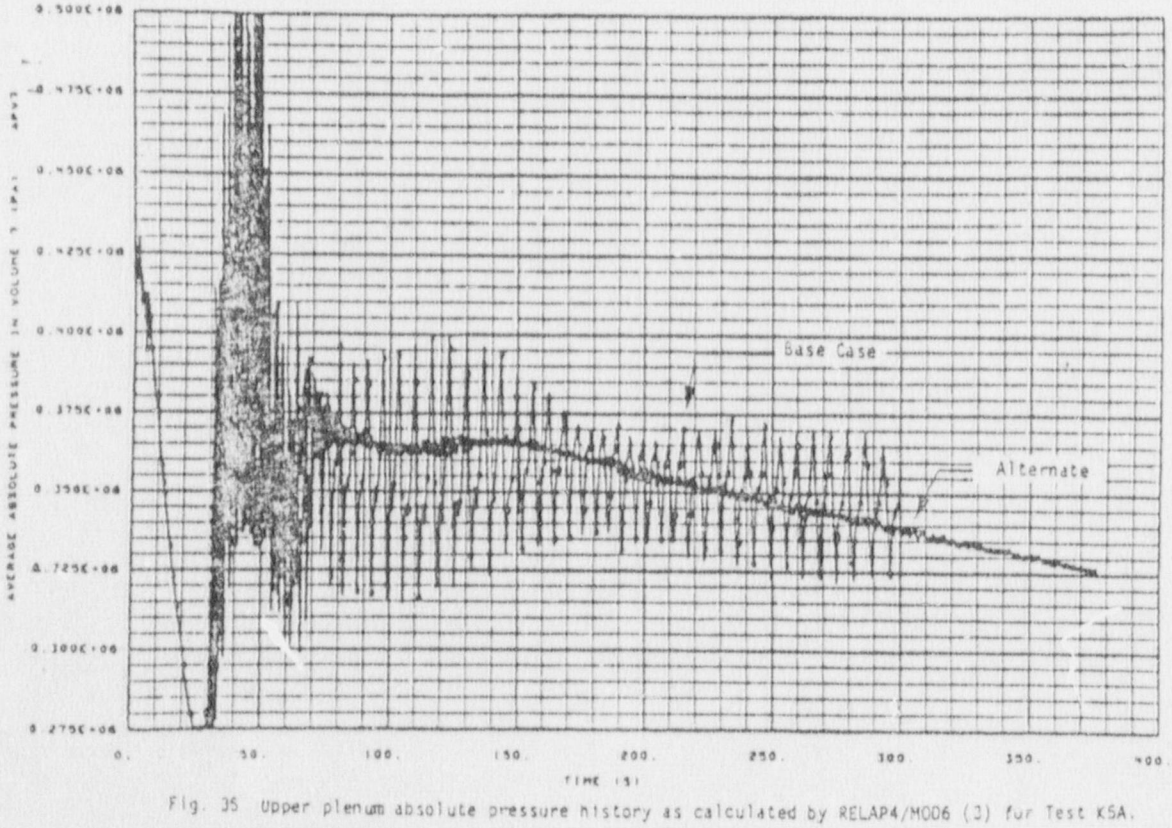

Fig. 35 Upper plenum absolute pressure history as calculated by RELAP4/MOD6 (3) for Test K5A.

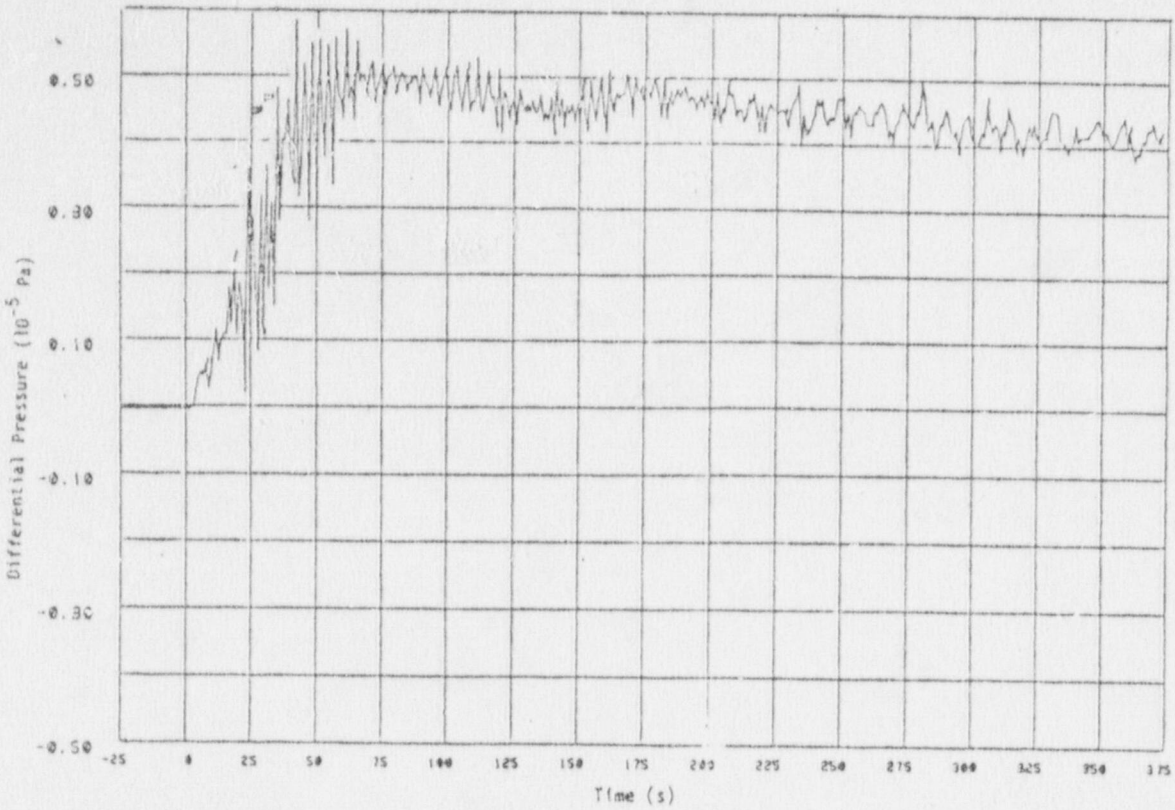

Fig. 36 Experimental differential pressure between upper plenum and upper annulus, Test KSA.

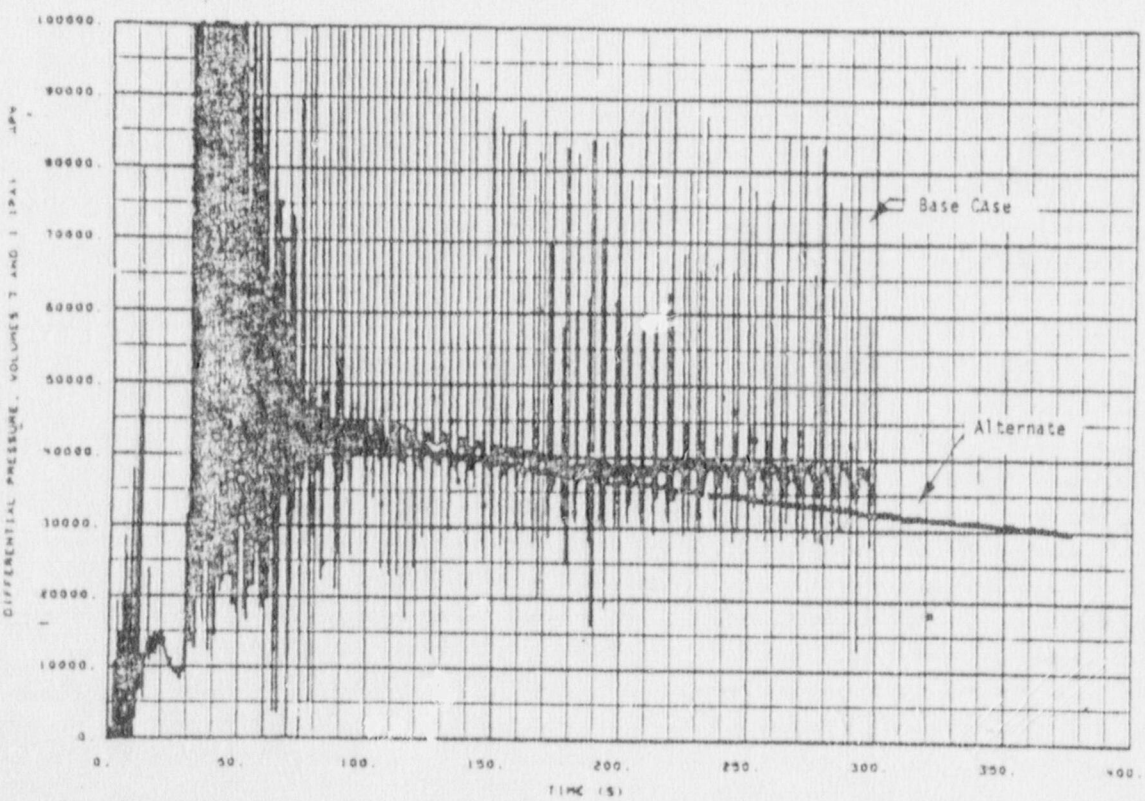

Fig. 37 Differential pressure between upper plenum and upper annulus as calculated by RELAP4/MOD6 (J) for Test KSA.

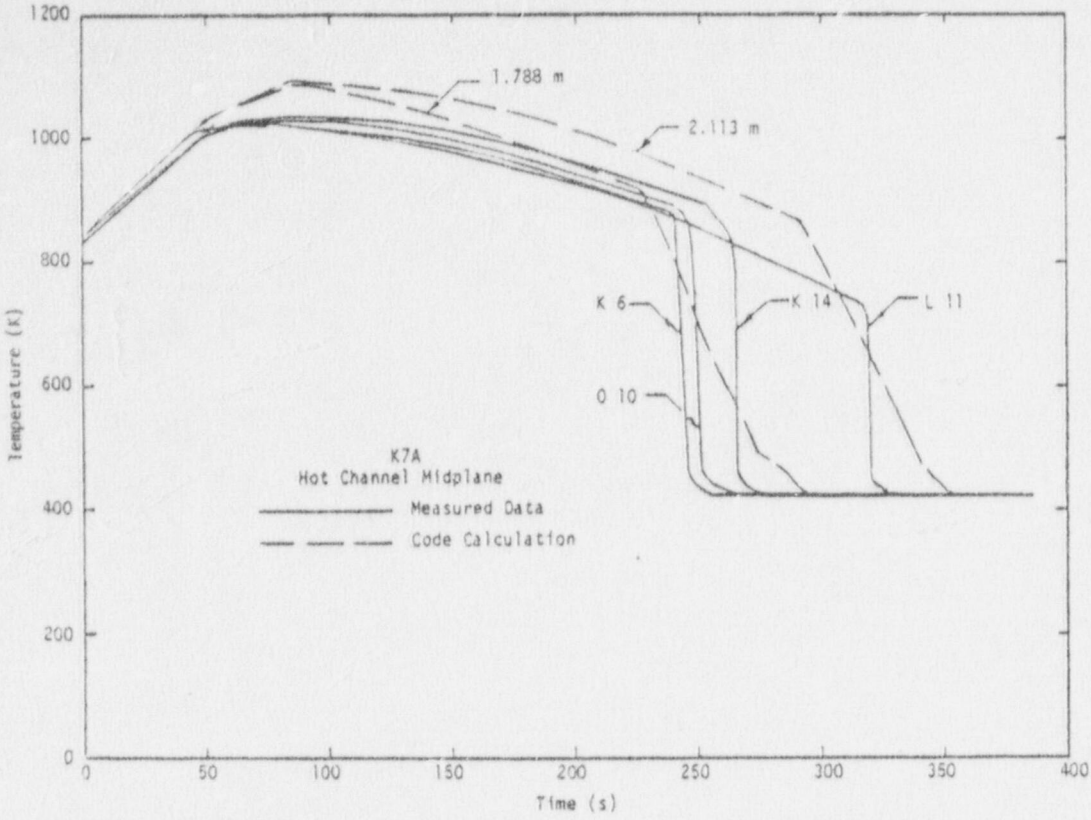

Fig. 38 Comparison of cladding temperature history at the midplane, Test K7A.

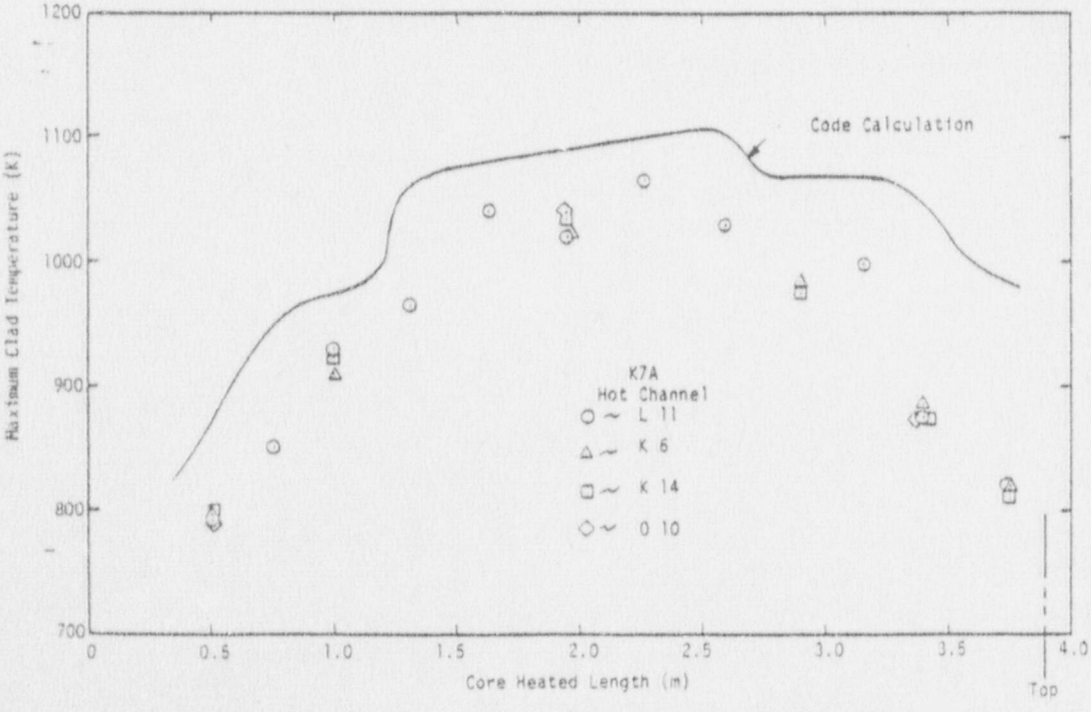

Fig. 39 Maximum rod surface temperature distribution over the core heated l
K7A hot channel.

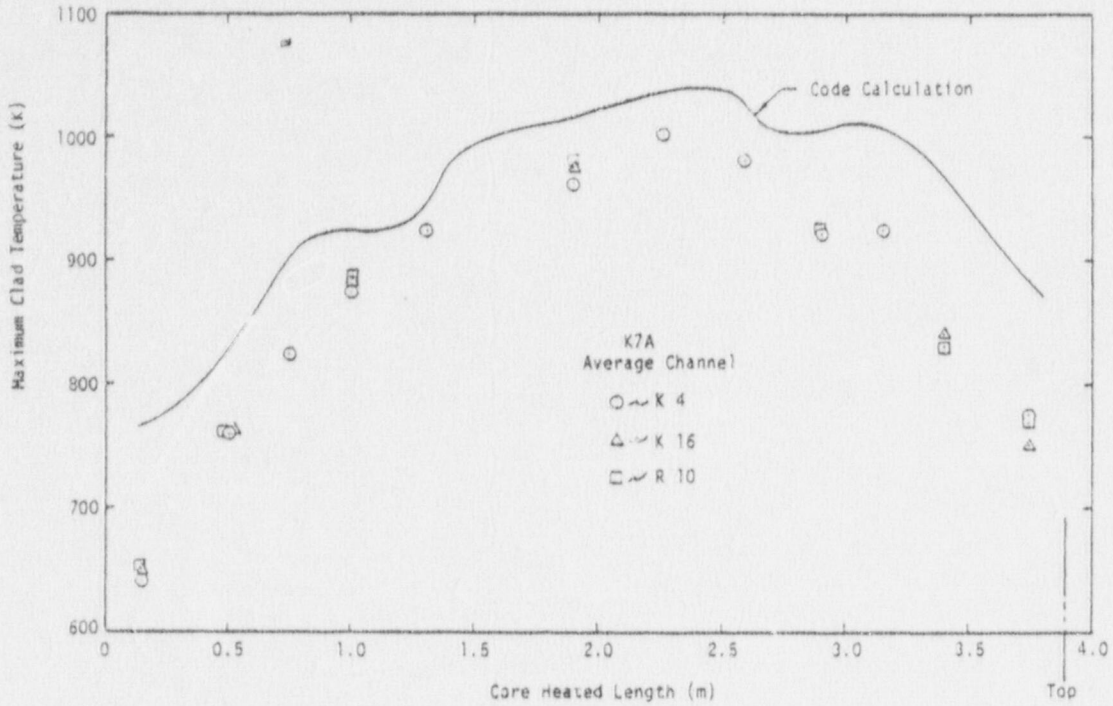

Fig. 40 Maximum rod surface temperature distribution over the core heated length, K7A average channel.

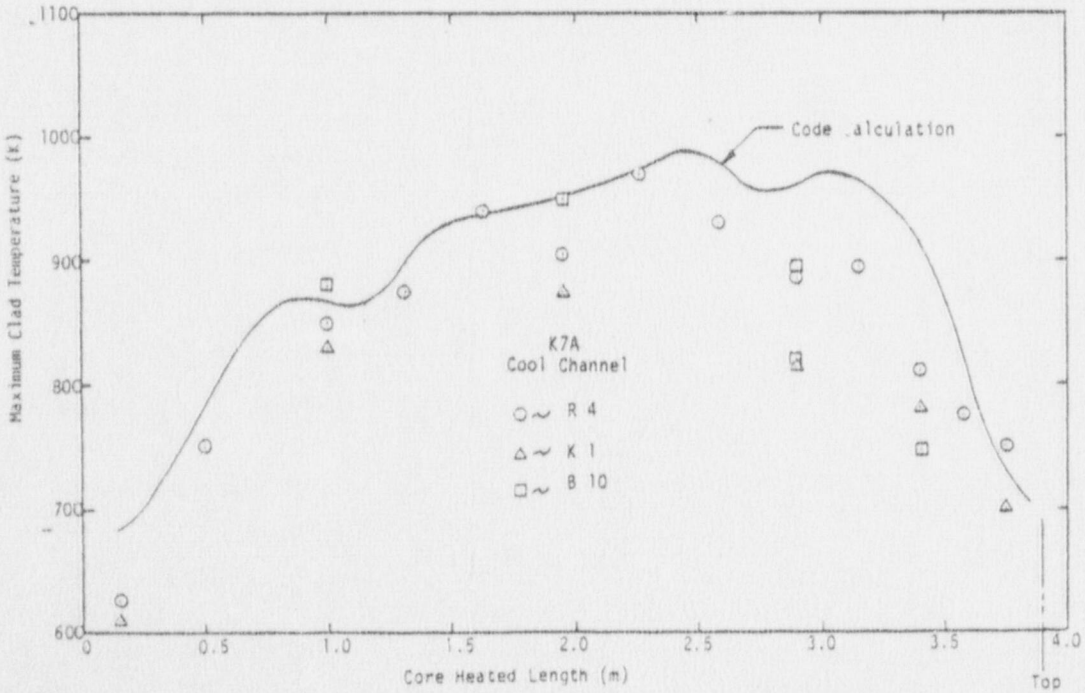

Fig. 41 Maximum rod surface temperature distribution over the core heated length, K7A cool channel.

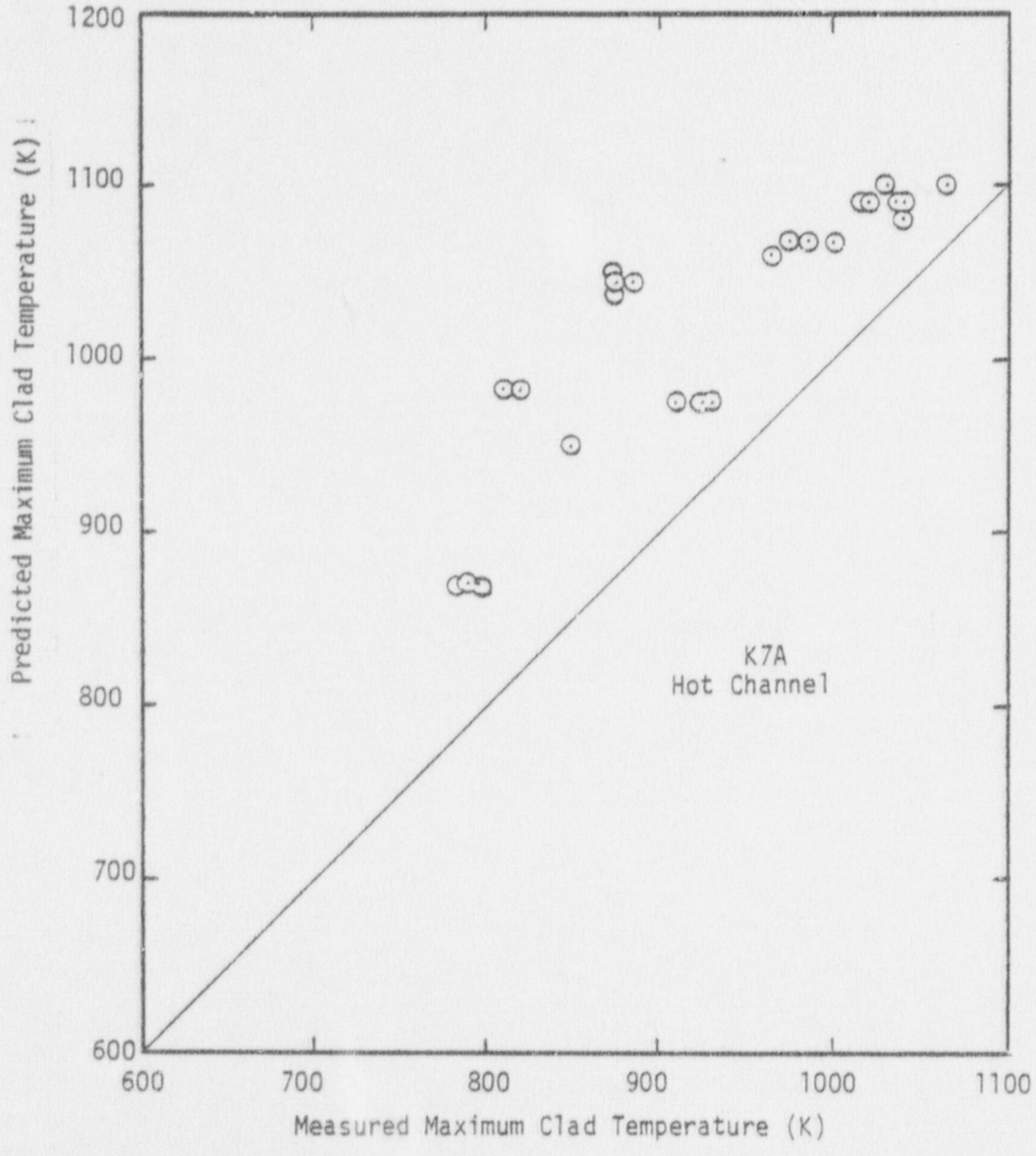

Fig. 42 Predicted vs. measured rod surface temperature, K7A hot channel.

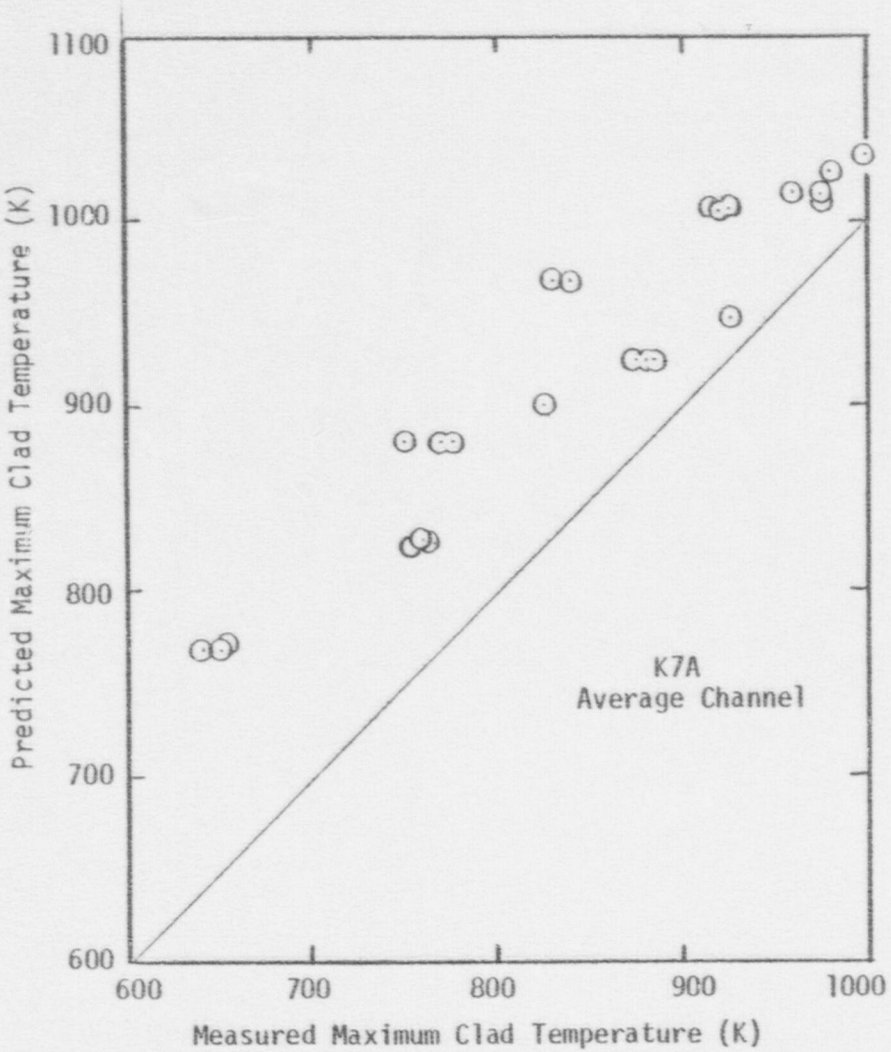

Fig. 43 Predicted vs. measured rod surface temperature, K7A average channel.

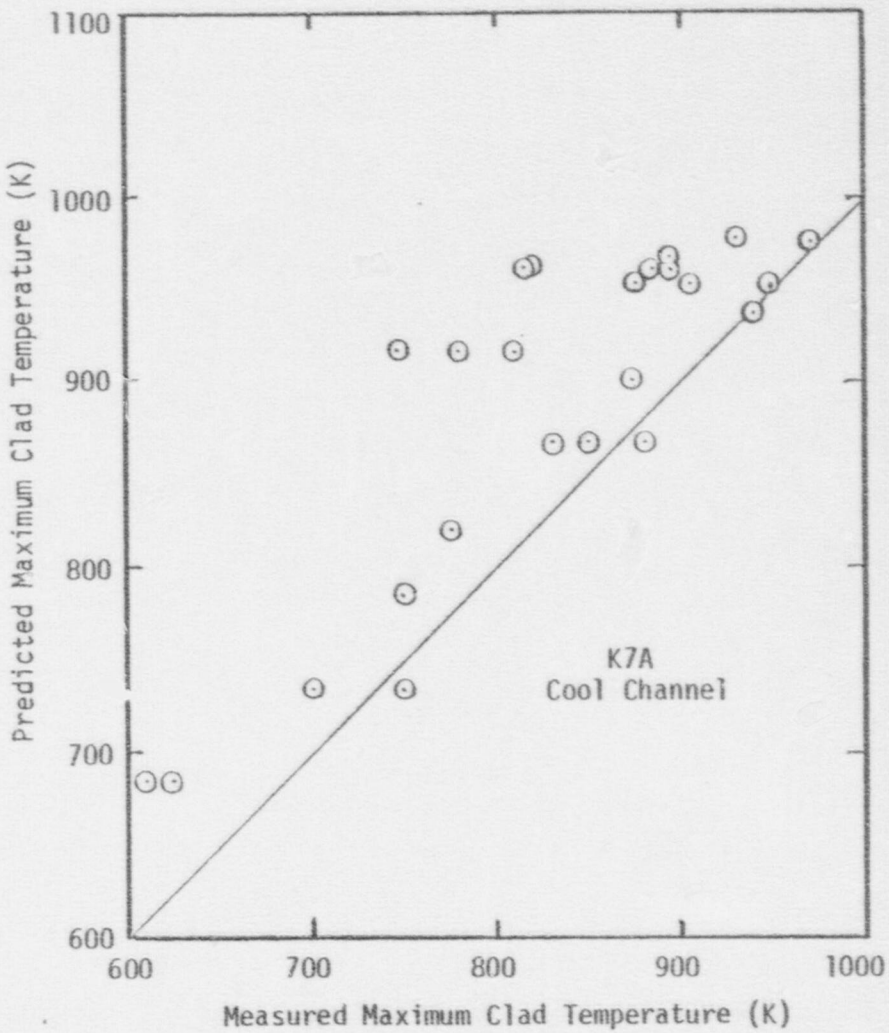

Fig. 44 Predicted vs. measured rod surface temperature, K7A cool channel.

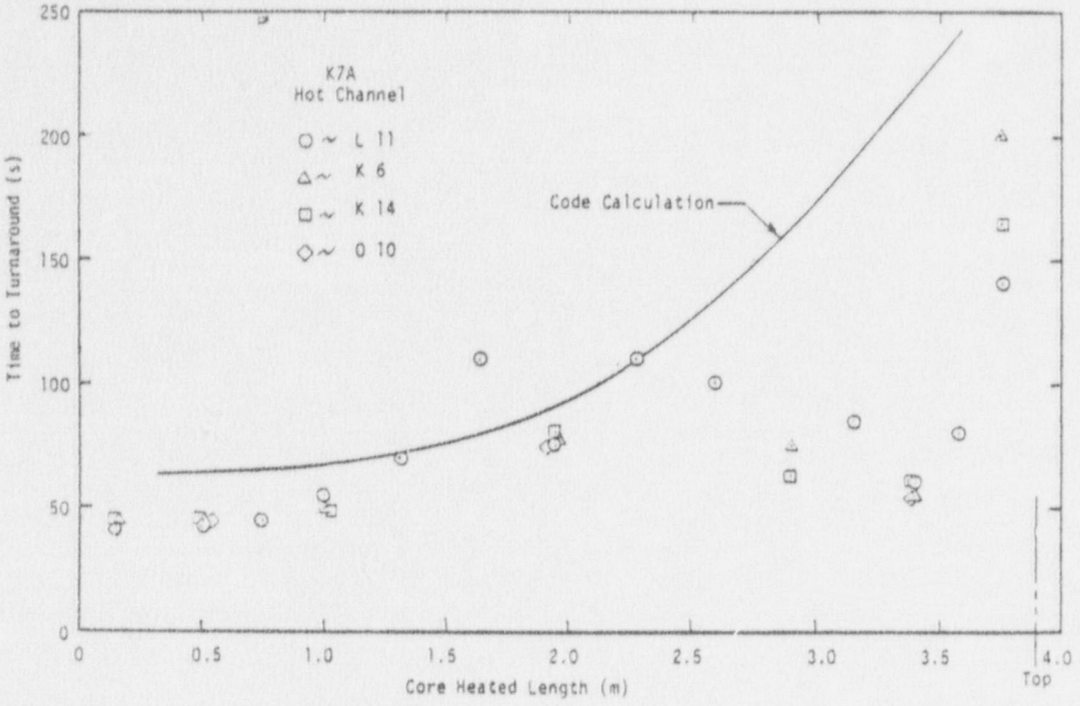

Fig. 45 Time to turnaround vs. core heated length, K7A hot channel.

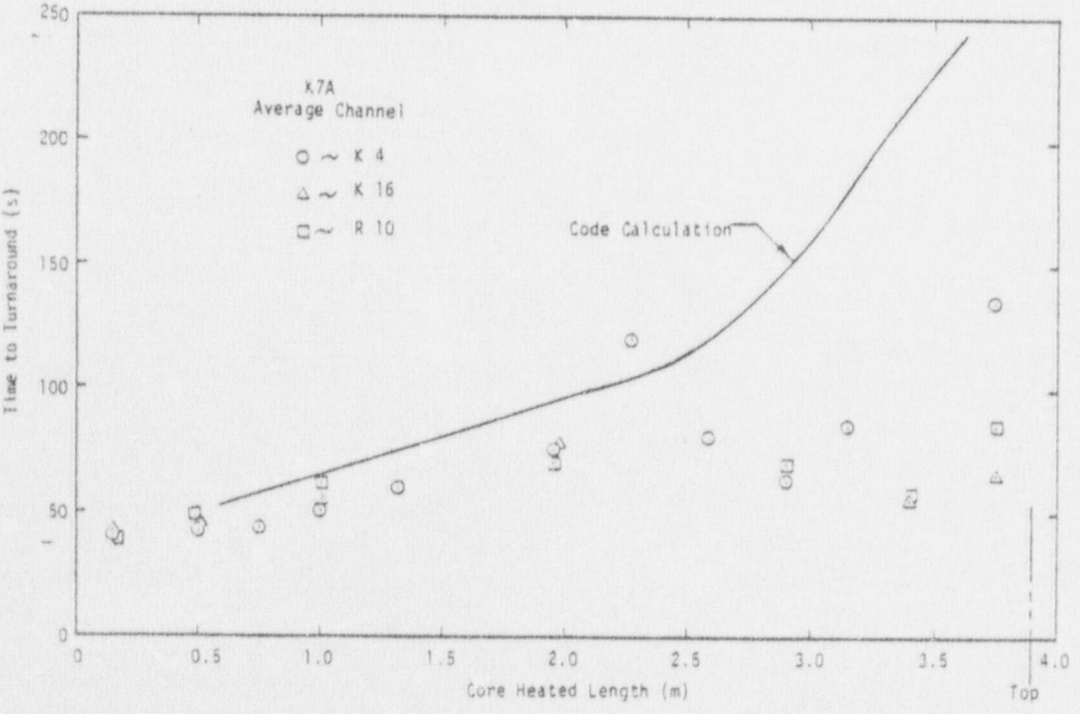

Fig. 46 Time to turnaround vs. core heated length, K7A average channel.

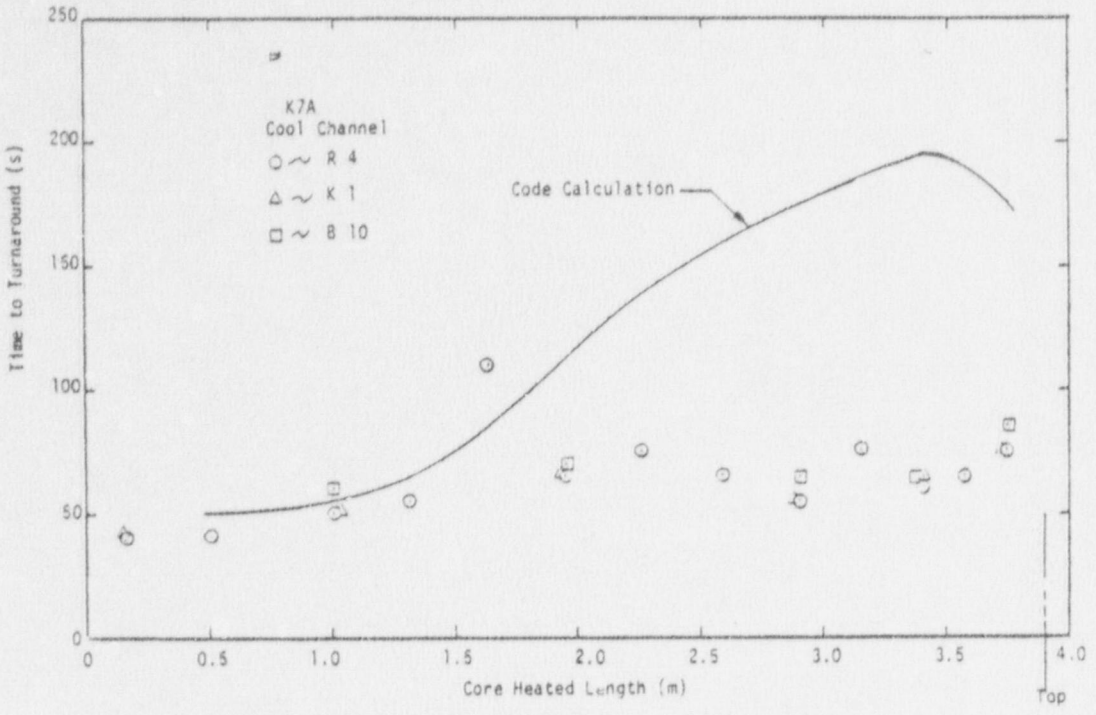

Fig. 47 Time to turnaround vs core heated length, K7A cool channel.

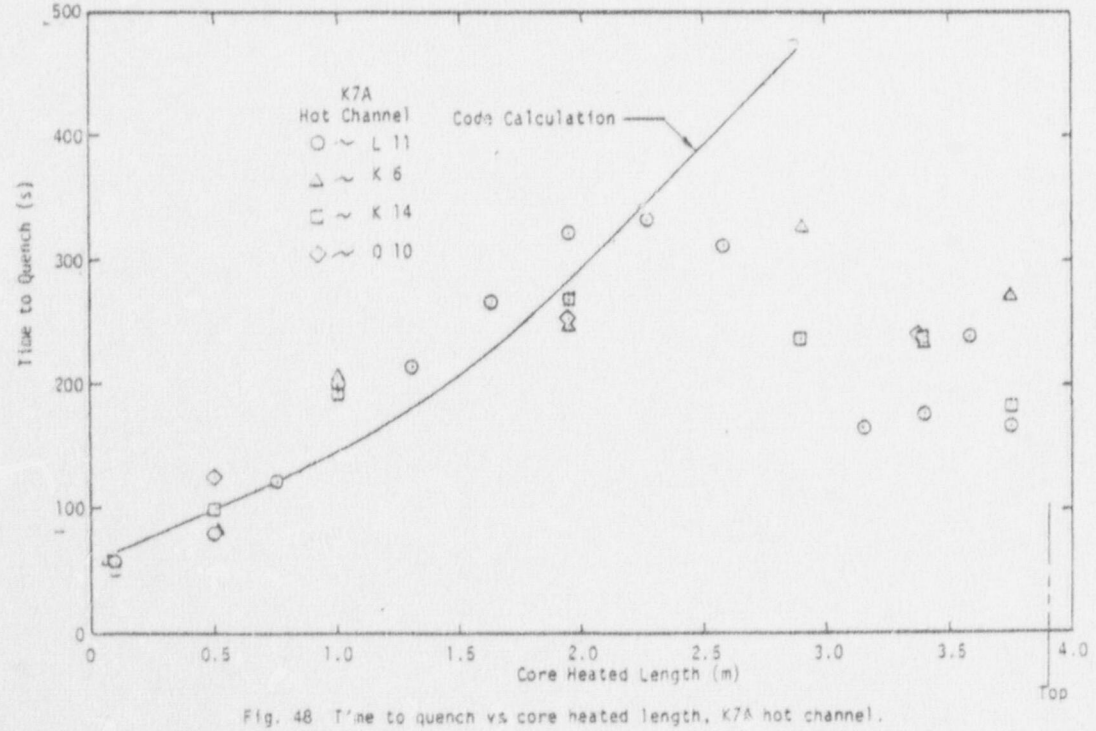

Fig. 48 Time to quench vs core heated length, K7A hot channel.

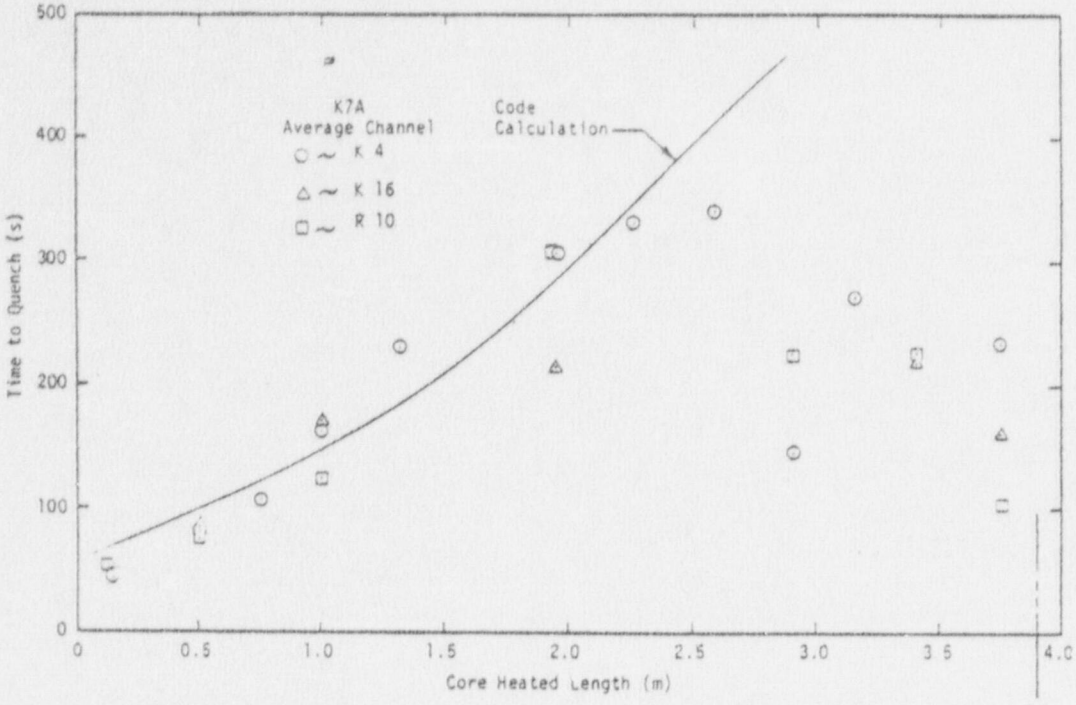

Fig. 49 Time to quench vs core heated length, K7A average channel.

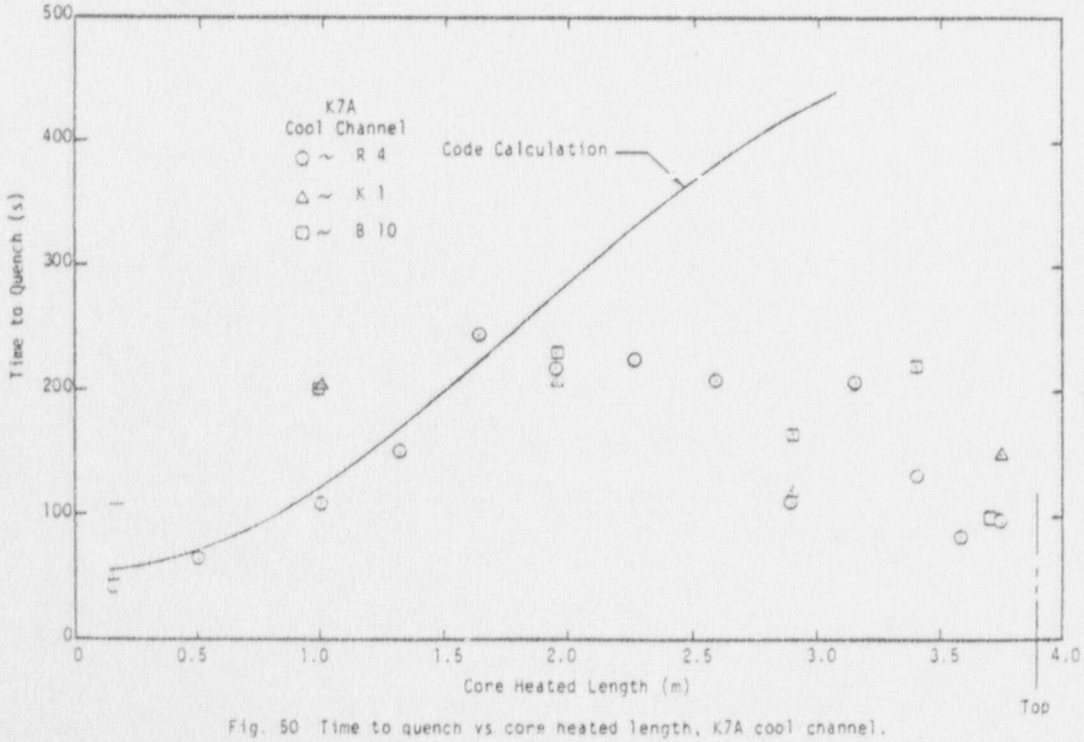

Fig. 50 Time to quench vs core heated length, K7A cool channel.

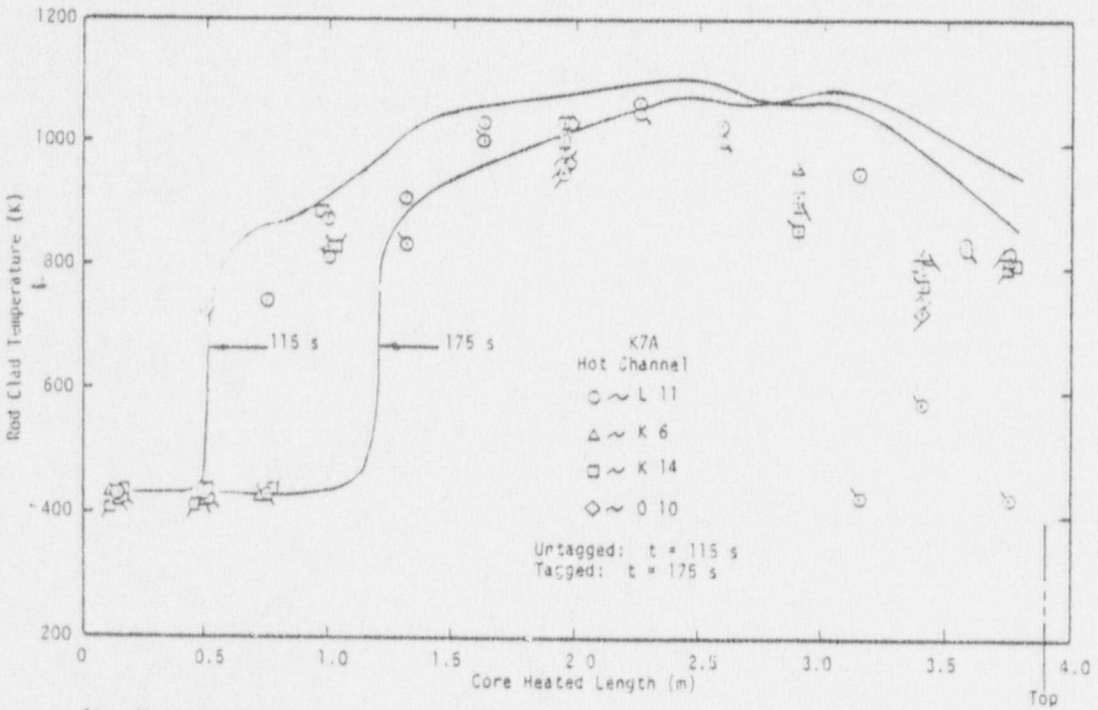

Fig. 51 Axial distribution of rod surface temperature at 115 s and 175 s, K7A hot channel.

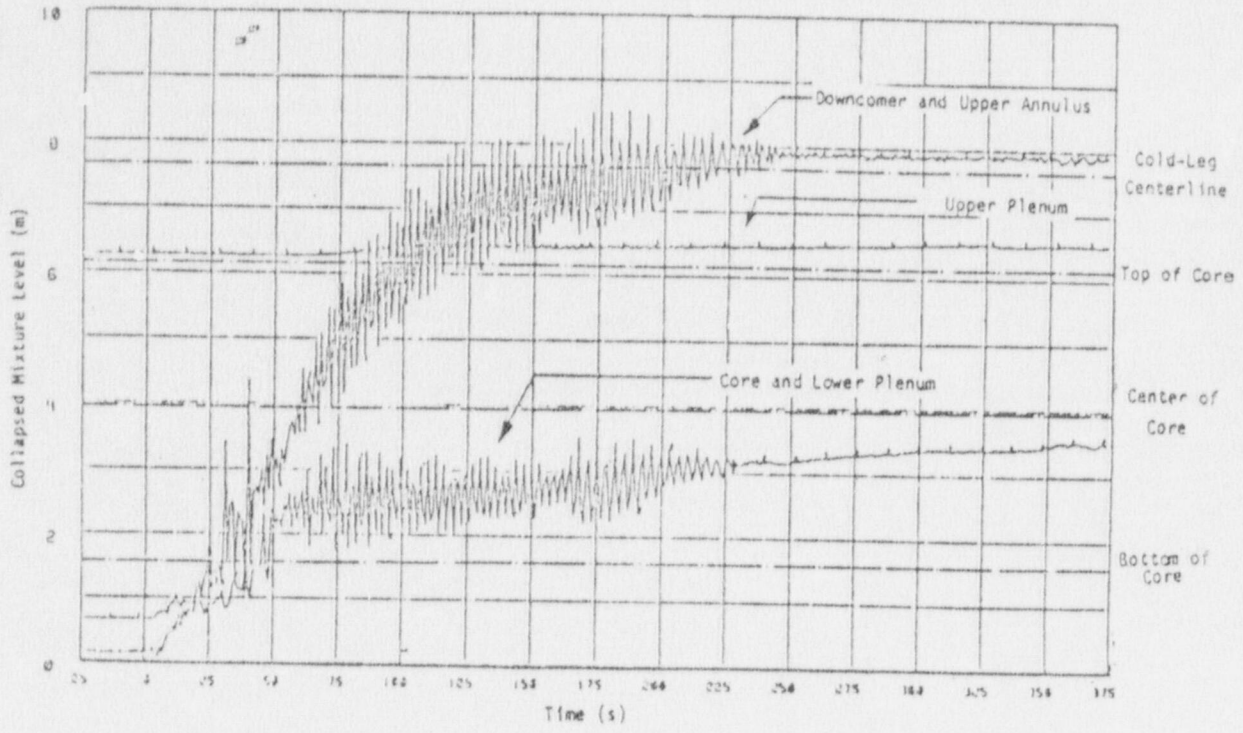

Fig. 52 Mixture level history in the vessel and downcomer for Test K7A.

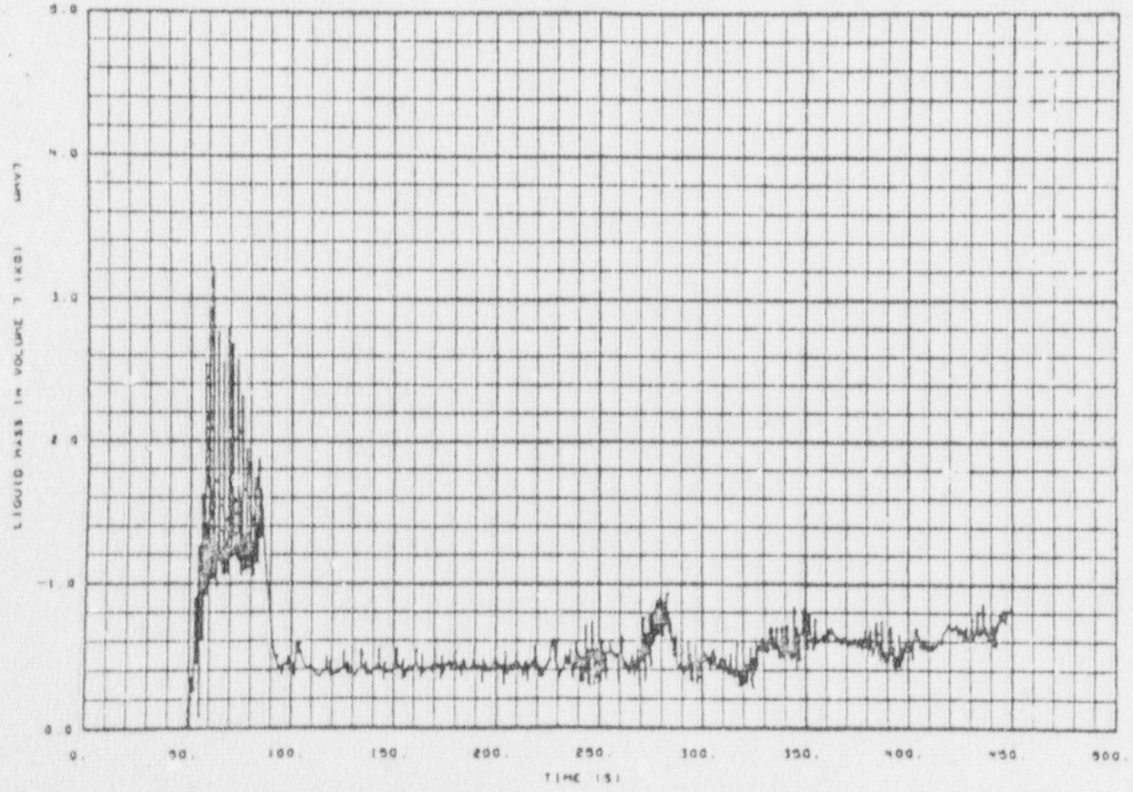

Fig. 53 Total mass in the upper plenum as calculated by RELAP4/MOD6 (3) for Test K7A.

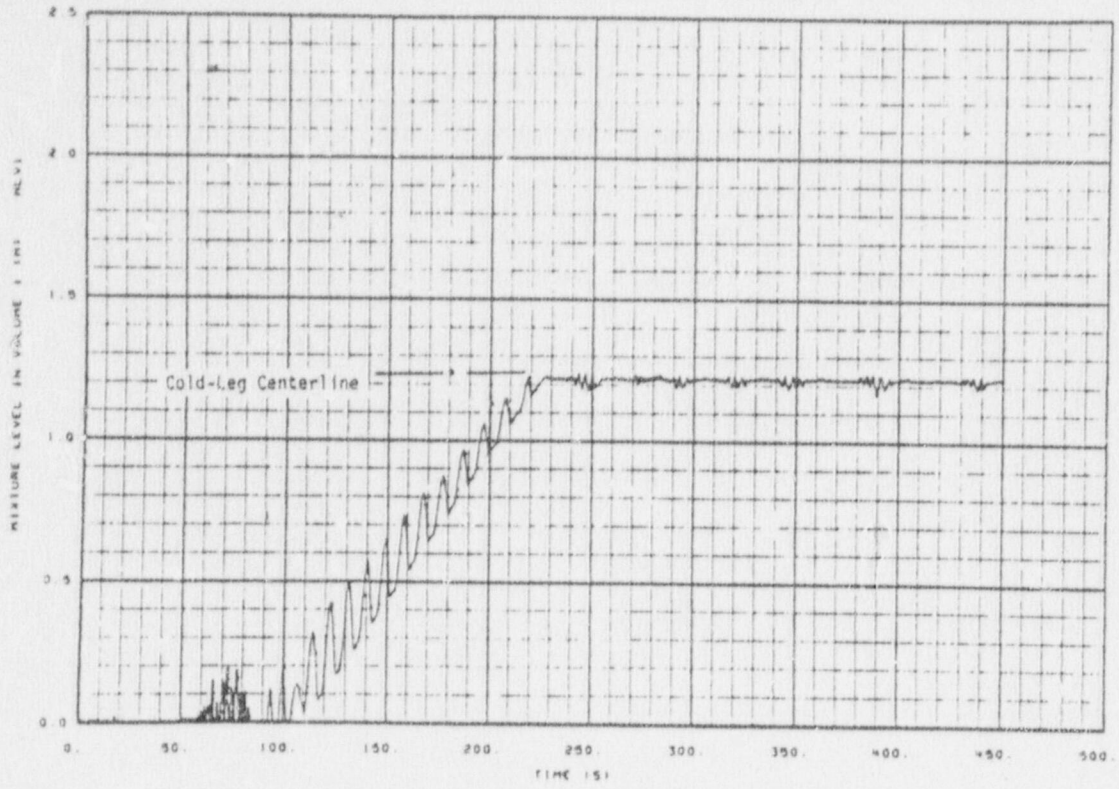

Fig. 54 Mixture level history in the upper annulus as calculated by RELAP4/MOD6 (3) for Test K7A.

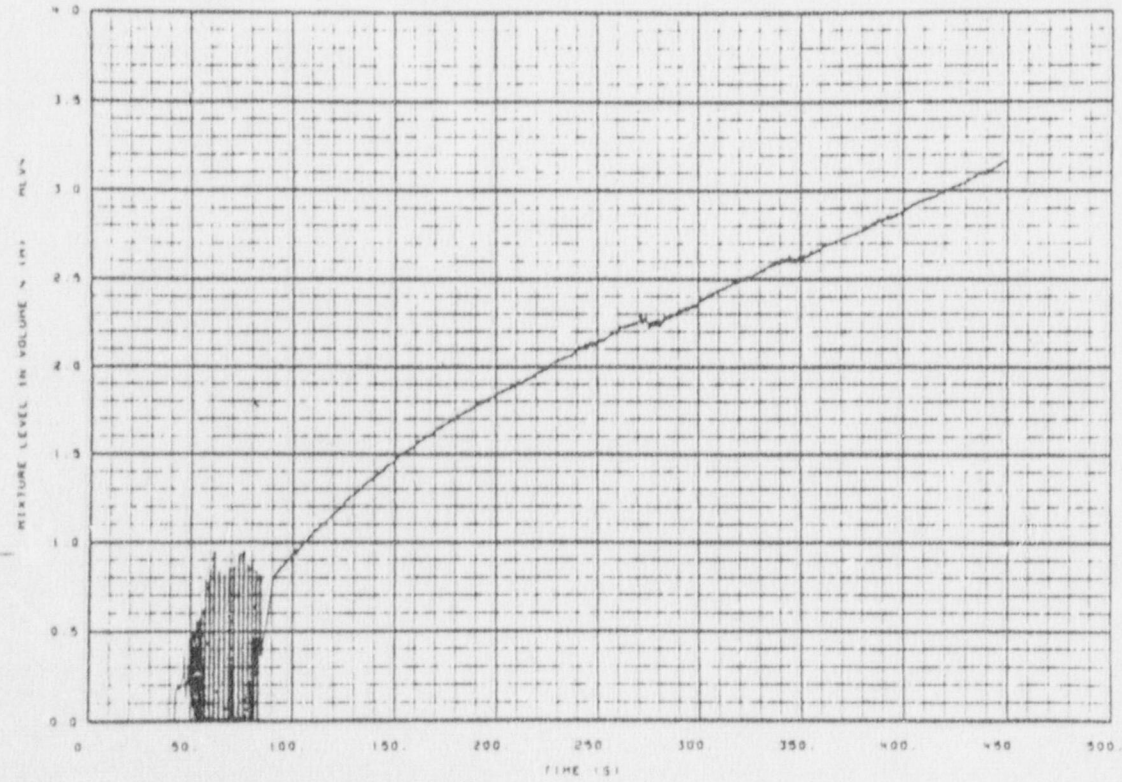

Fig. 55 Mixture level history in the core hot channel as calculated by RELAP4/MOD6 (3) for Test K7A.

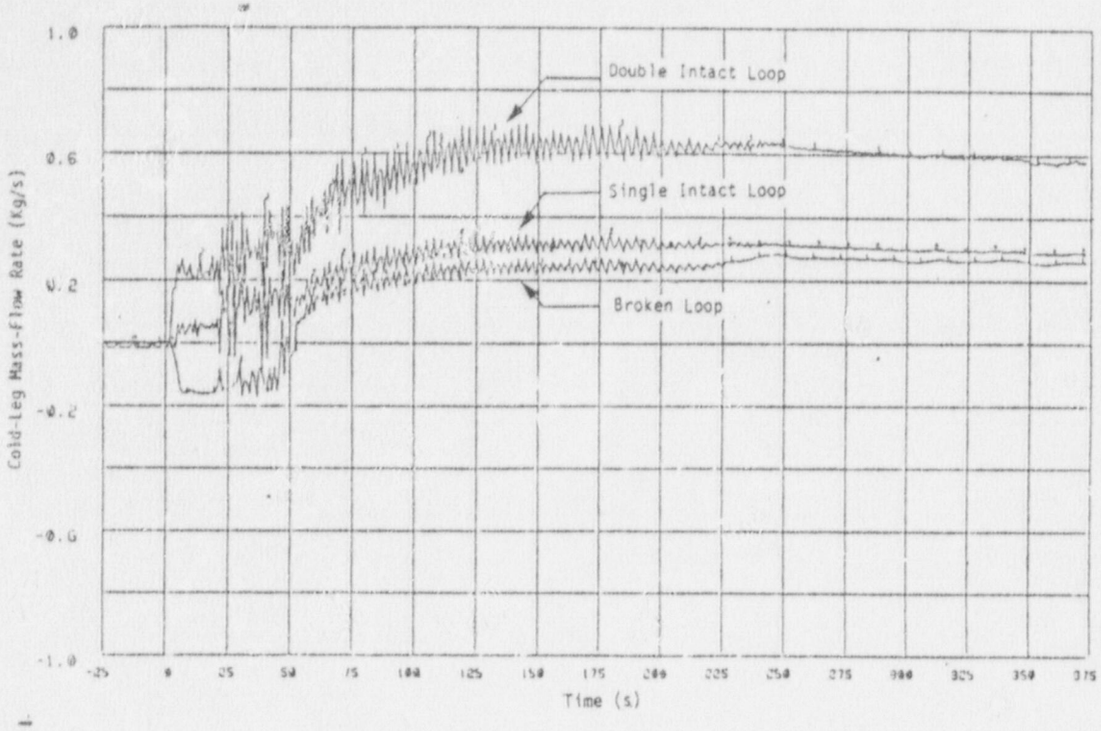

Fig. 56 Experimental cold-leg mass-flow-rate history for Test K7A.

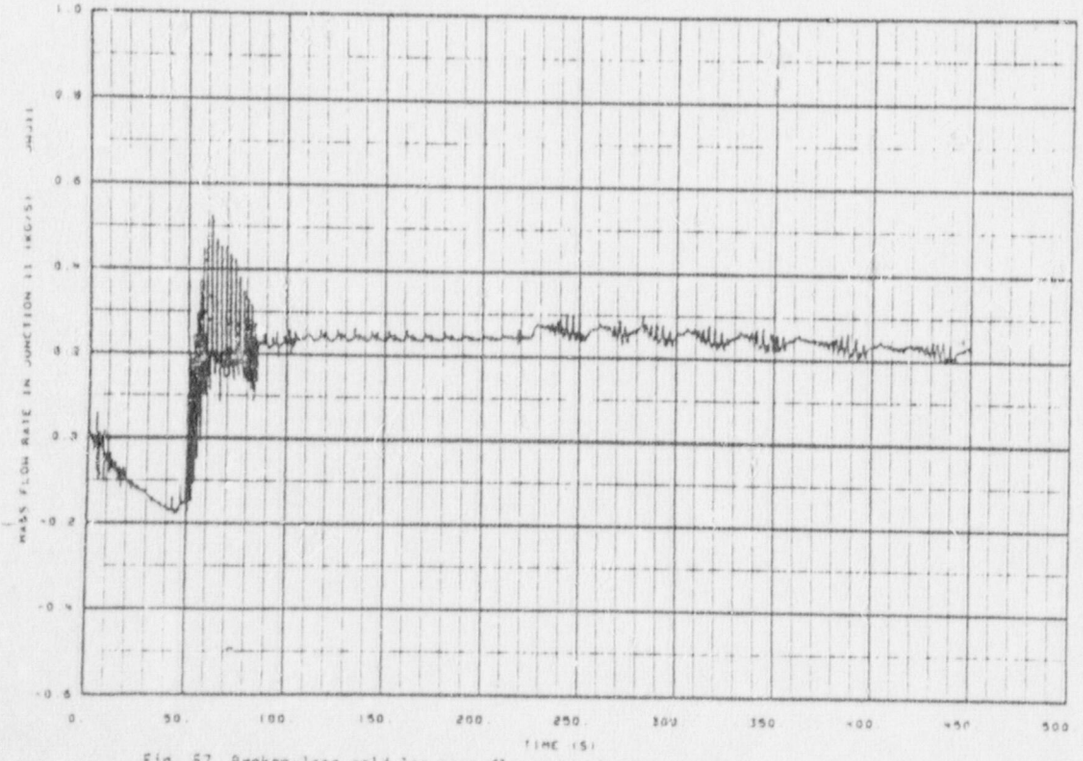

Fig. 57 Broken-loop cold-leg mass-flow-rate history as calculated by RELAP4/MOD6 (3) for Test K7A.

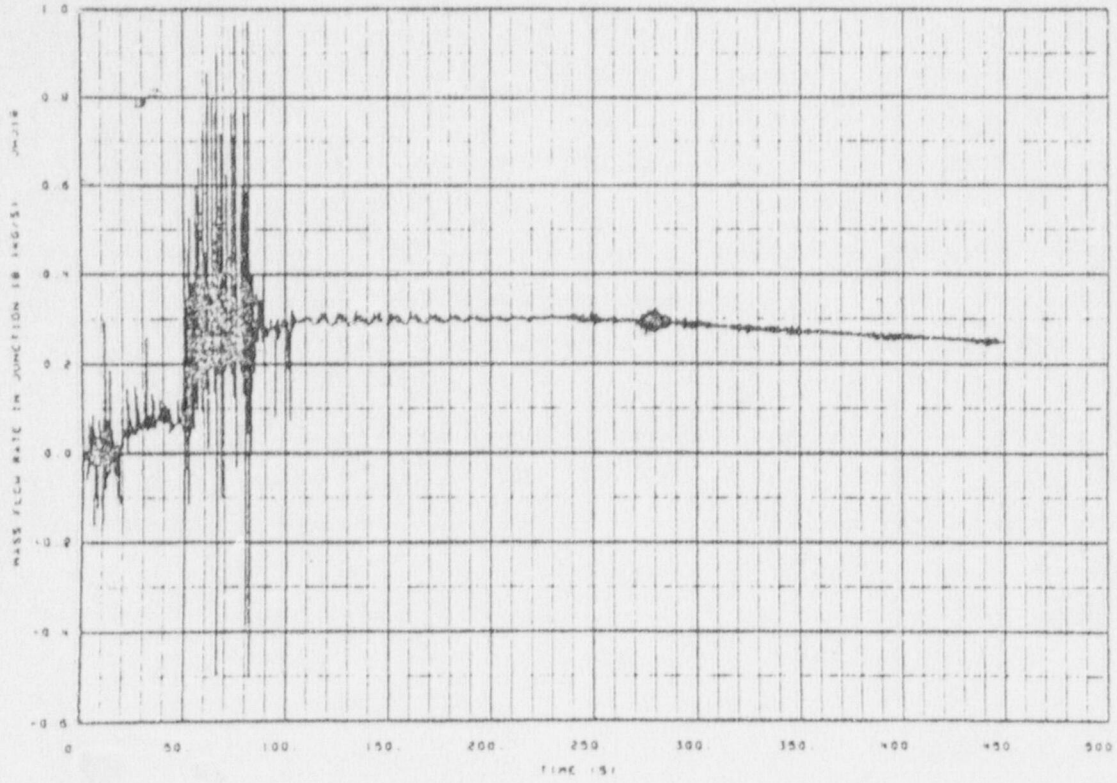

Fig. 58 Single-intact-loop cold-leg mass-flow-rate history as calculated by RELAP4/MOD6 (3) for Test K7A.

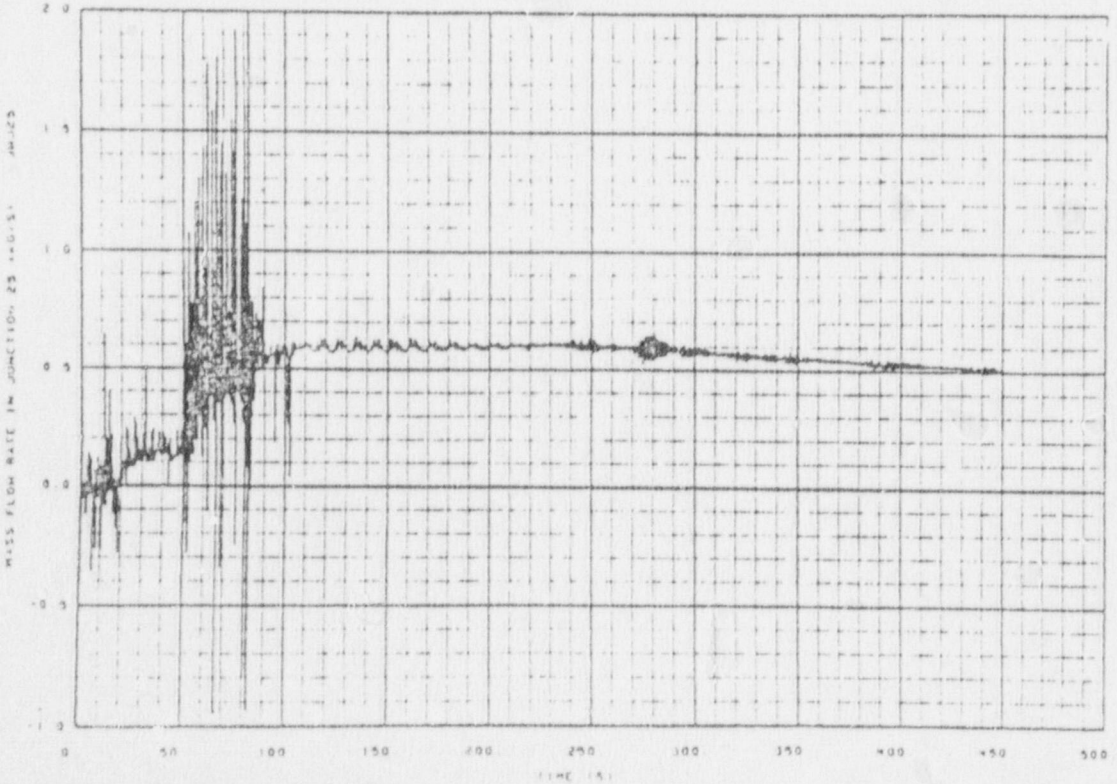

Fig. 59 Double-intact-loop cold-leg mass-flow-rate history as calculated by RELAP4/MOD6 (3) for Test K7A.

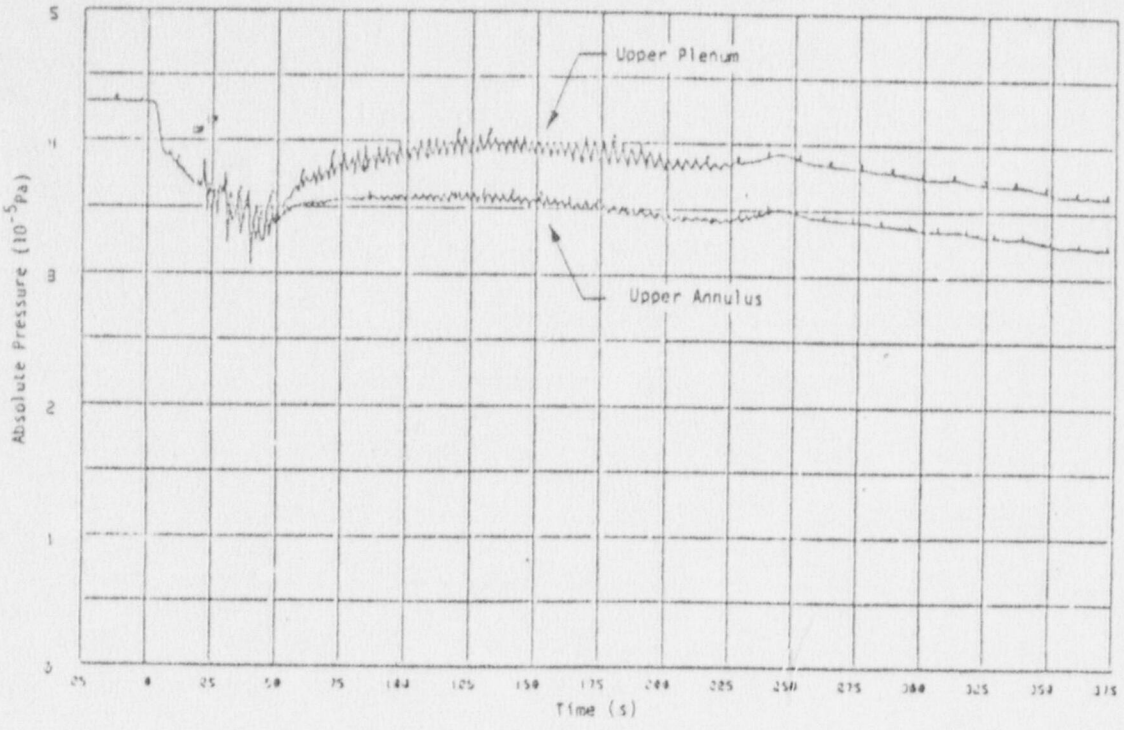

Fig. 60 Upper plenum and upper annulus experimental absolute pressure history for Test K7A.

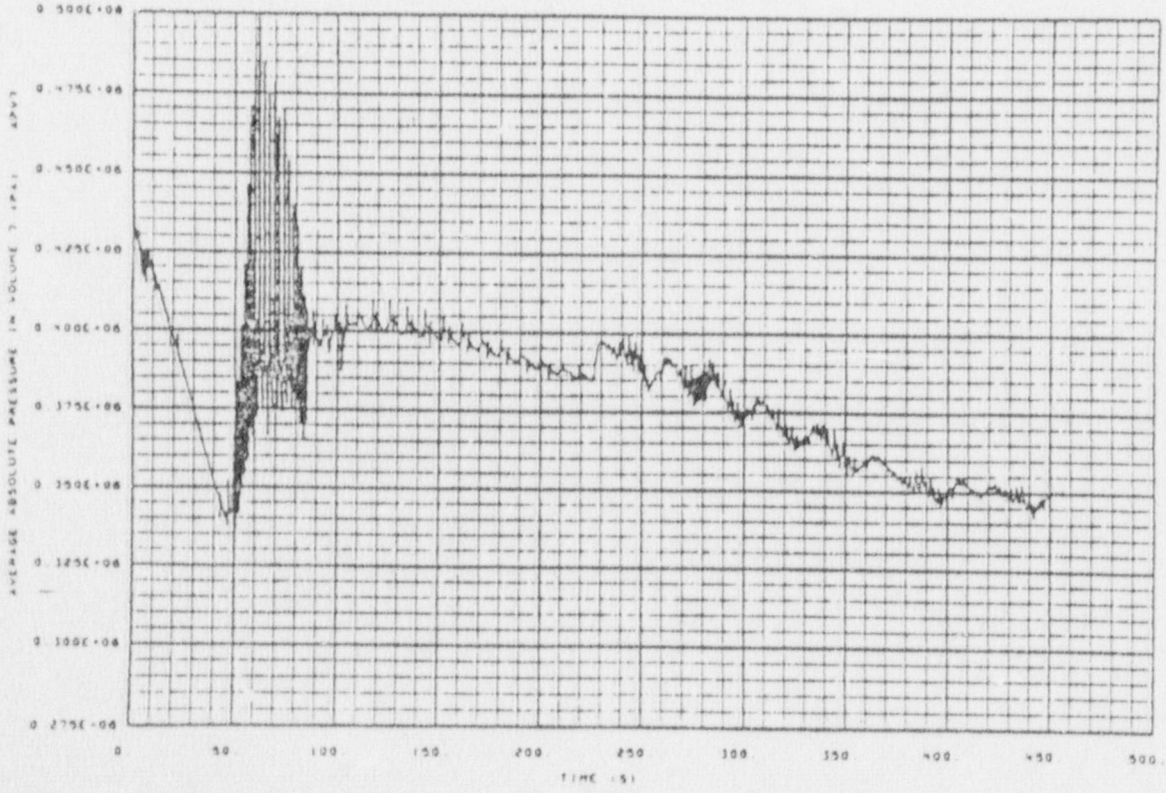

Fig. 61 Upper Plenum absolute pressure history as calculated by RELAP4/MOD6 (3) for Test K7A.

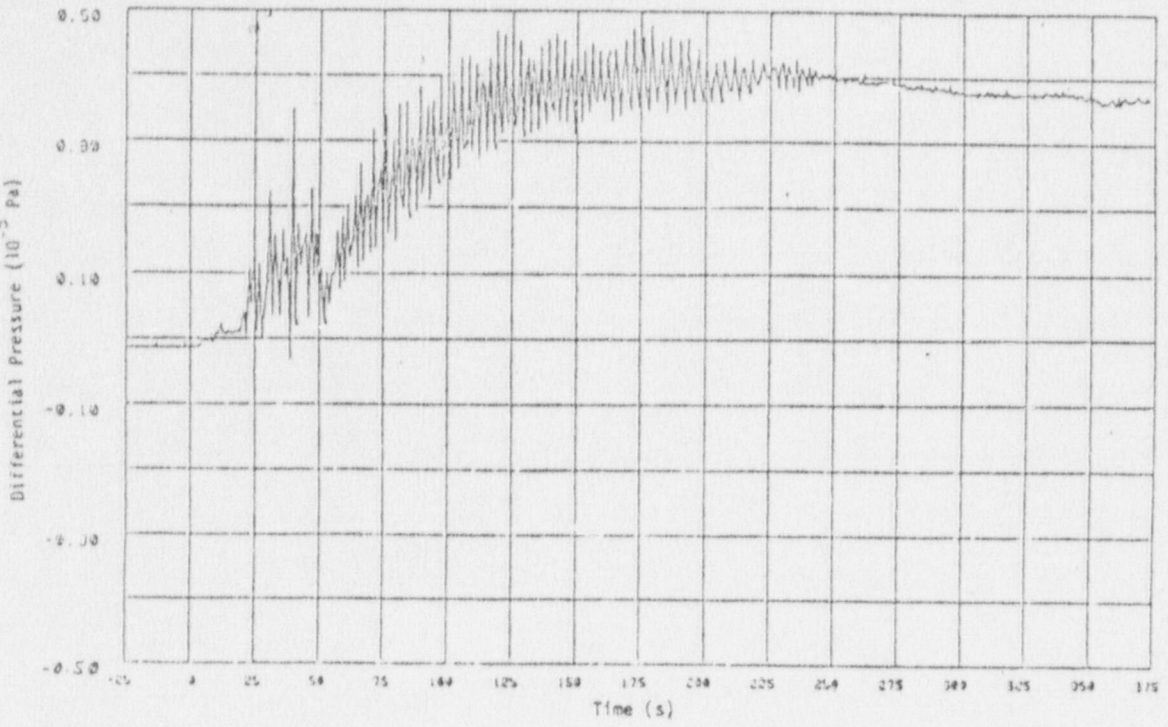

Fig. 62 Experimental differential pressure between upper plenum and upper annulus, test K7A.

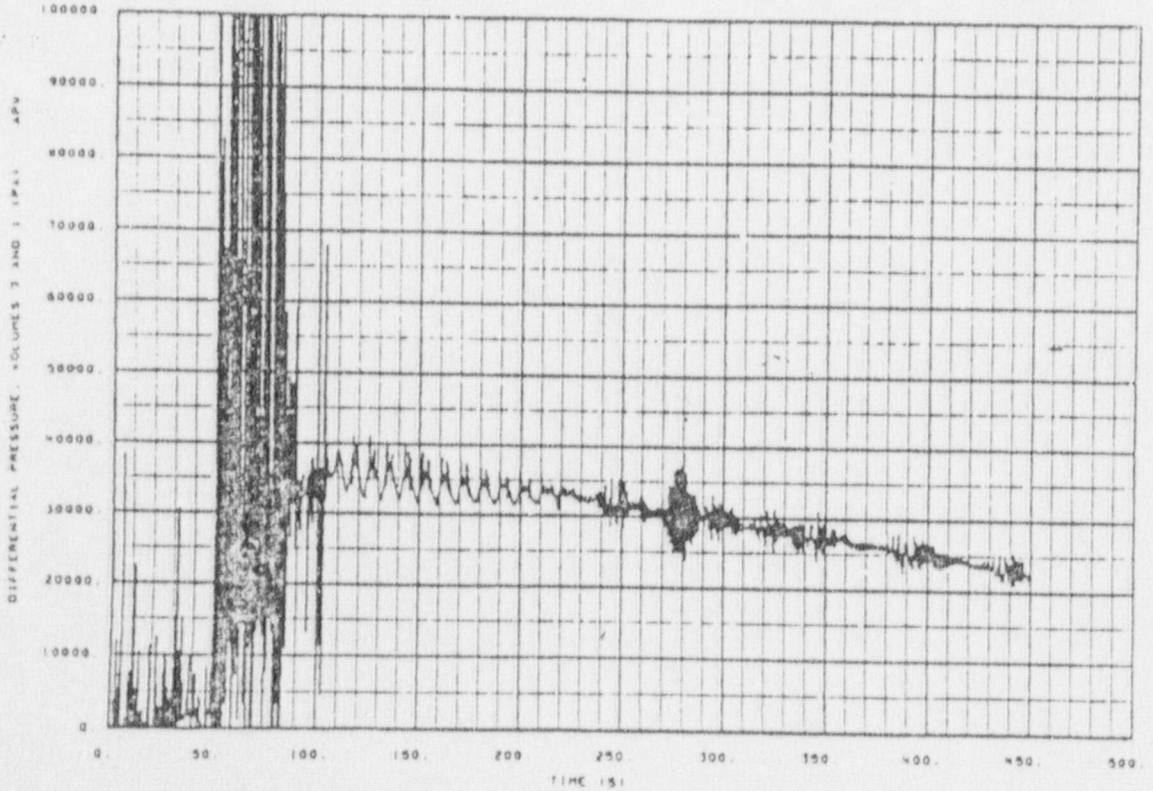

Fig. 63 Differential pressure between upper plenum and upper annulus as calculated by RELAP4/MOD6 (3) for Test K7A.

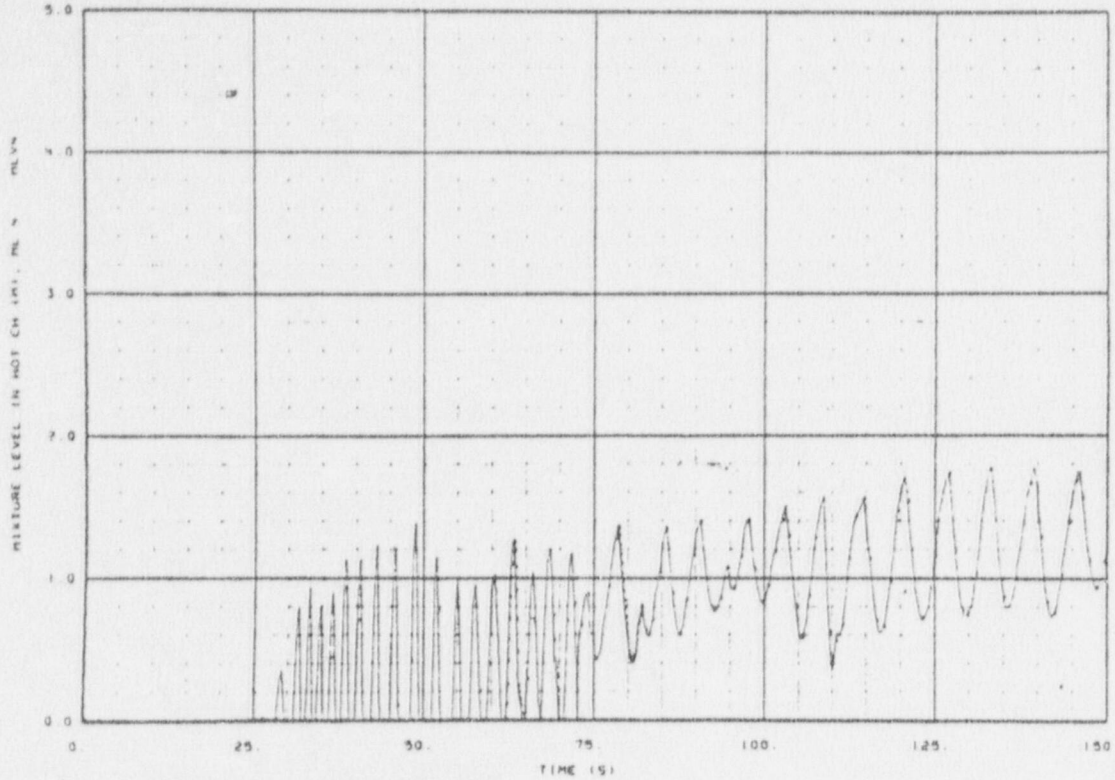

Fig. 64 Core hot-channel mixture-level history when undivided steam-generator inlet-side primary volumes were used.

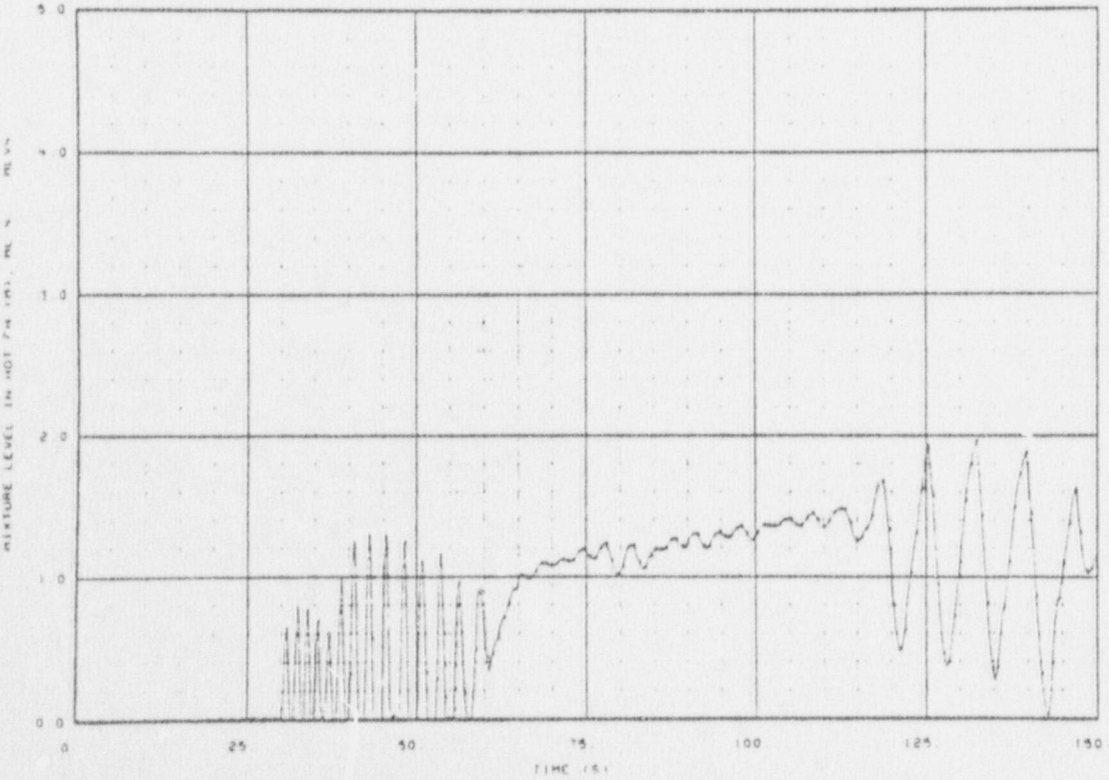

Fig. 65 Core hot-channel mixture-level history when steam-generator inlet-side primary volumes were divided in half.

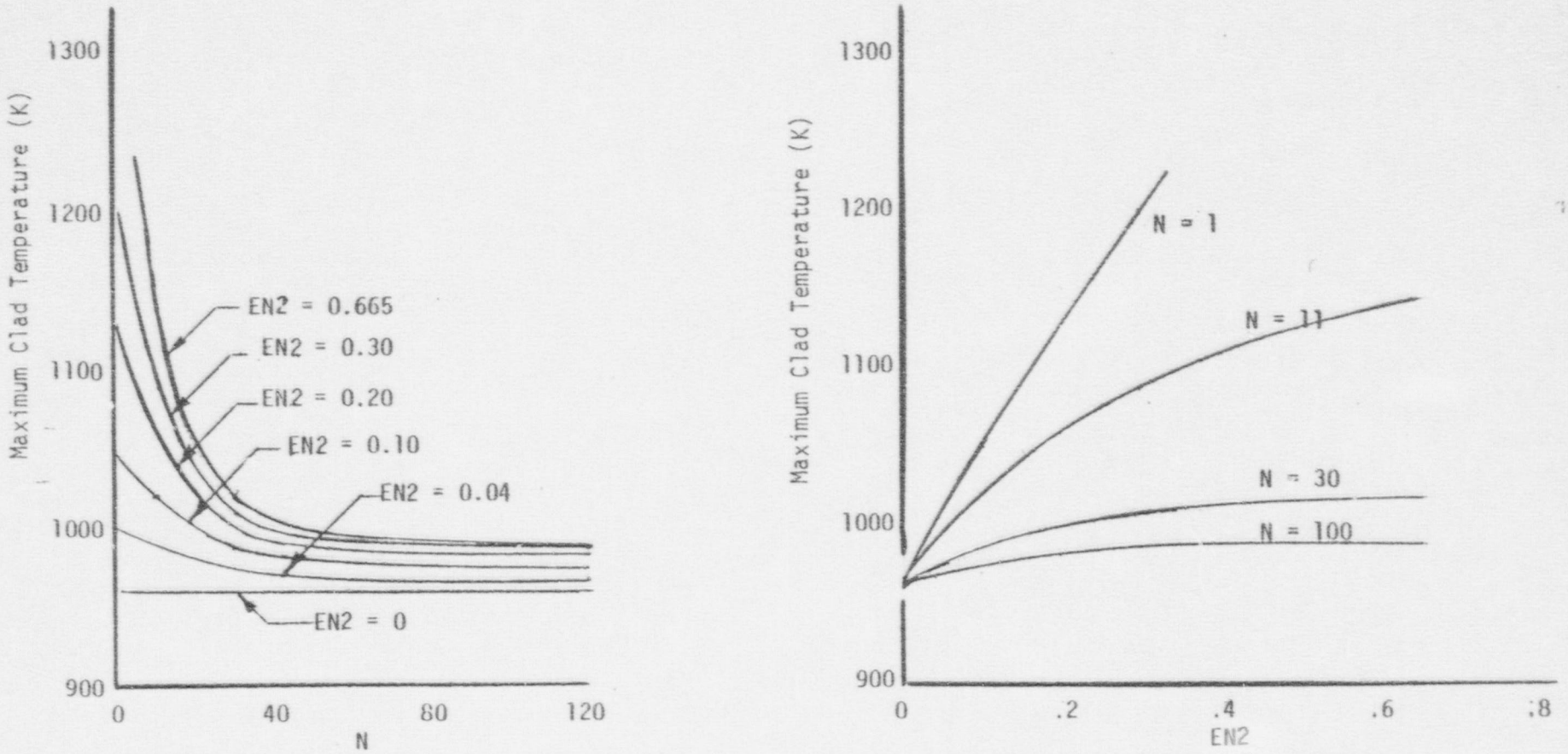

Fig. 66 Effect of varying N and EN2 on maximum rod surface temperature.

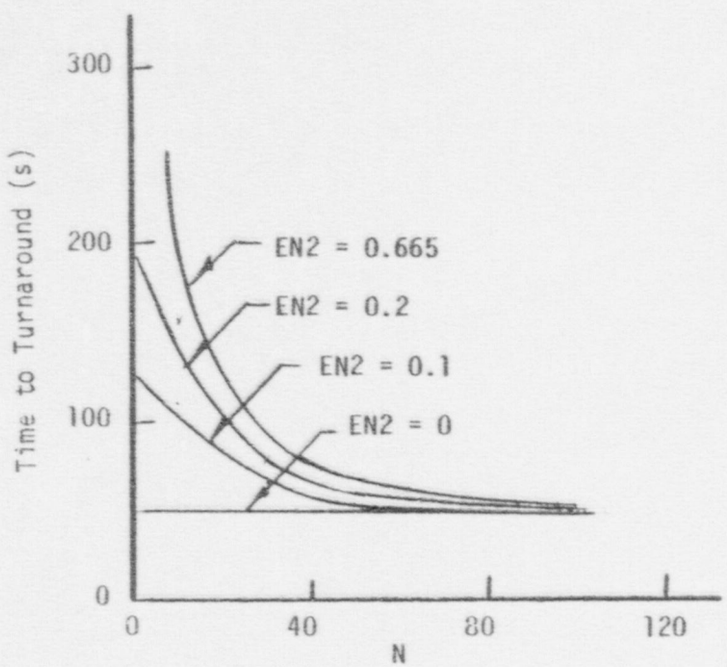

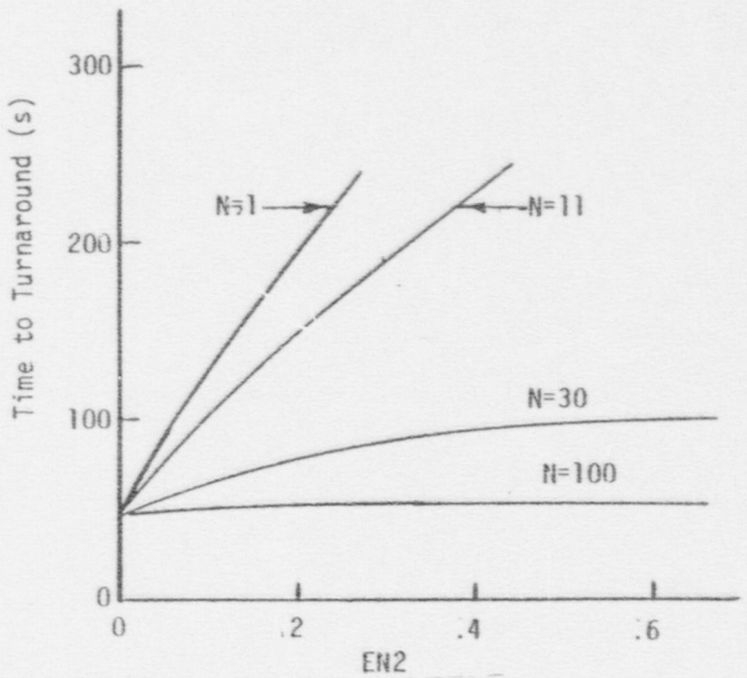

Fig. 67 Effect of varying N and EN2 on time to turnaround.

PCT = Peak Cladding Temperature

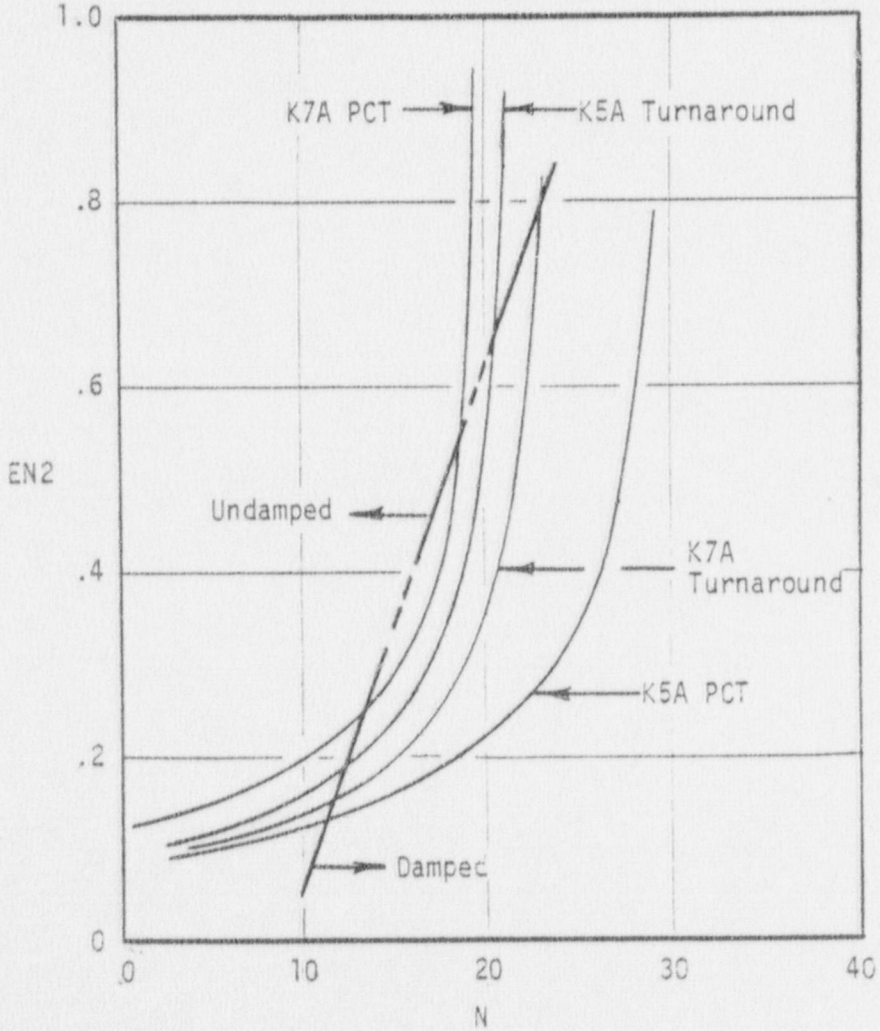

Fig. 68 N and EN2 relationships for PKL tests

APPENDIX A

TEST PREDICTION FOR KWU PKL TEST K5A
USING RELAP4/MOD6, UPDATE 3

Bill

MAR 6 1978

Mr. R. E. Tiller, Director
Reactor Operations and Programs Division
Idaho Operations Office - DOE
Idaho Falls, ID 83401

TEST PREDICTION FOR KMU PKL TEST K5A USING RELAP4/MOD6, UPDATE 3 - JAD-45-78

Ref: (a) S. Fabic ltr to Attendees of Nov 18, 1977 Denver meeting, Independent Verification of Codes, Nov 28, 1977
(b) 189 Number A0047 (I-106), Independent Verification, Dec 1977

Dear Mr. Tiller:

This report presents pertinent results calculated for the Kraftwerk Union (KMU) PKL Reflood Test K5A using RELAP4/MOD6, Update 3. The calculations represent a "blind" test prediction, so called because they were made without prior study of experimental system behavior and without access to test K5A results.

A detailed pretest prediction report similar to those produced by Semiscale and PBF was not produced at this time. The main objective of this letter is to show proof of the calculation and expedite release of the data for future analysis. This objective is in contrast to requirements of the experimental programs for detailed test prediction reports which can be used in test planning, instrumentation needs, etc. Detailed analysis of the predicted experiment behavior and evaluation of code capabilities and deficiencies will be presented in separate documentation prepared after comparing the prediction with experimental data.

The KMU PKL facility is a three-loop simulation of a West German pressurized water reactor, fabricated in a reduced scale that maintains prototype volume-to-power ratio. It was designed specifically for system experiments simulating the reflood phase of hypothetical loss-of-coolant accidents. The full length electrically-heated 340-rod core is divided into hot, average, and cool channels and has an overall power capacity of 1.45 MW and a peak power of 1.5 MW/M. The RELAP4 nodalization of this facility is attached in Figure 1 and the core channel and heat-slab description is attached in Figure 2.

Test K5A is a 200% cold-leg-break experiment with ECC injection into the intact-loop cold legs and into the upper annulus; this injection was simulated in the RELAP4 modeling by upper annulus injection. Boundary conditions used were as-tested functions of core power, injection rate, and suppression tank pressure, shown vs. time in Figures 3-5, attached.

The data presentation consists of two separate calculations: (a) a "base-case calculation" and (b) an "alternate calculation". The effort to provide the test prediction is unique in that it is a specific attempt to conduct code calculations within independent verification guidelines. These guidelines were set forth by the NRC in Reference (a) and were followed as closely as possible in developing the base-case calculation. However, because of anomalies that resulted in severe system hydraulic oscillations, the results of the calculation were not believed to be a realistic forecast of probable PKL experiment behavior. Therefore, an alternate calculation was made with an identical model except for the following: (a) A new default input option was used for core dispersed-flow heat transfer. (The new default value was issued with RELAP4/MOD6, Update 4) (b) A modified liquid entrainment fraction was used. The alternate calculation is believed to have provided a more realistic test prediction. The two calculations will be evaluated separately in the code-data comparison and carefully distinguished in subsequent documentation.

Figures 6-20 present typical results that will be compared to in-core thermocouple data and system pressure data. Significant differences and results for the two calculations are as follows:

	Base-Case	Alternate
Liquid Entrainment Fraction, EN2	0.30	0.665
Liquid Weighting Factor for Dispersed Flow Heat Transfer, N	11.0	30.0
Core Oscillation Damping	Undamped	Damped at 70 s
Peak Clad Temperature	1090 K	1020 K
Turnaround Time at the Hot Spot (2.44 M elevation)	200 S	100 S
Quench Time at the Hot Spot (2.44 M elevation)	Not Quenched at 300 seconds	310 S

The data from Experiment K5A are currently in the possession of the Idaho NRC office. It is recommended that the NRC now instruct the Idaho office to release the data to EG&G for use in evaluating the prediction.

This transmittal is in partial satisfaction of work agreed to in Reference (b). Scheduled final completion of this work will be described in the next edition of the WRSR Status Summary Report.

Very truly yours,

Original signed by

J. A. Dearien, Manager
Code Verification and
Applications Program

YSC:vjd

Attachments:
As stated

cc: S. Fabic, NRC-RSR
G. N. Lauben, NRC-DSS
W. H. Lovelace, NRC-MIPC, w/o attach.
W. C. Lovelace, NRC-MIPC, w/o attach.
W. C. Lyon, NRC-RSR - 3
R. M. Scroggins, NRC-RSR
L. S. Tong, NRC-RSR
R. W. Kiehn, EG&G Idaho, w/o attach

bcc: Y. S. Chen
J. A. Dearien - 2
~~W. S.~~ Haigh
R. E. Rice
P. H. Vander Hyde, w/o attach.
L. J. Ybarrondo
Central Files
File 15.1

KWU - PKL 3-LOOP RELAP4/MOD6 NODALIZATION

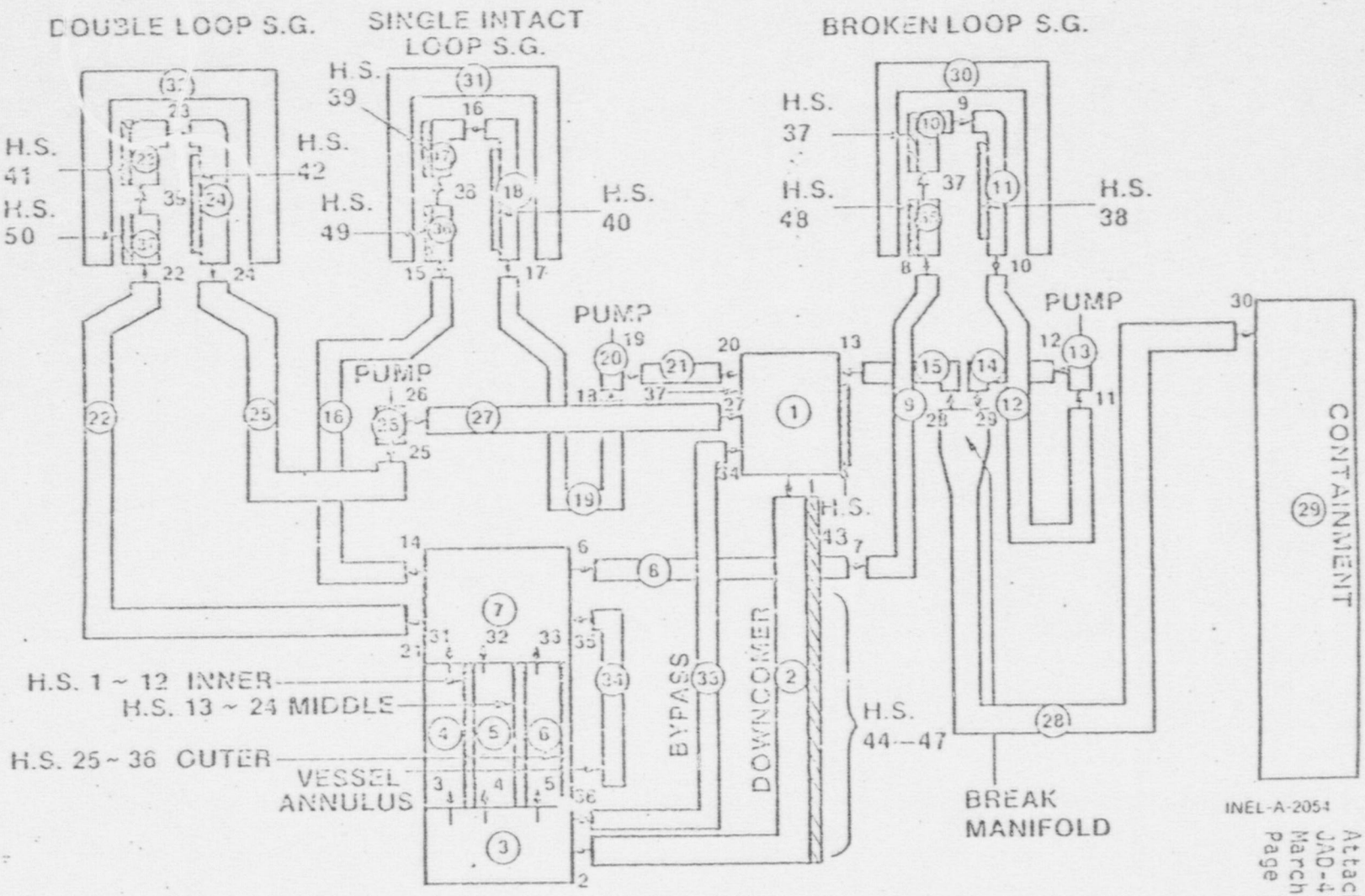

Fig. 1 KWU-PKL three-loop RELAP4/MOD6 nodalization.

Attachment 1
JAD-45-78
March 6, 1978
Page 1 of 20

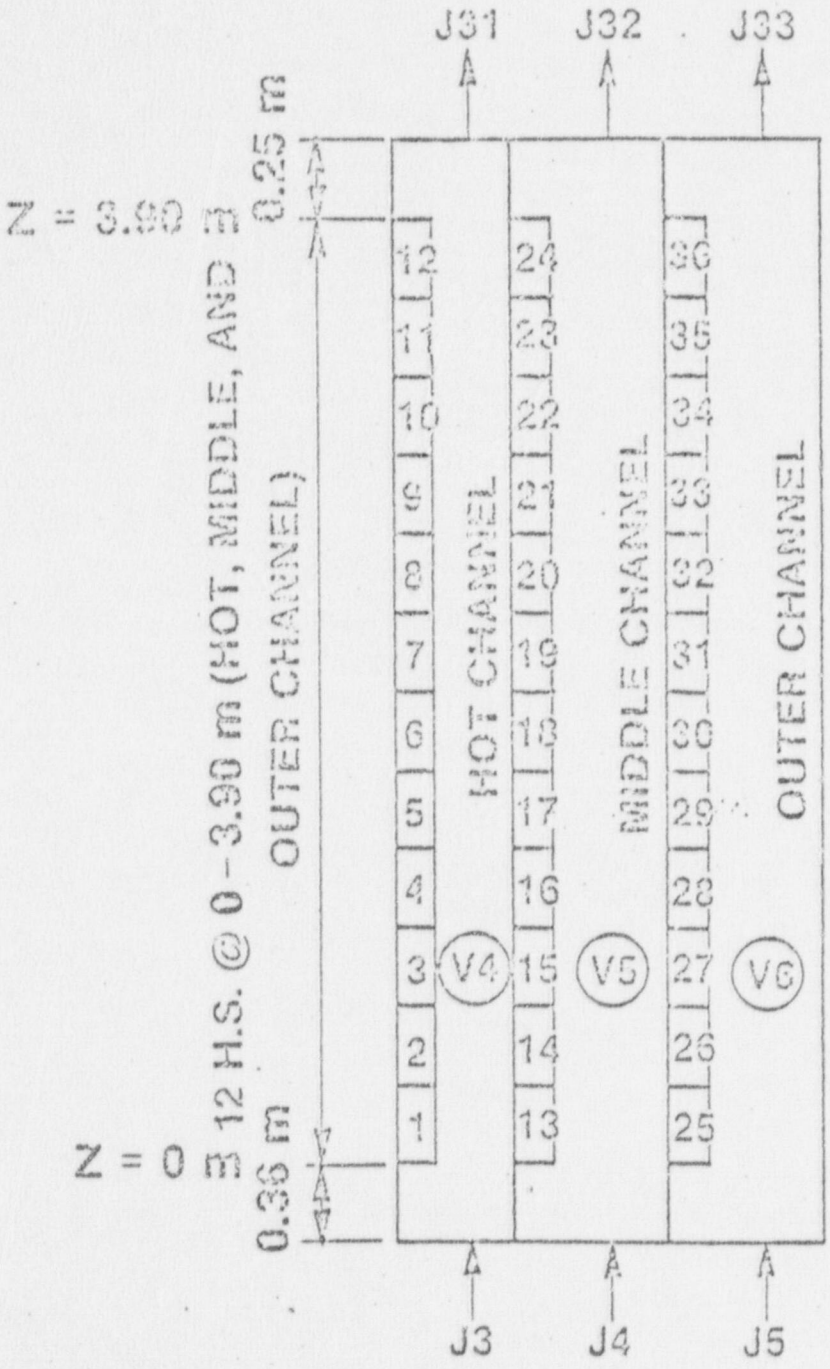

Fig. 2 Core heat slab structure.

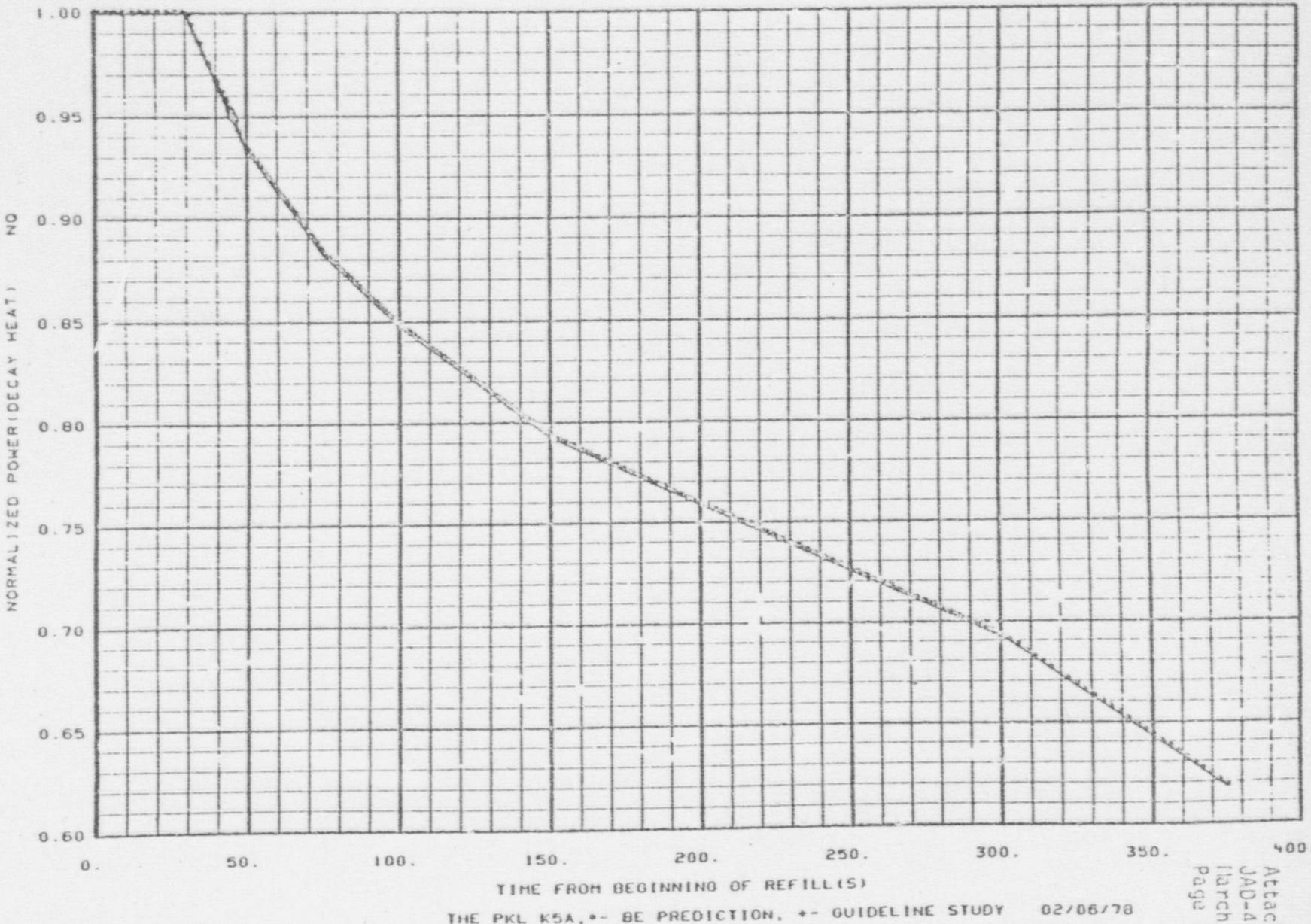

Fig. 3 Total normalized pwer vs. time.

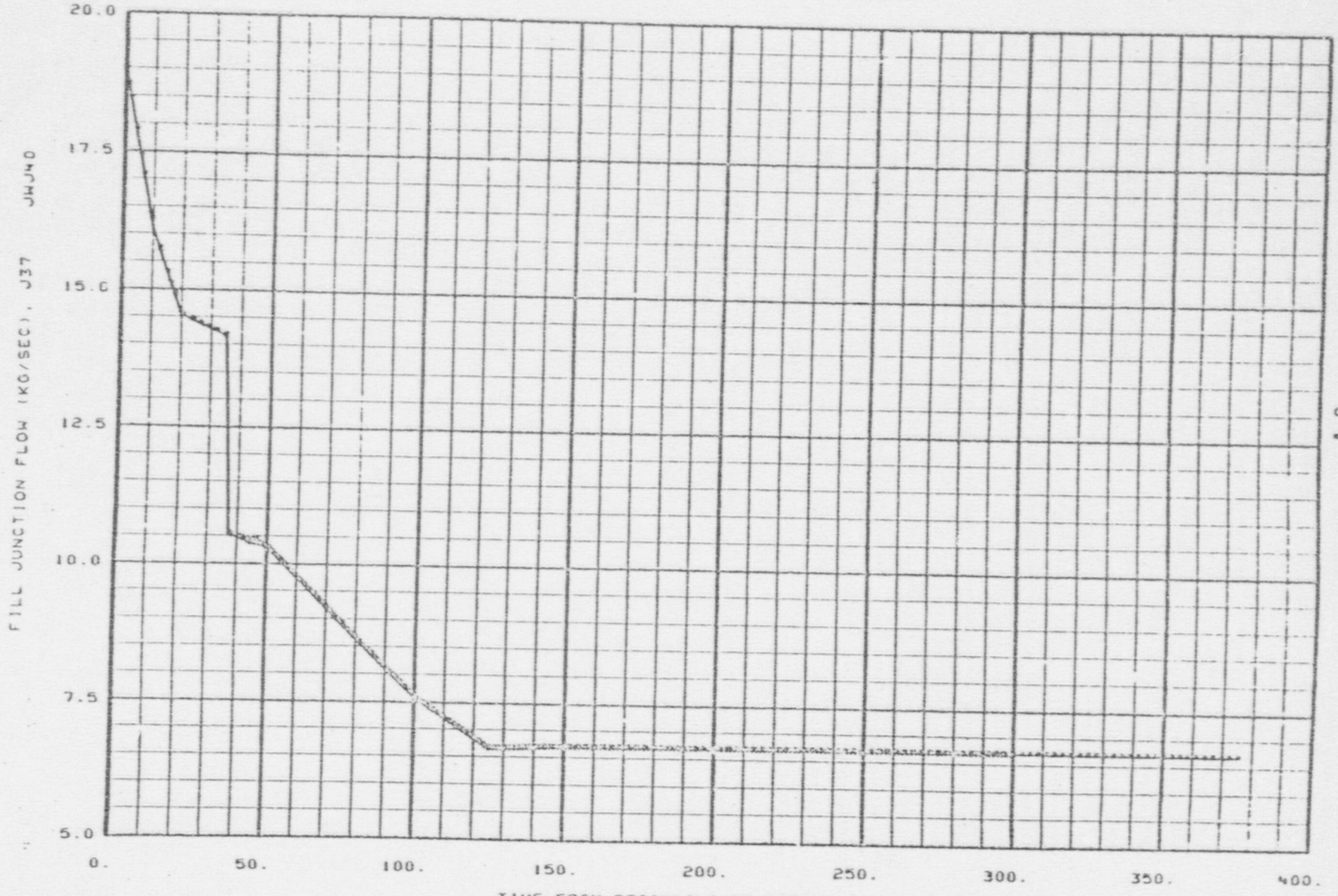

Fig. 4 Total ECC injection rate vs. time.

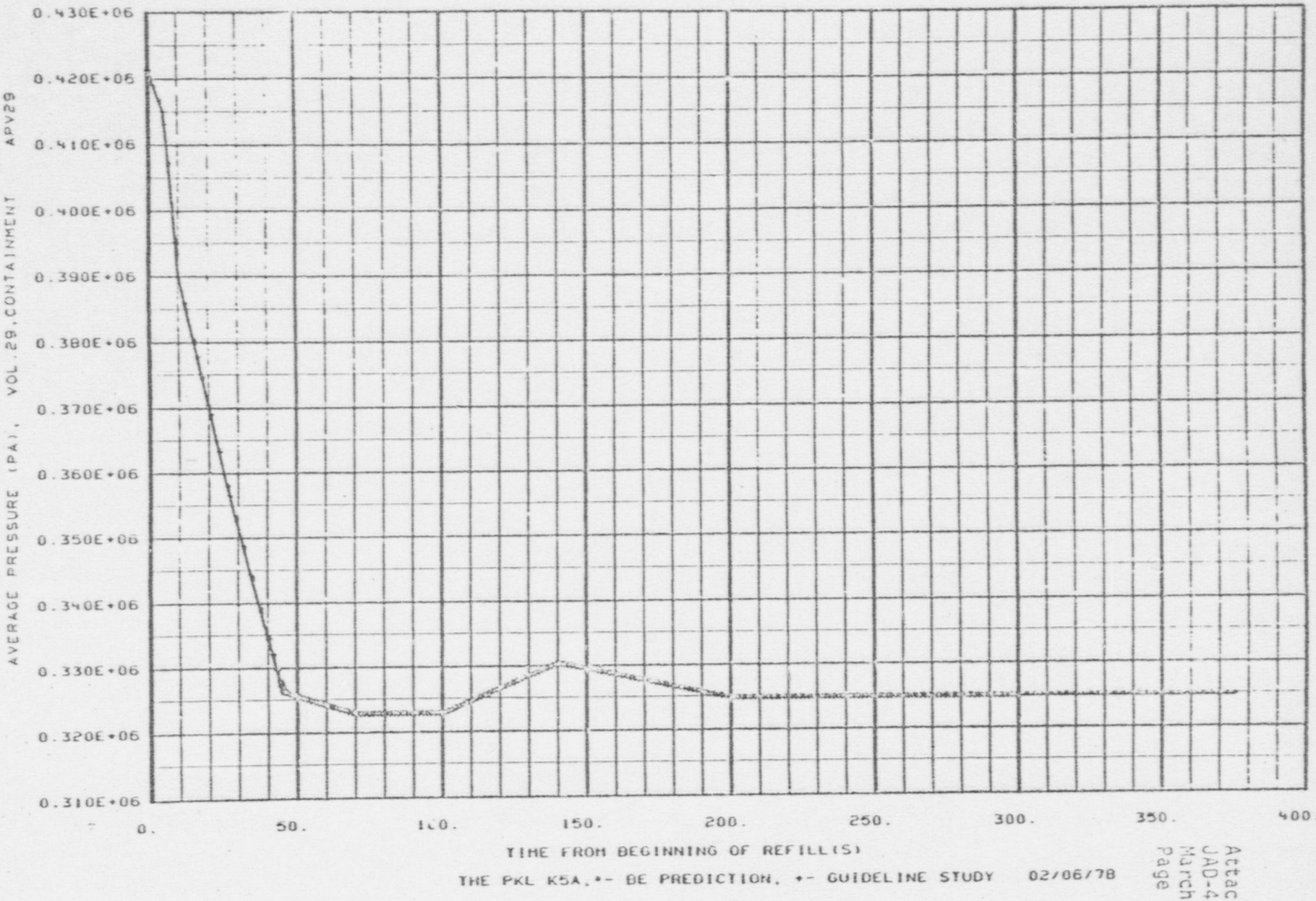

Fig. 5 Containment pressure vs. time

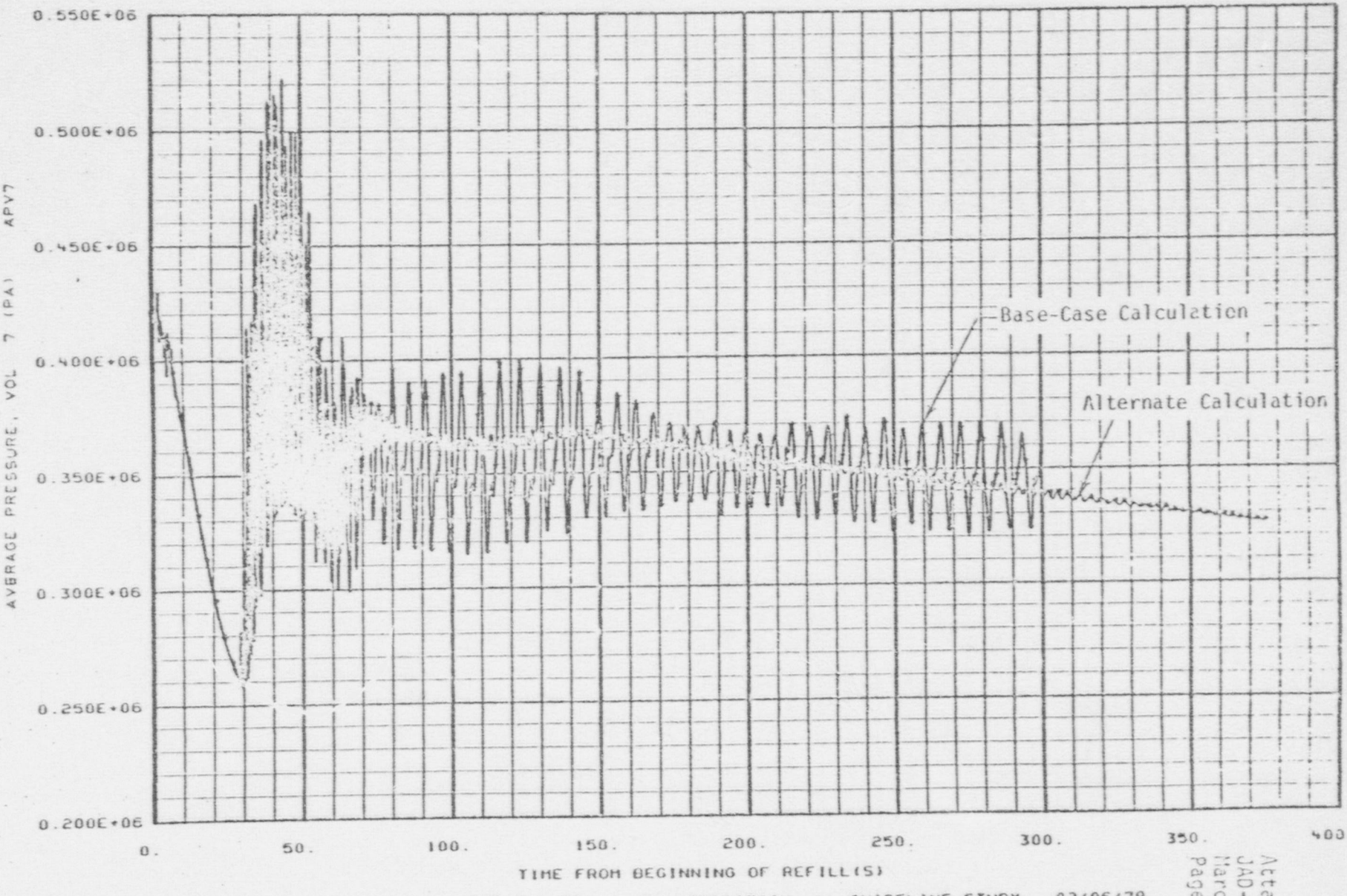

Fig. 6 Upper plenum pressure vs. time.

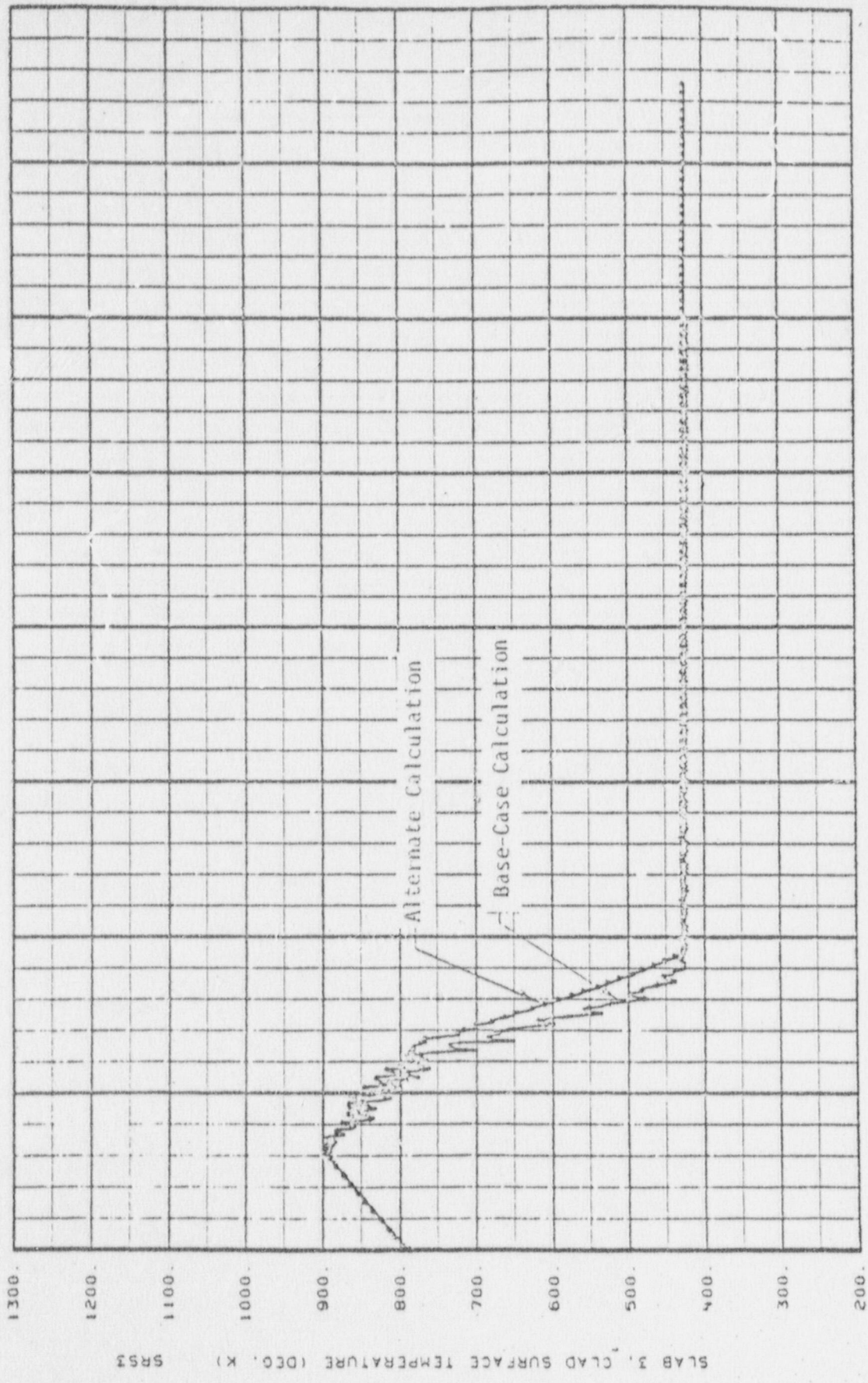

Fig. 7 Hot channel rod surface temperature at Z = 0.85 m vs. time.

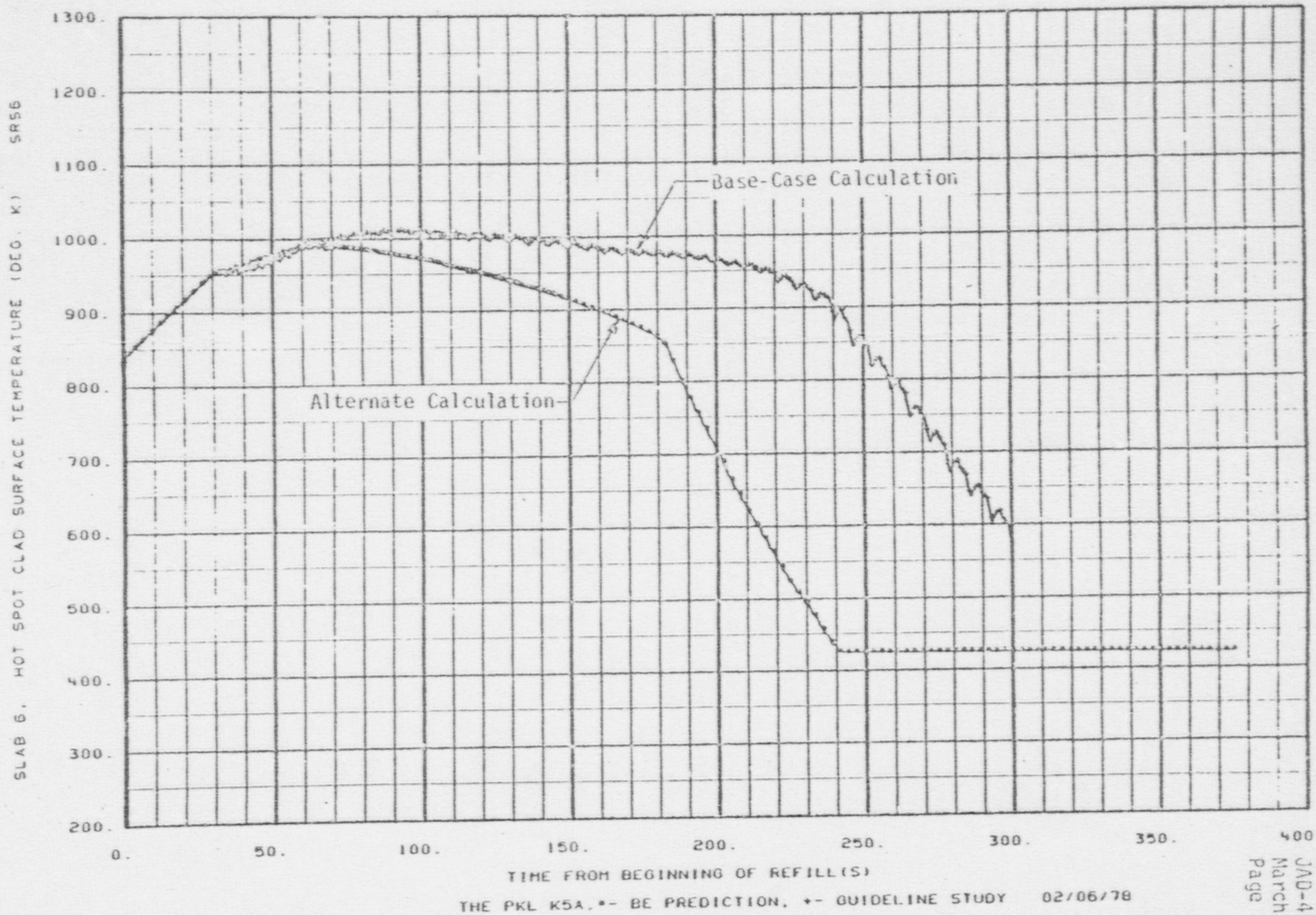

Fig. 8 Hot channel rod surface temperature at Z = 1.79 m vs. time.

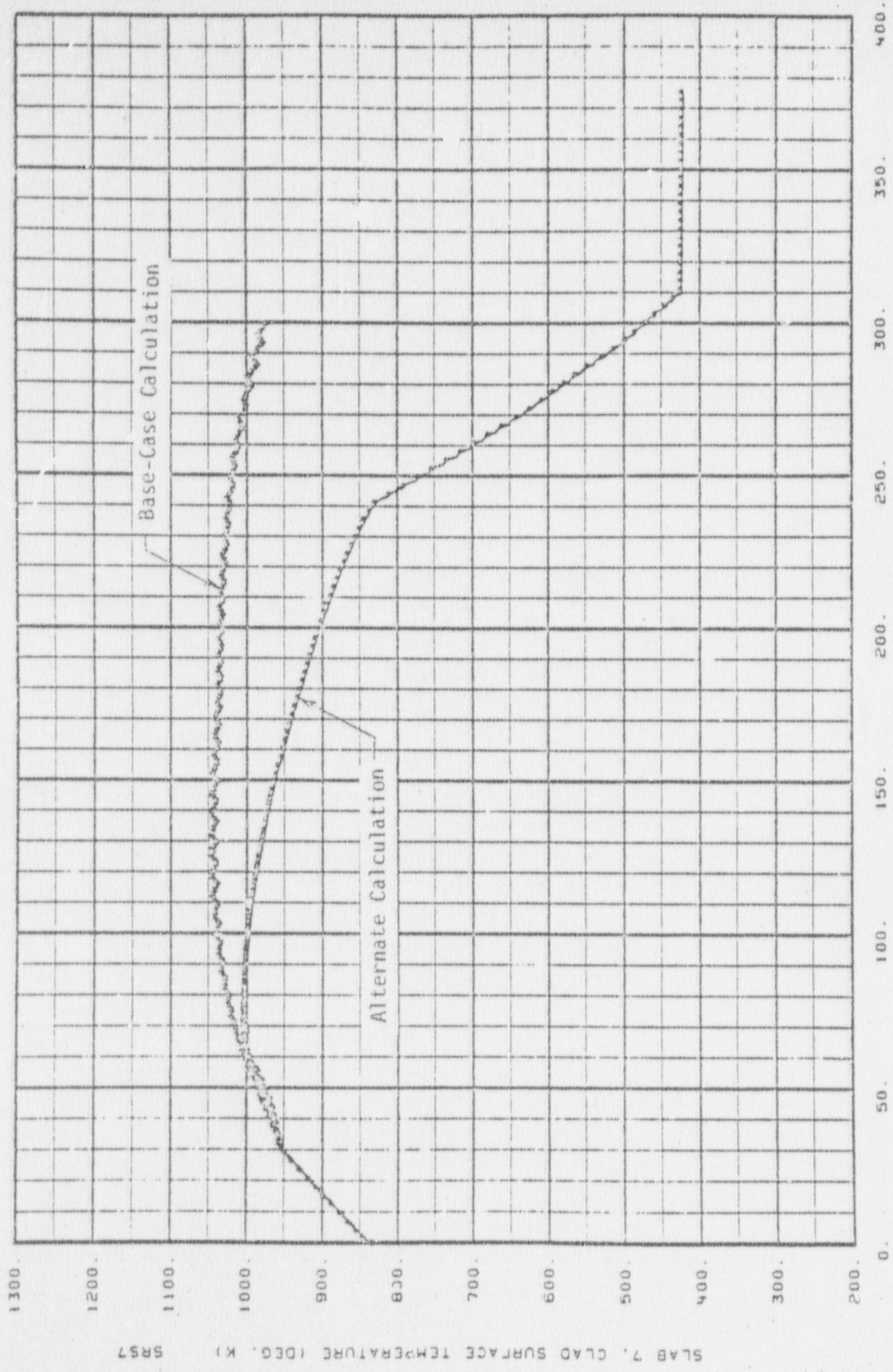

Fig. 9 Hot channel rod surface temperature at z = 2.11 m vs. time.

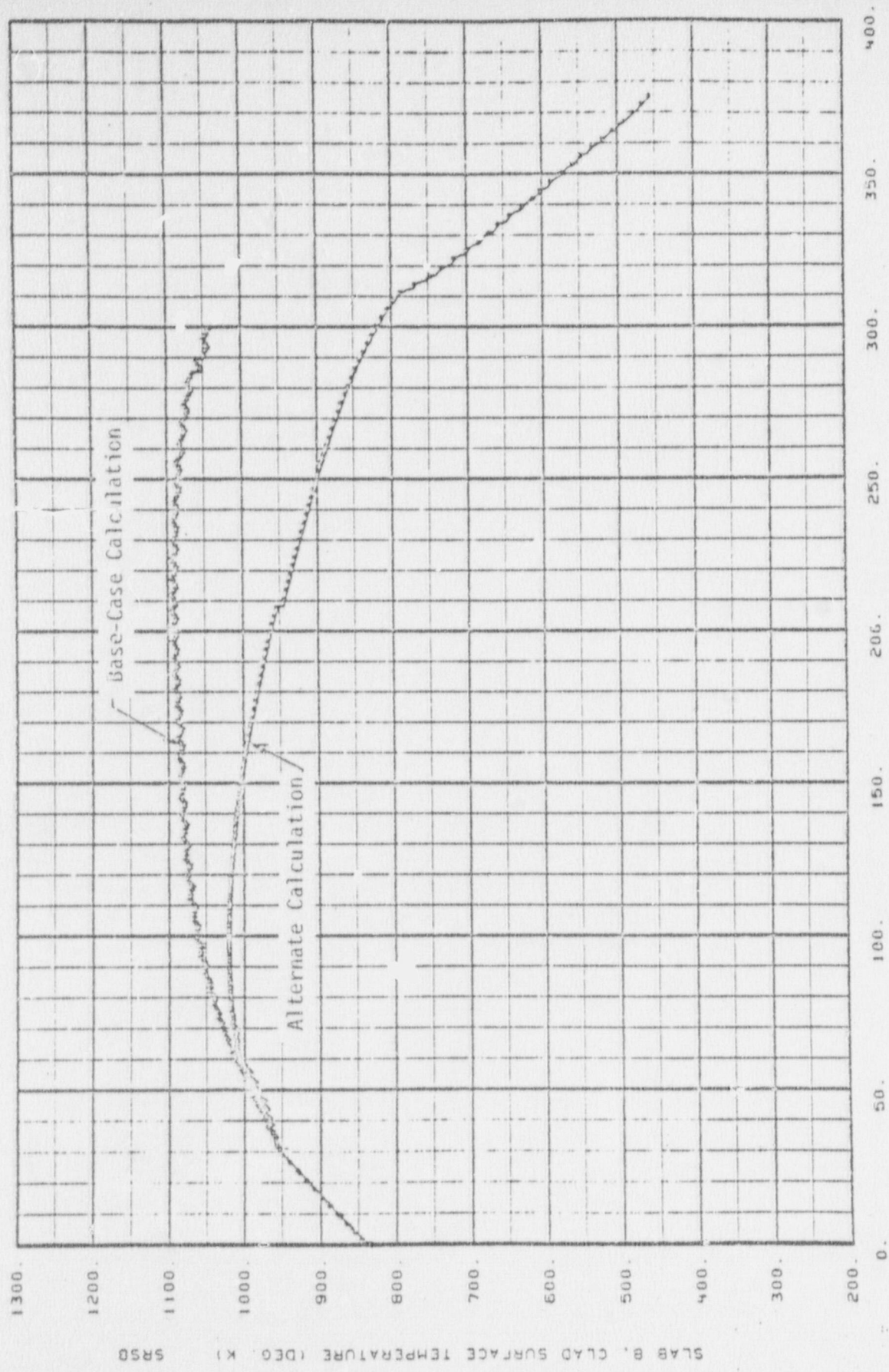

Fig. 10. Hot channel rod surface temperature at Z = 2.44 m vs. time.

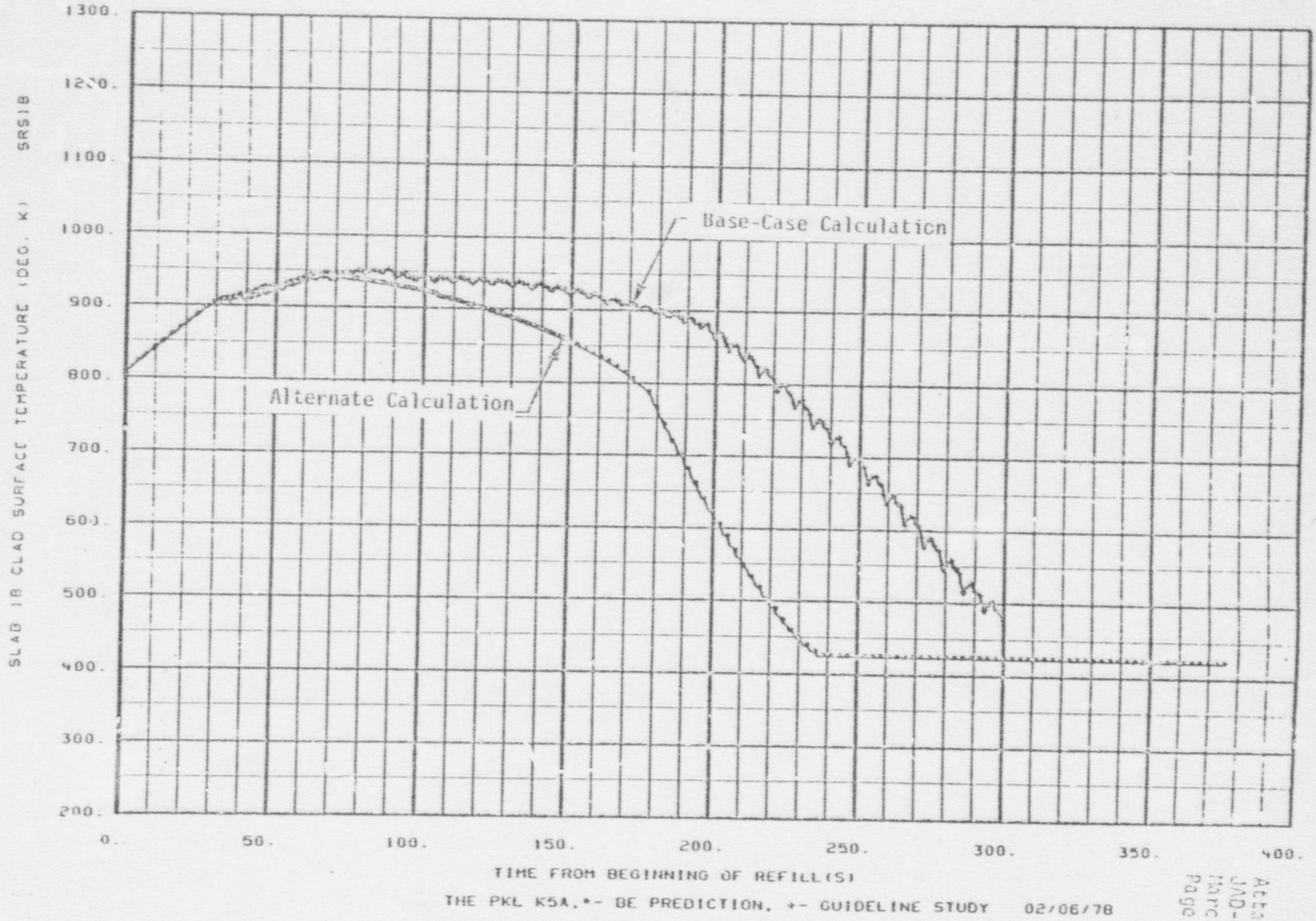

Fig. 11 Average channel rod surface temperature at Z = 1.79 m vs. time.

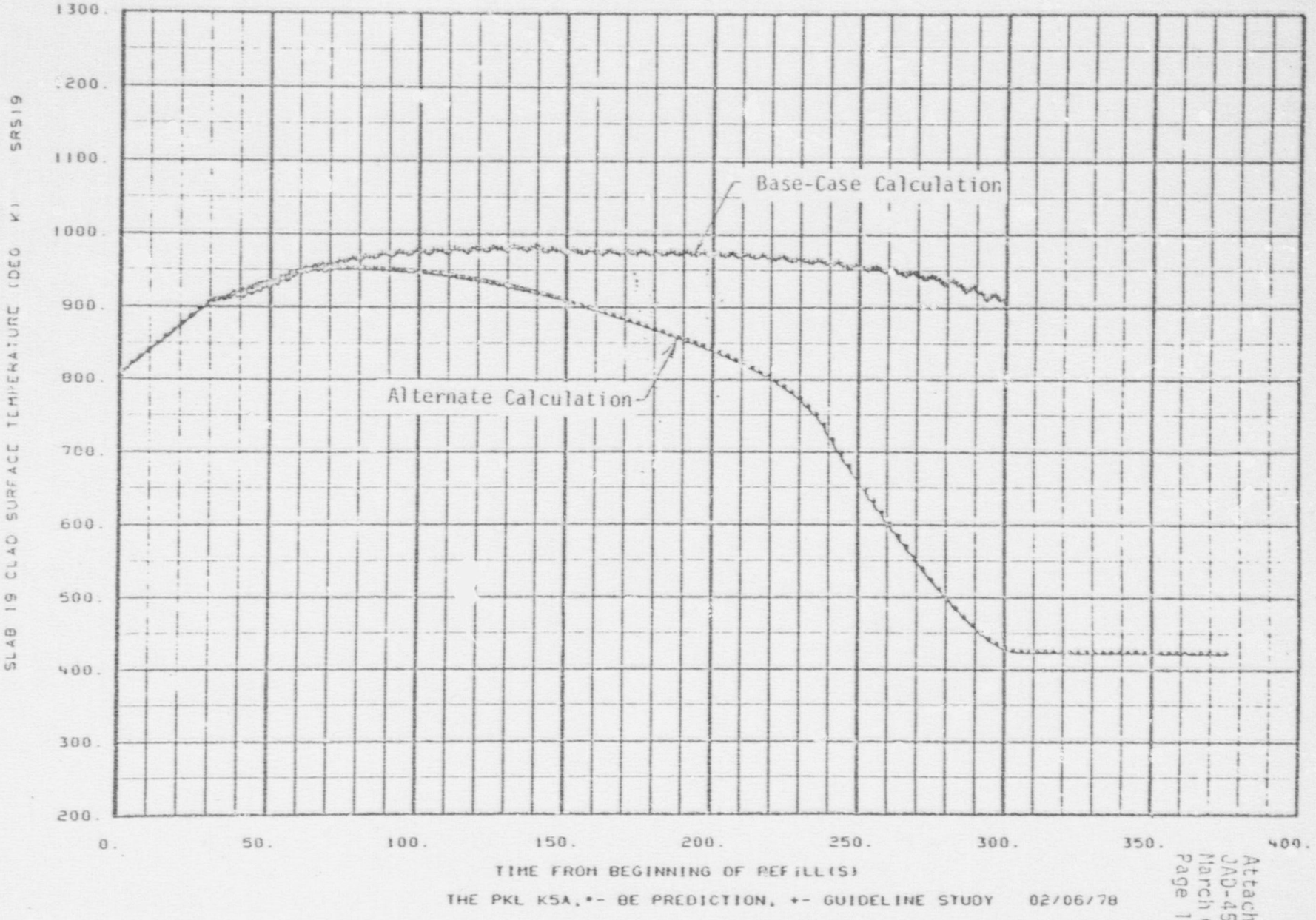

Fig. 12 Average channel rod surface temperature at $\bar{z}$ = 2.11 m vs. time.

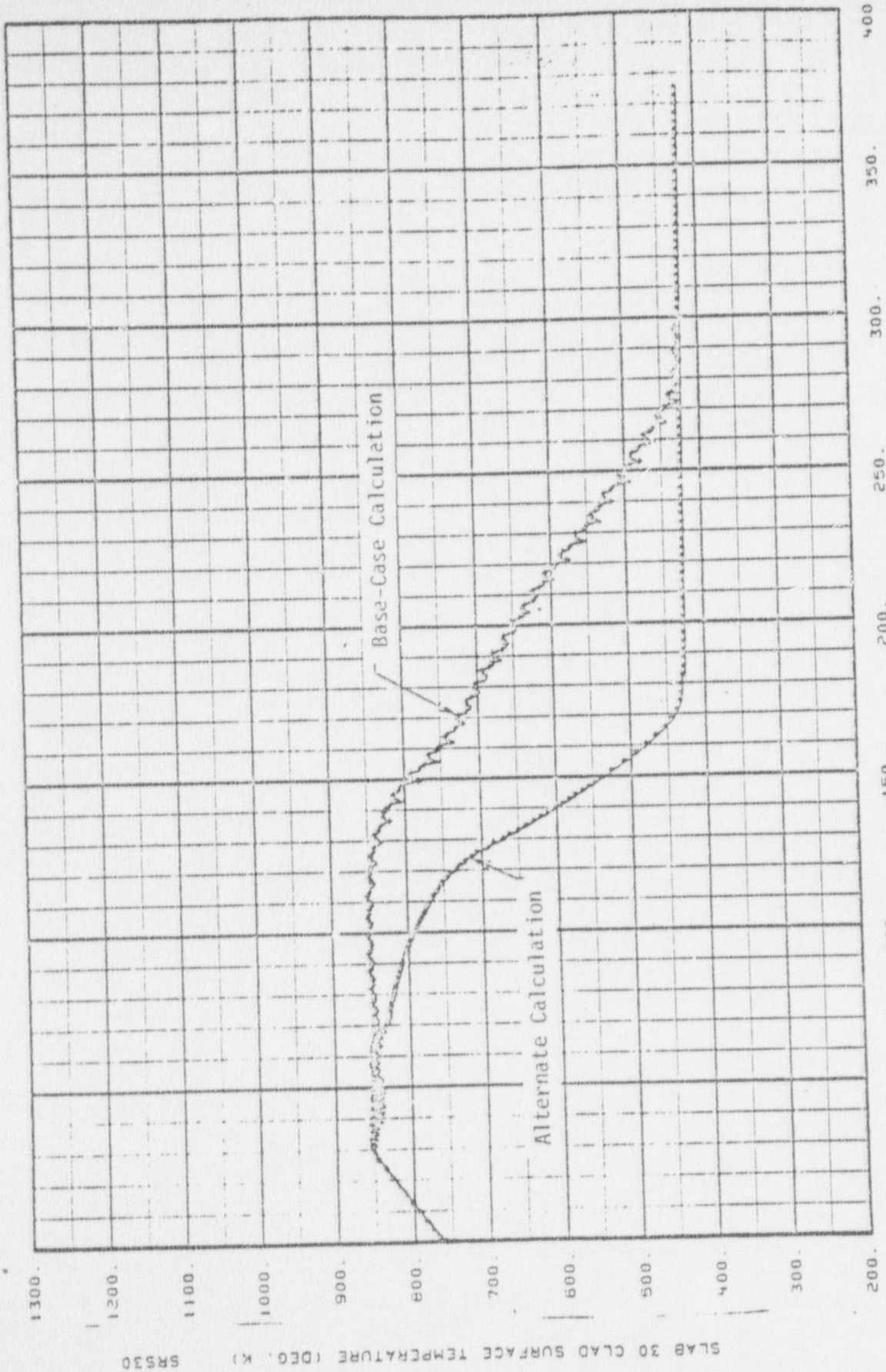

Fig. 13 Cool channel rod surfa... at Z = 1.79 m vs. time.

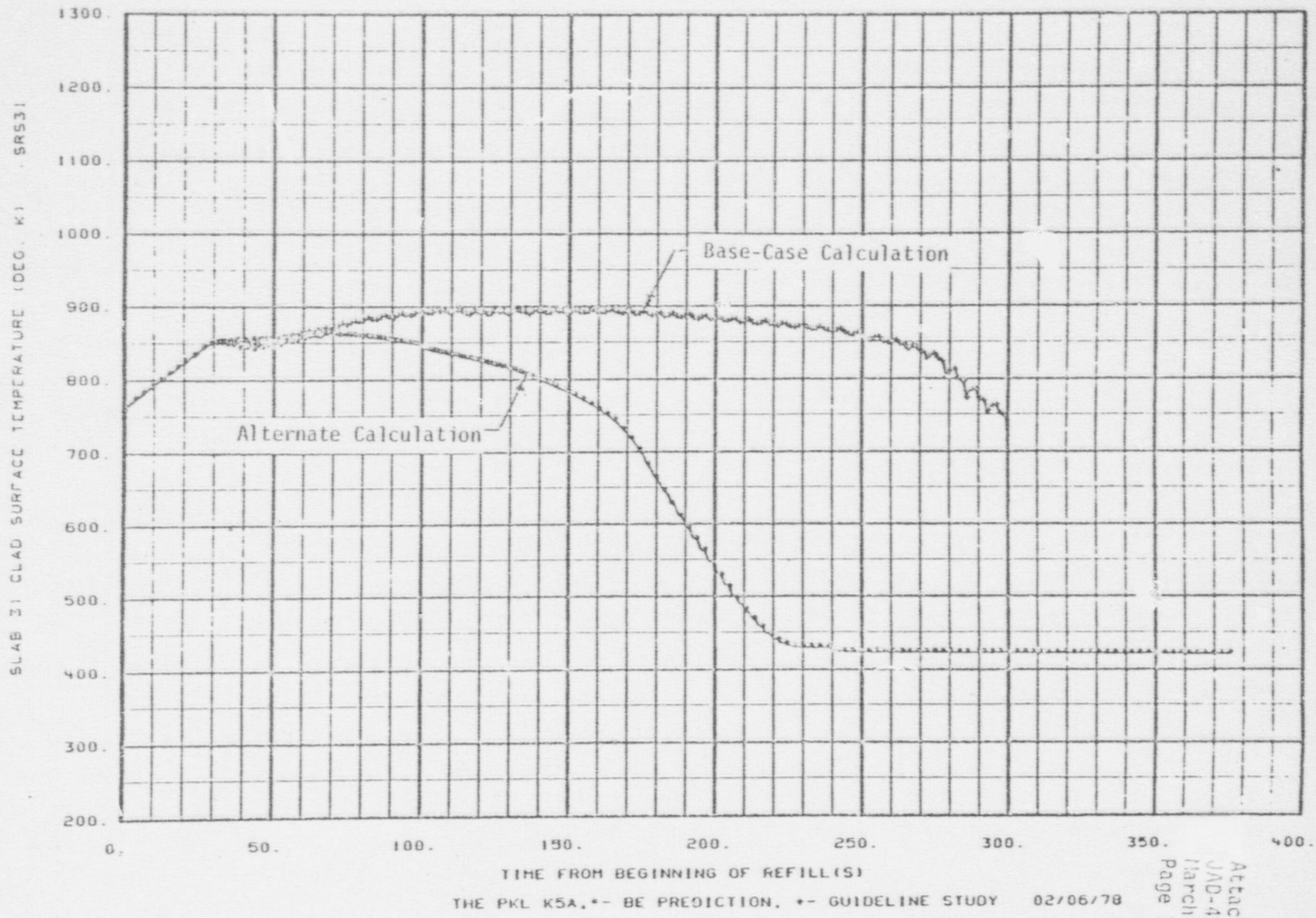

Fig. 14 Cool channel rod surface temperature at Z = 2.11 m vs. time.

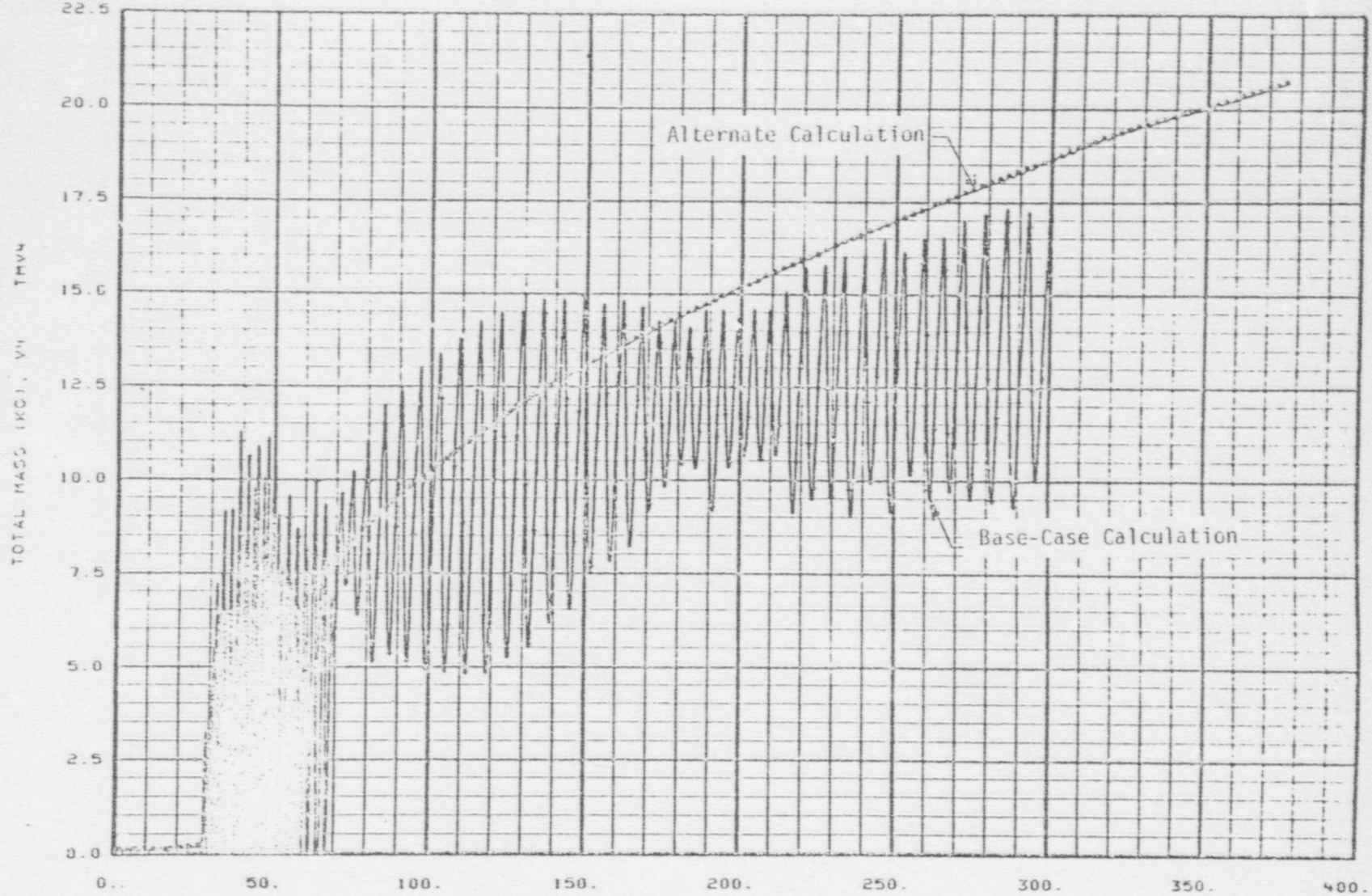

Fig. 15 Total mass in hot channel vs. time.

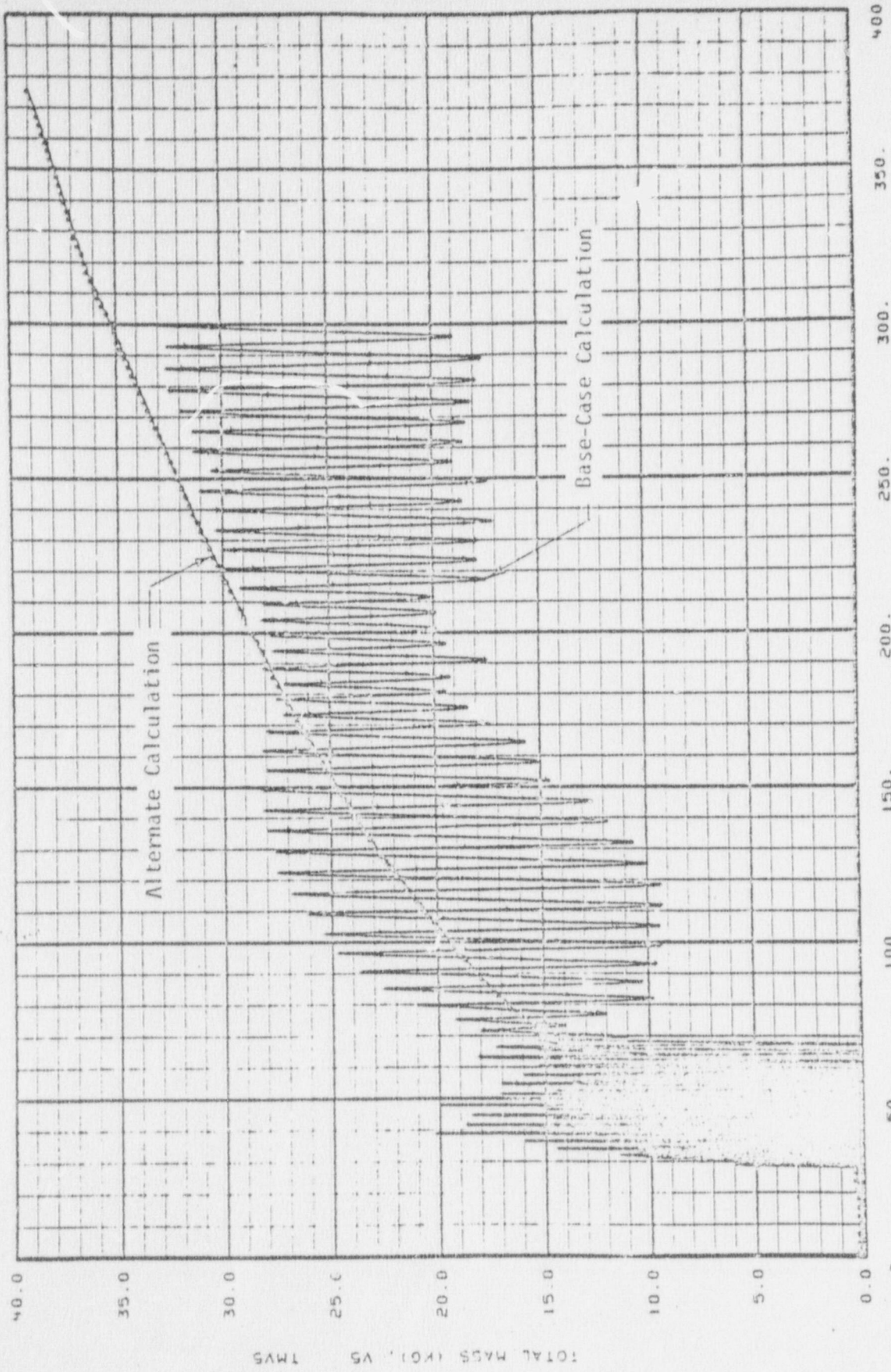

Fig. 16 Total mass in average channel vs. time.

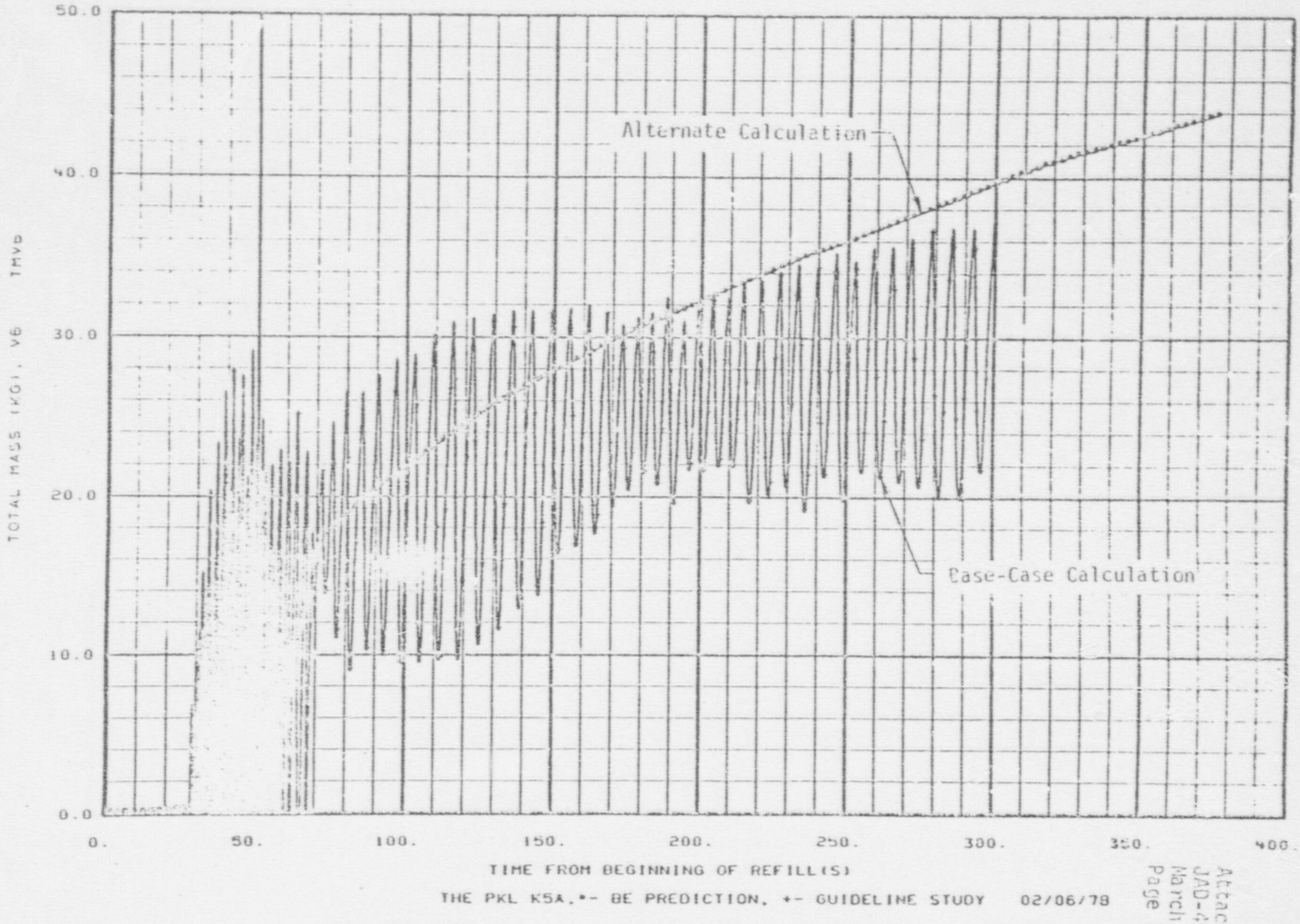

Fig. 17 Total mass in cool channel vs. time.

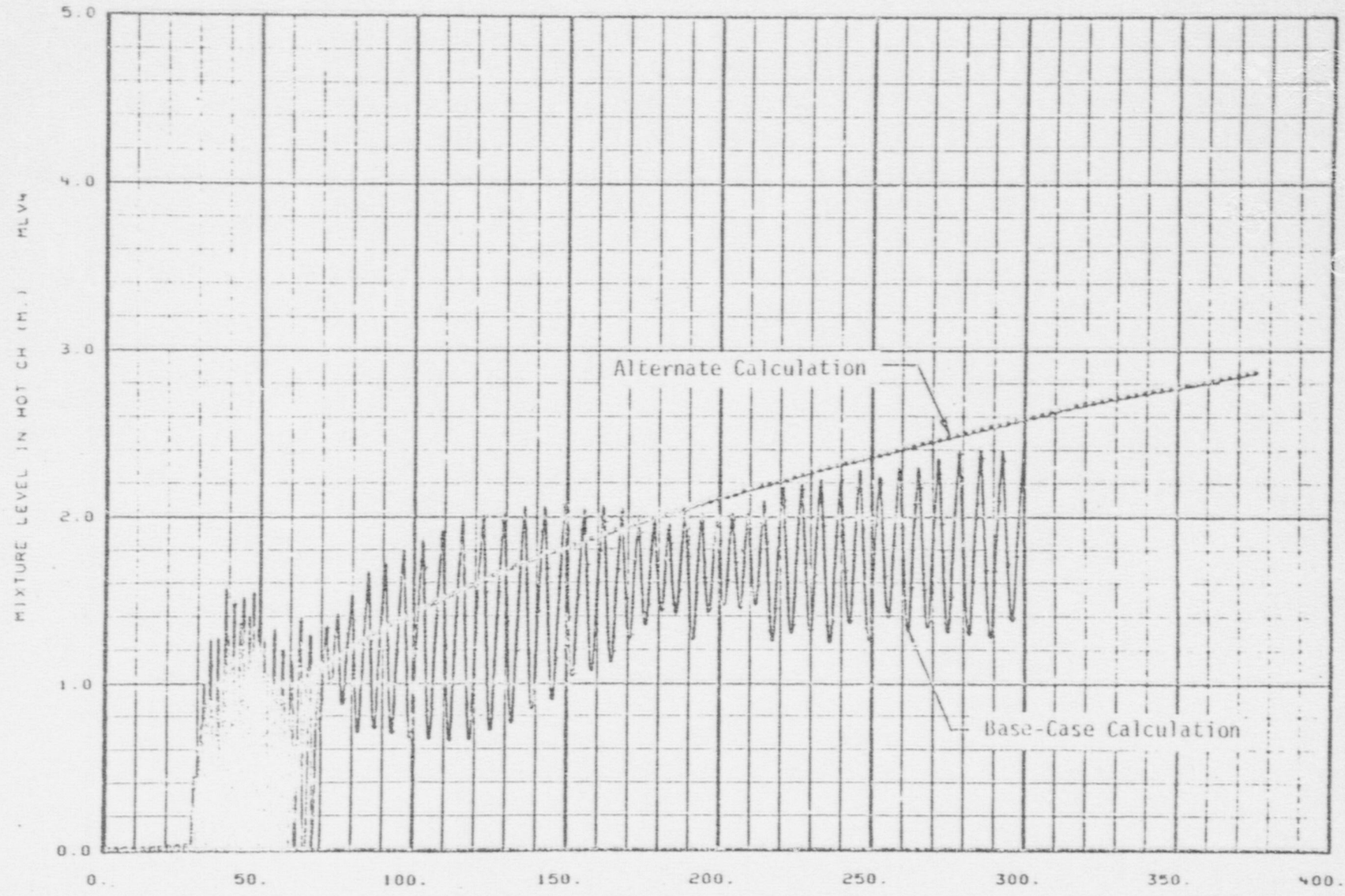

Fig. 18 Hot channel mixture level vs. time.

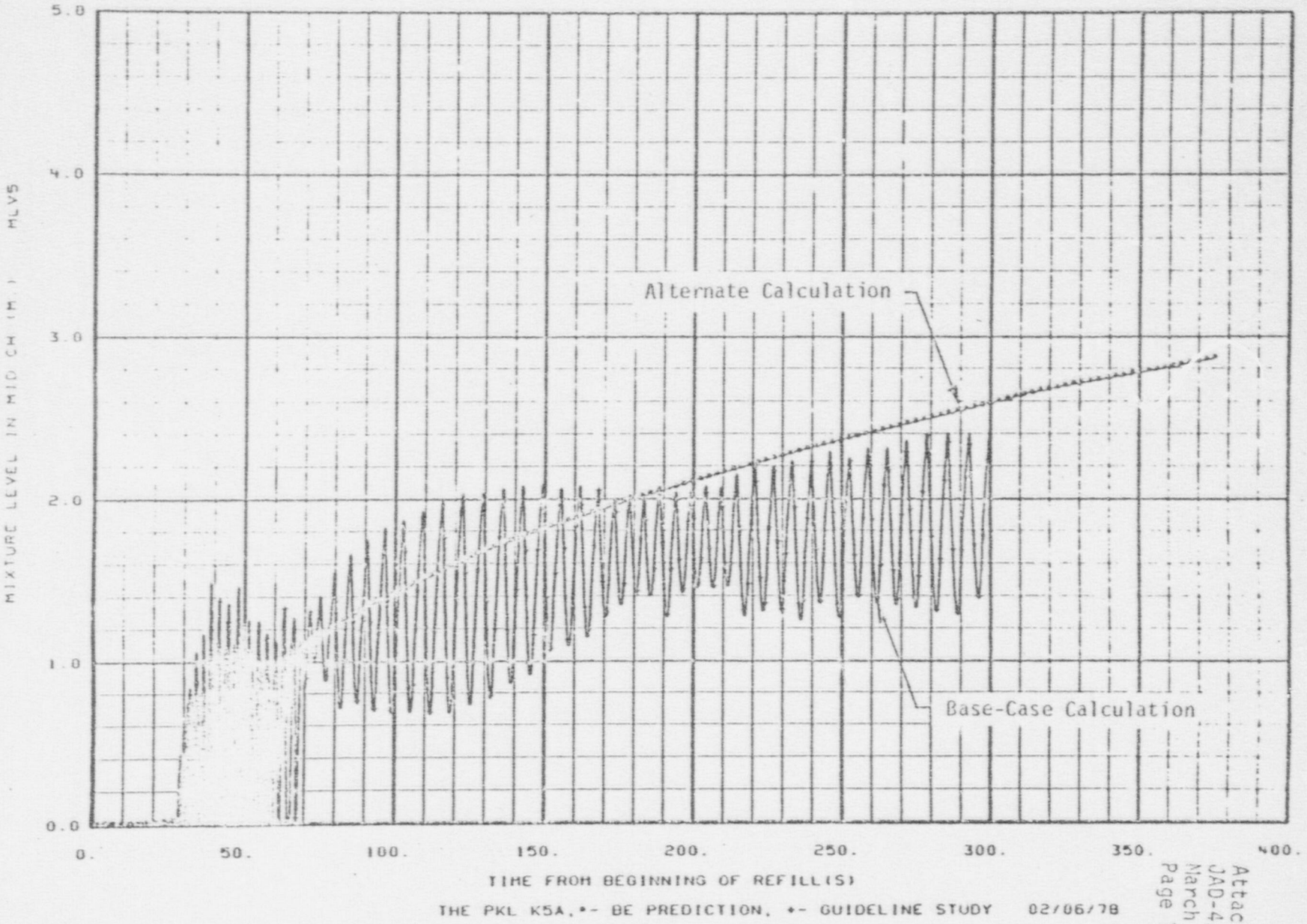

Fig. 19 Average channel mixture level vs. time.

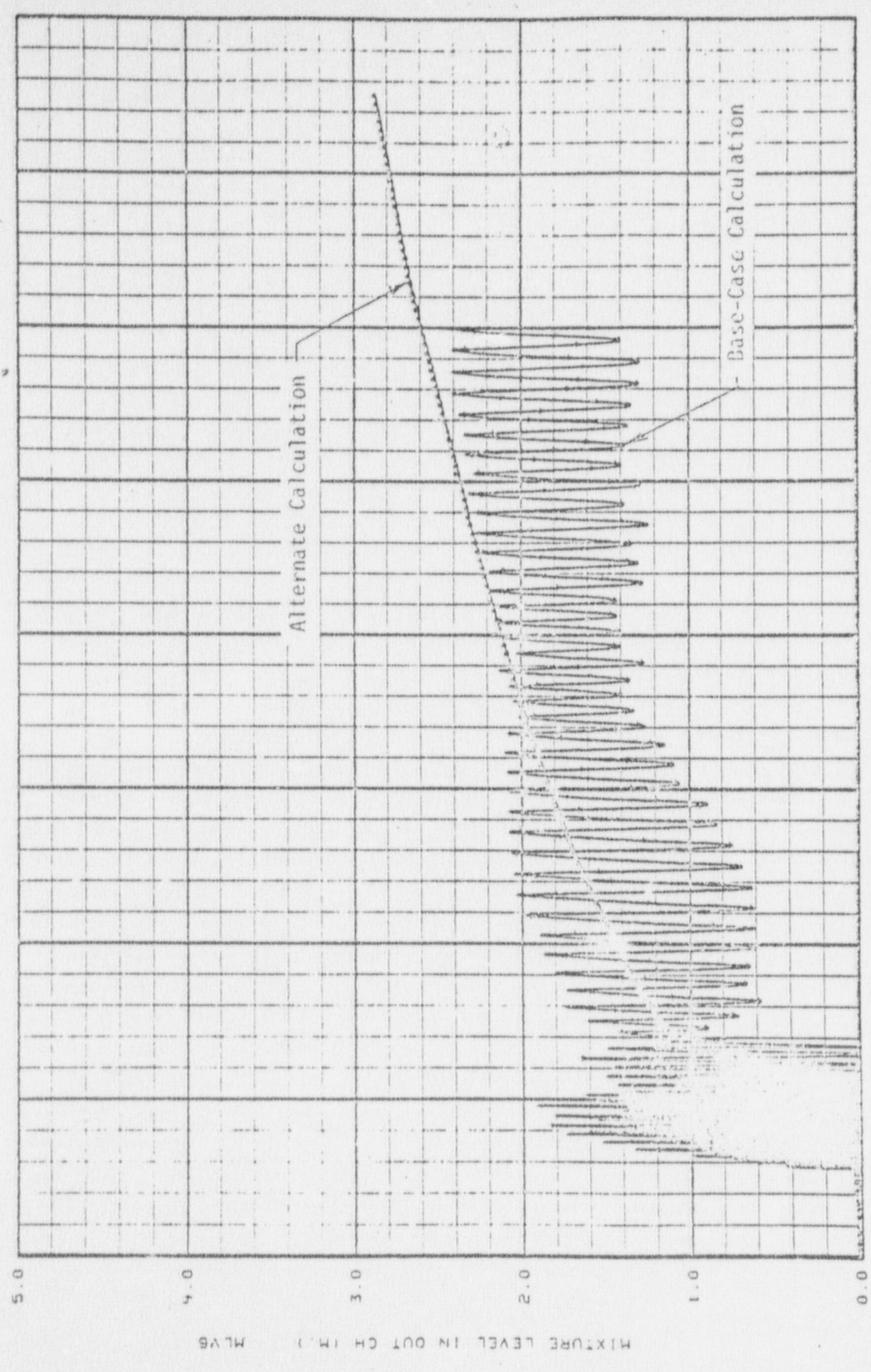

Fig. 20 Cool channel mixture level vs. time.

APPENDIX B

TEST PREDICTION FOR KWU PKL TEST K7A
USING RELAP4/MOD6, UPDATE 3

EG&G Idaho, Inc.

P. O. Box 1625
Idaho Falls, Idaho 83401

March 28, 1978

Mr. R. E. Tiller, Director
Reactor Operations and Programs Division
Idaho Operations Office - DOE
Idaho Falls, ID 83401

TEST PREDICTION FOR KWU PKL TEST K7A USING RELAP4/MOD6, UPDATE 3 - JAD-68-78

Ref: (a) S. Fabic Ltr to Attendees of Nov 18, 1977 Denver meeting, Independent Verification of Codes, Nov 28, 1977
(b) Status Summary Report WRSR, Office of Nuclear Regulatory Research, Jan 13, 1978

Dear Mr. Tiller:

The enclosure is a presentation of pertinent results calculated for the KWU (Kraftwerk Union) PKL Reflood Test K7A. The calculation was the second of two "blind" test predictions made using RELAP4/MOD6, Update 3 without prior study of experimental system behavior and without access to experimental results. The contents of the enclosure were handed to the NRC representative in Idaho on March 8, 1978 to show proof of calculation and to expedite the release of experimental data for future analysis.

A detailed pretest prediction report similar to those prepared by Semiscale and PBF was not produced at this time. The main objective of this letter is to make formal transmittal of calculated results. This objective is in contrast to requirements of the experimental programs for detailed test prediction reports that can be used in test planning, instrumentation needs, etc. Detailed analysis of the predicted experiment behavior and evaluation of code capabilities and deficiencies will be presented in separate documentation prepared after comparing the prediction with experimental data.

The KWU PKL facility is a three-loop simulation of a West German pressurized water reactor, fabricated in a reduced scale that maintains prototype volume-to-power ratio. It was designed specifically for system experiments simulating the reflood phase of hypothetical loss-of-coolant accidents. The full-length, electrically heated,

340-rod core is divided into hot, average, and cool channels and has an overall power capacity of 1.45 MW with a peak power of 1.5 KW/M. The RELAP4 nodalization of this facility and the core channel and heat-slab description are presented in the enclosure.

Test K7A is a 200% cold-leg-break experiment with ECC injection representative of prototype ECC injection into two of the three intact-loop cold legs. Boundary conditions used were as-tested core power, injection rate, and suppression tank pressure shown as functions of time in the enclosure. The "blind" calculation made to predict the results of the K7A experiment was conducted within the independent verification guidelines set forth by the NRC in Reference (a). Modeling and code input options described in released RELAP4 manuals were used in the analysis.

The data from Experiment K7A are not presently available at the INEL. It is recommended that the NRC release these data so that the test prediction may be evaluated.

This transmittal satisfies the requirement for issue of a test-prediction transmittal letter for Test K7A by April 1, 1978. This requirement is identified in the March 6, 1978 update of Reference (b), LOCA Analysis Verification.

Very truly yours,

Original signed by

J. A. Dearien, Manager
Code Verification and
Applications Program

WSH:vjd

Enclosure:
"RELAP4/MOD6 Prediction of KWU PKL Test K7A Behavior", Y. S. Chen, March 7, 1978

cc: S. Fabic, NRC-RSR
G. N. Lauben, NRC-DSS
W. H. Lovelace, NRC-MIPC, w/o attach.
W. C. Lyon, NRC-RSR - 3
R. M. Scroggins, NRC-RSR
L. S. Tong, NRC-RSR
R. W. Kiehn, EG&G Idaho, w/o attach.

bcc: Y. S. Chen
J. A. Dearien - 2
W. S. Haigh WSH
R. E. Rice RER
P. H. Vander Hyde, w/o attach.
L. J. Ybarrondo LJY
Central Files
File 15.1

RELAP4/MOD6 PREDICTION OF KWU PKL TEST K7A BEHAVIOR

Y. S. Chen

March 7, 1978

Calculated results represented by the attached plots are on file on Tapes T9N478, T9V204, and T9W766 at the Idaho National Engineering Laboratory.

CONTENTS

KWU - PKL 3-LOOP RELAP4/MOD6 NODALIZATION

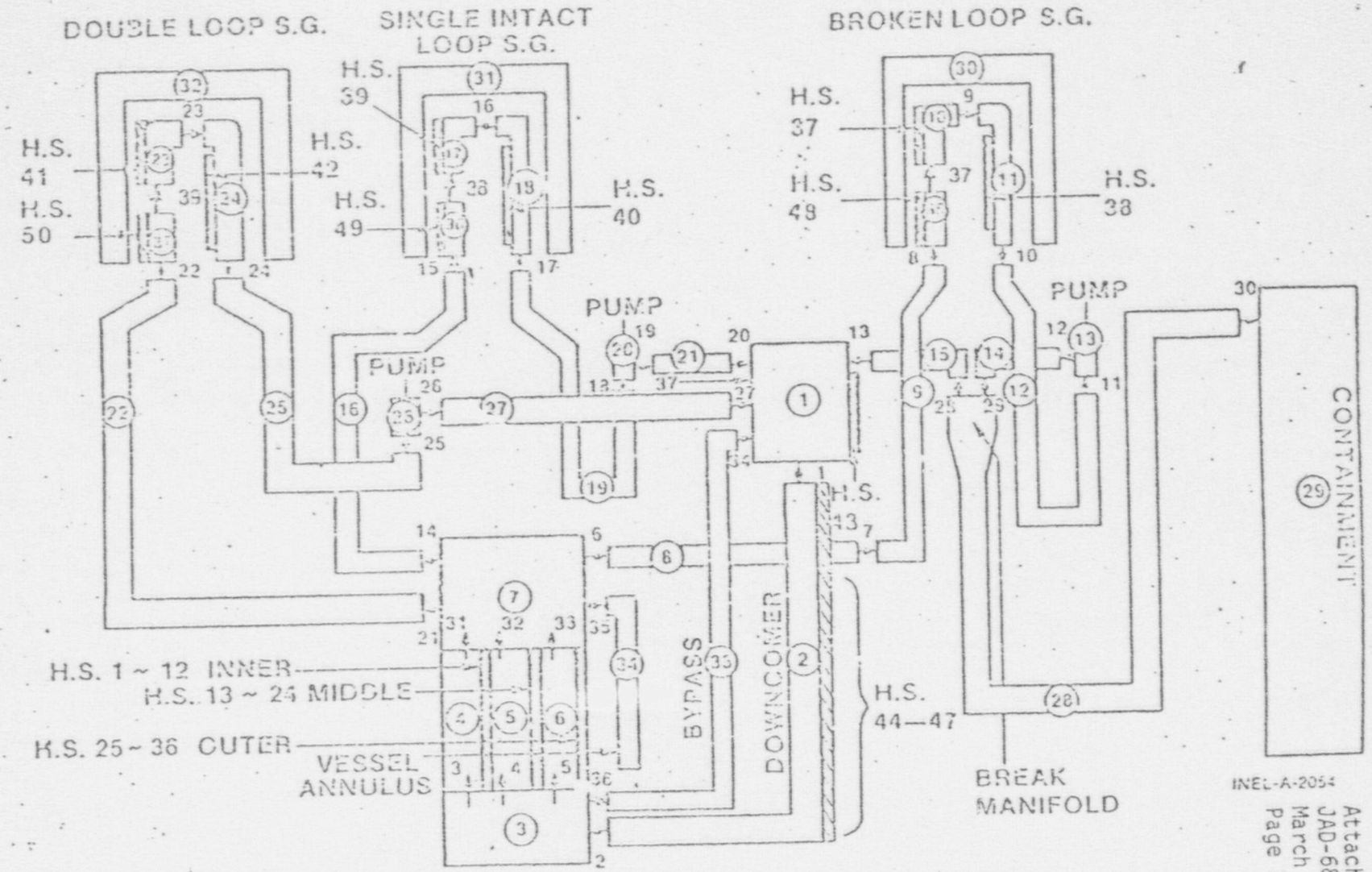

Fig. 1 KWU-PKL three-loop RELAP4/MOD6 nodalization.

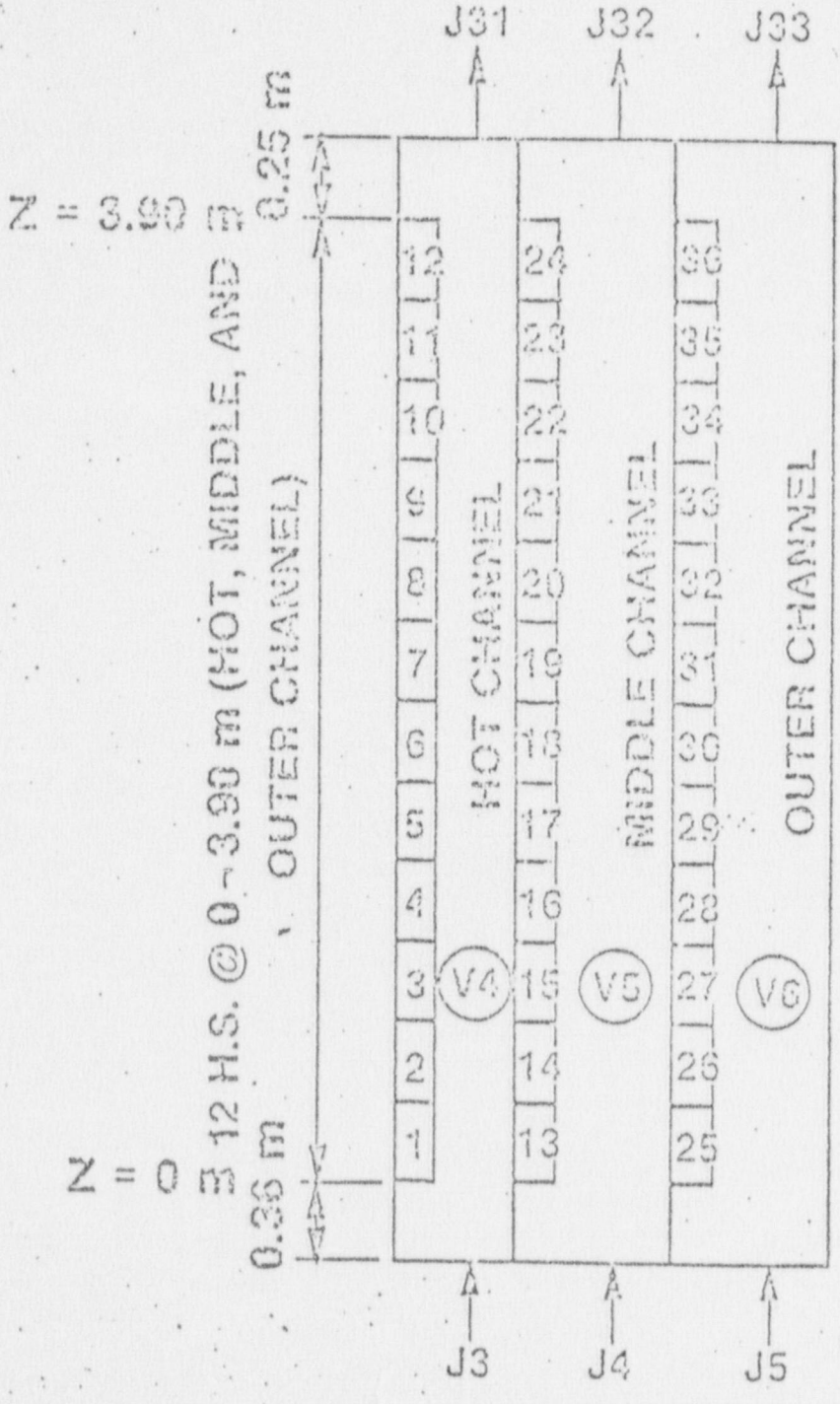

Fig. 2 Core heat slab structure.

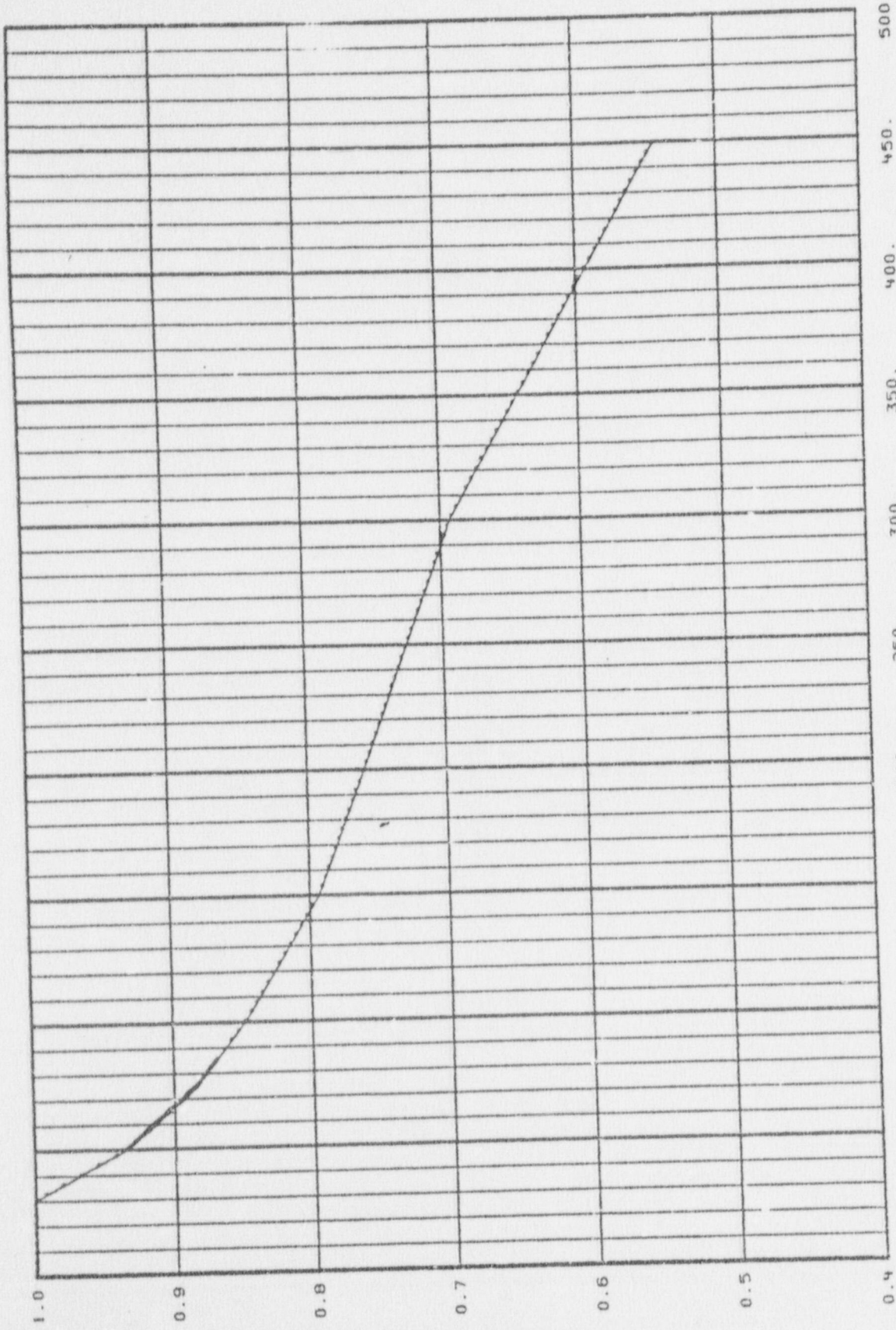

Fig. 3 Total normalized power vs. time.

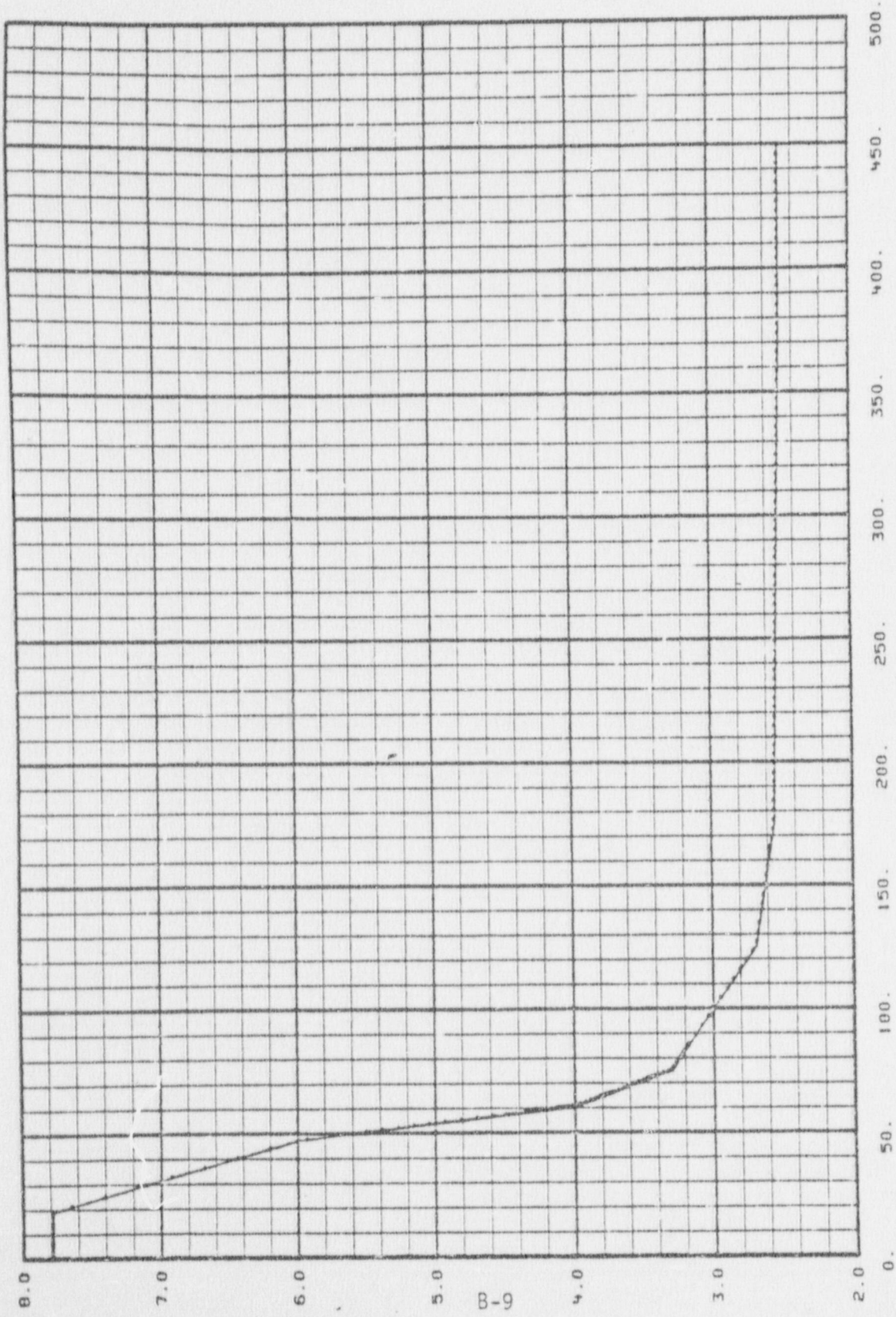

Fig. 4 Total ECC injection rate vs. time.

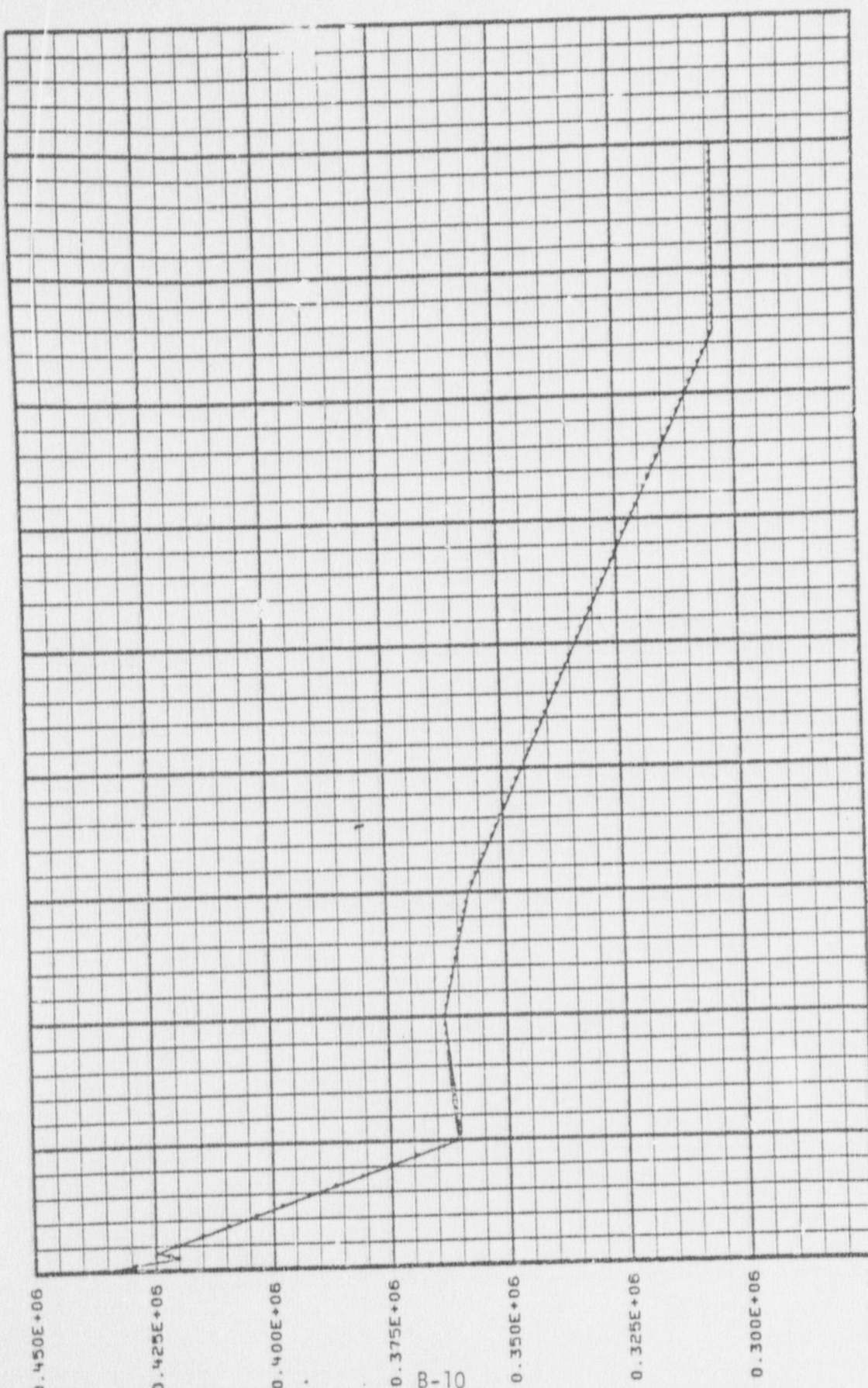

Fig. 5 Containment pressure vs. time.

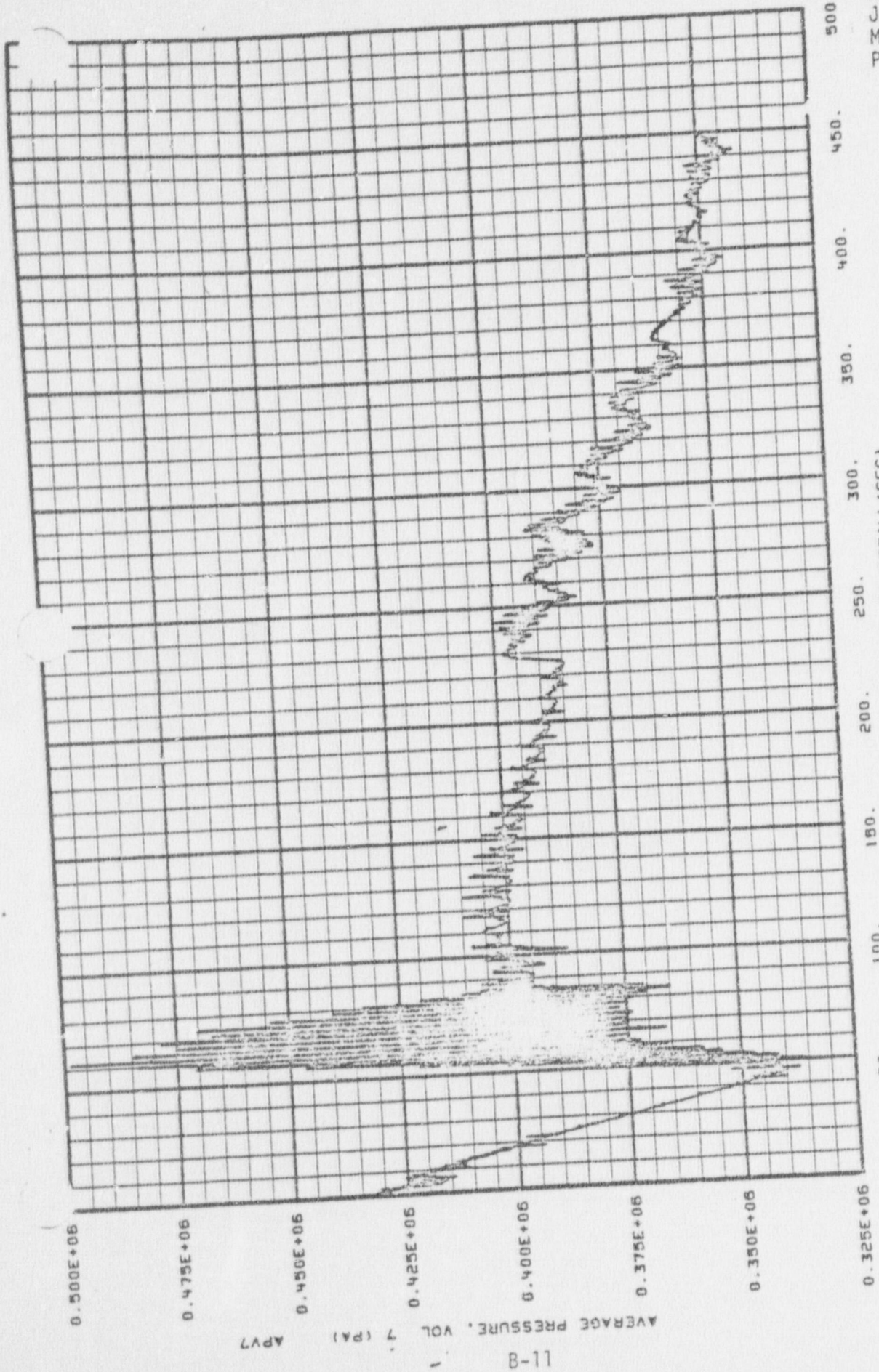

Fig. 6 Upper plenum pressure vs. time.

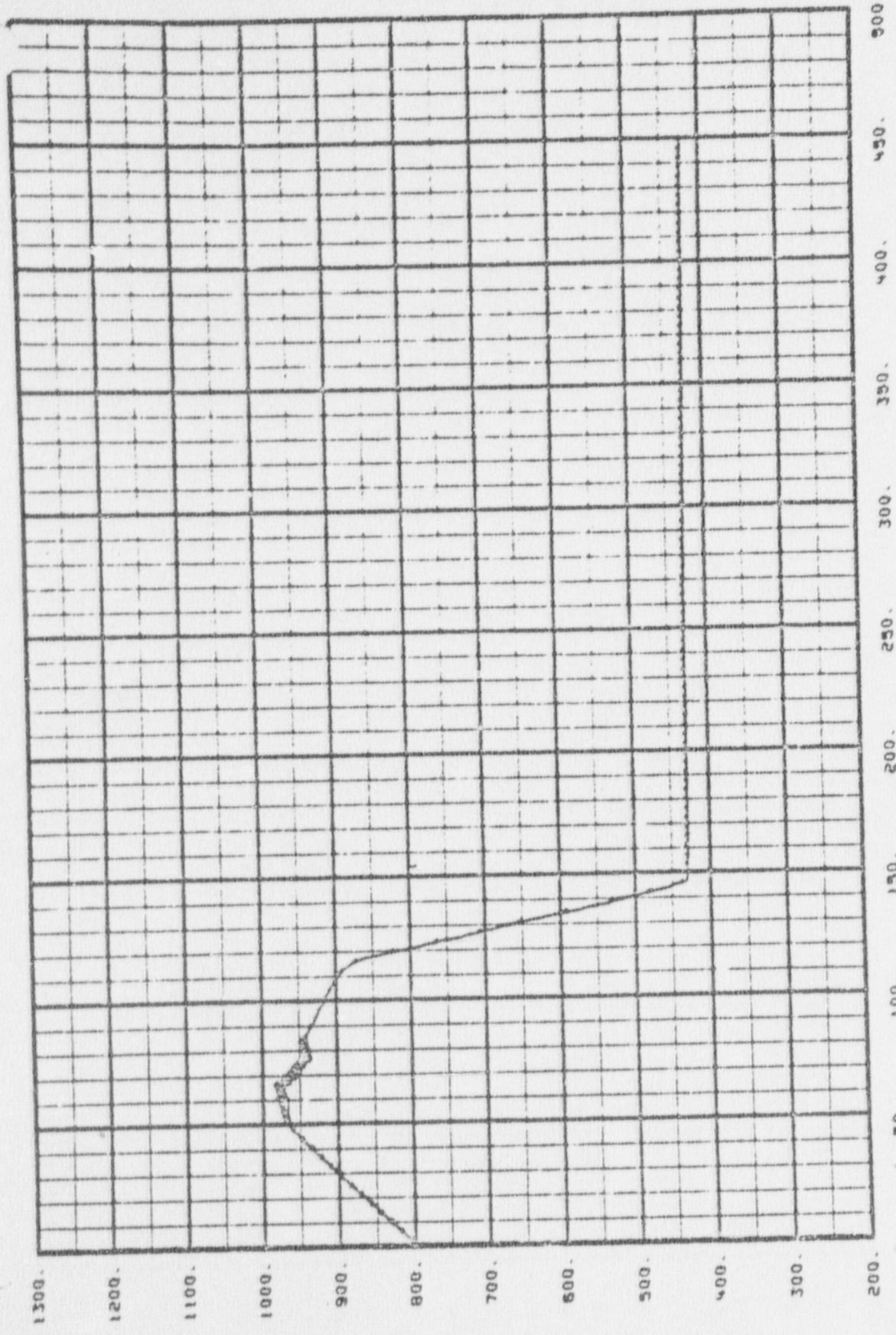

Fig. 7 Hot-channel rod surface temperature at Z = 0.85 m vs. time.

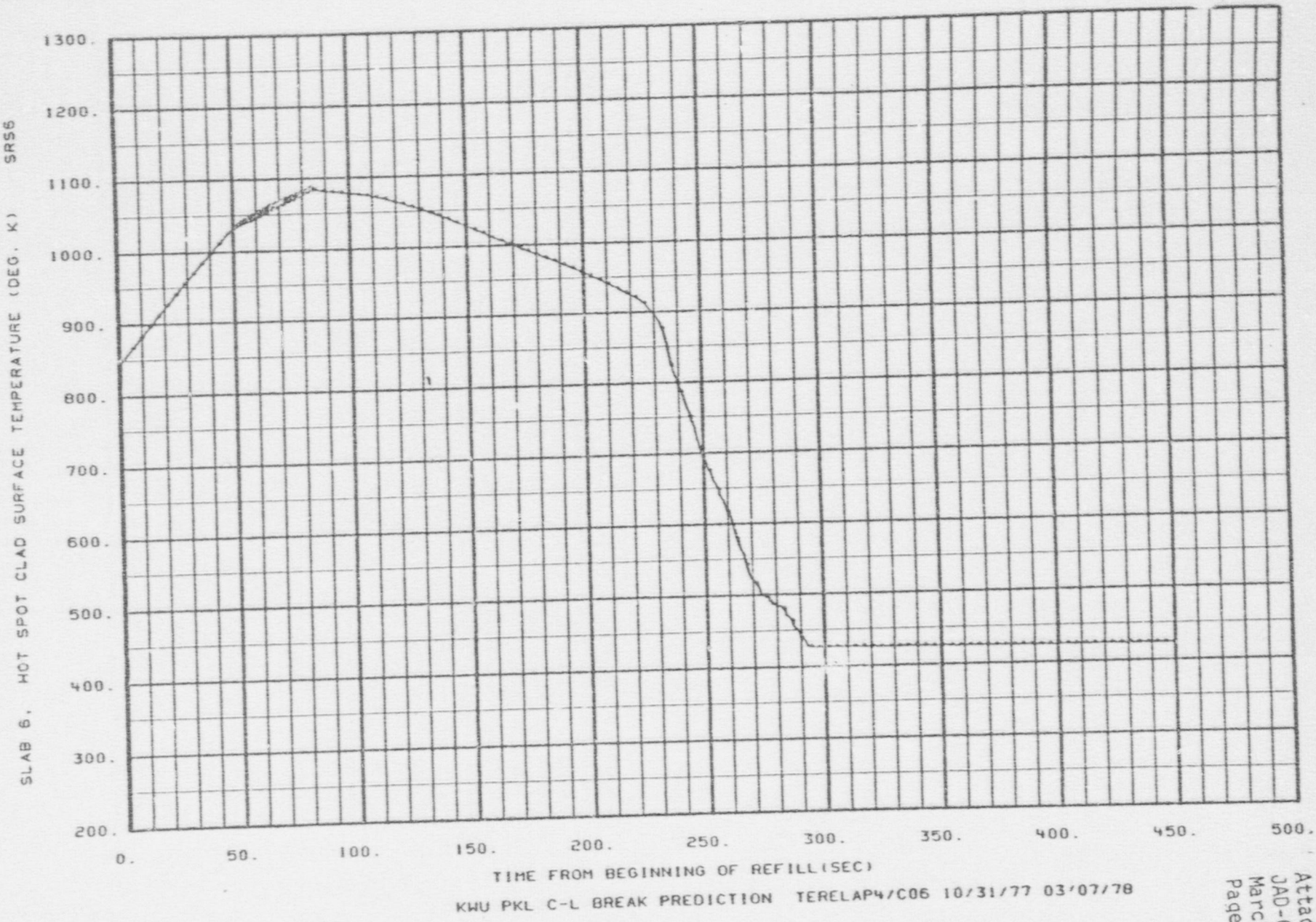

Fig. 8 Hot-channel rod surface temperature at $z = 1.79$ m vs. time.

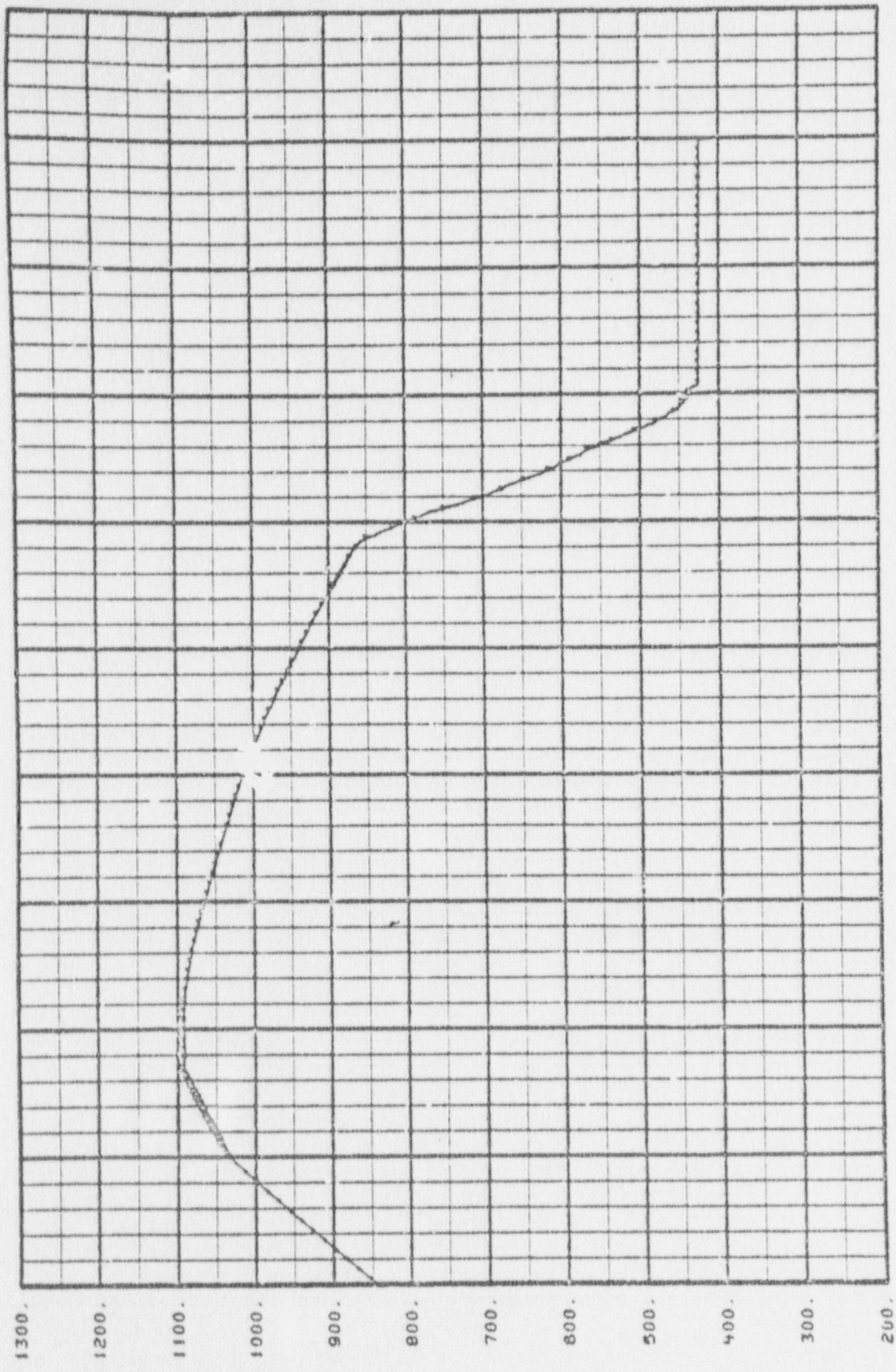

Fig. 9 Hot- channel rod surface temperature at Z = 2.11 m vs. time.

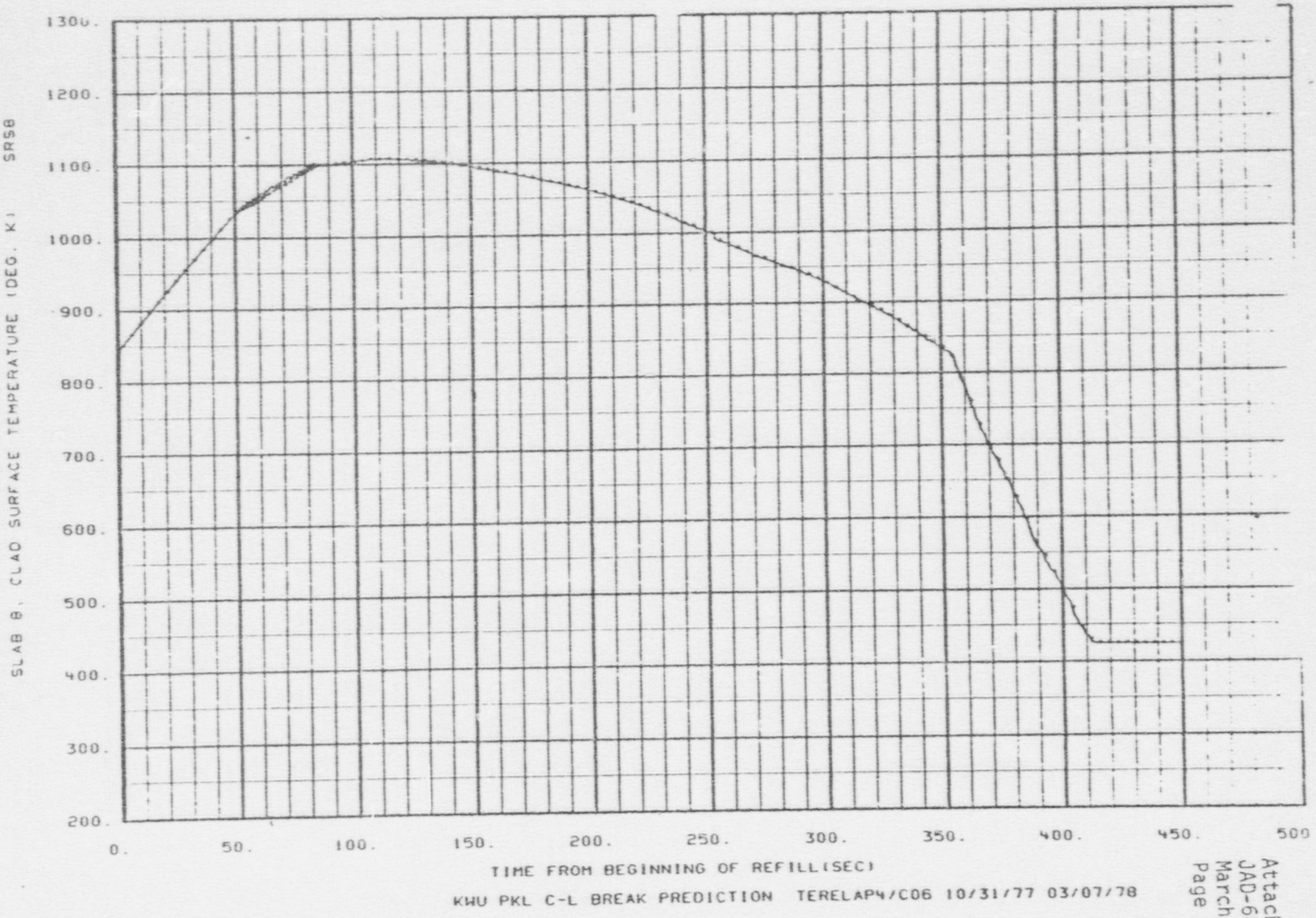

Fig. 10 Hot-channel rod surface temperature at $Z = 2.44$ m vs. time.

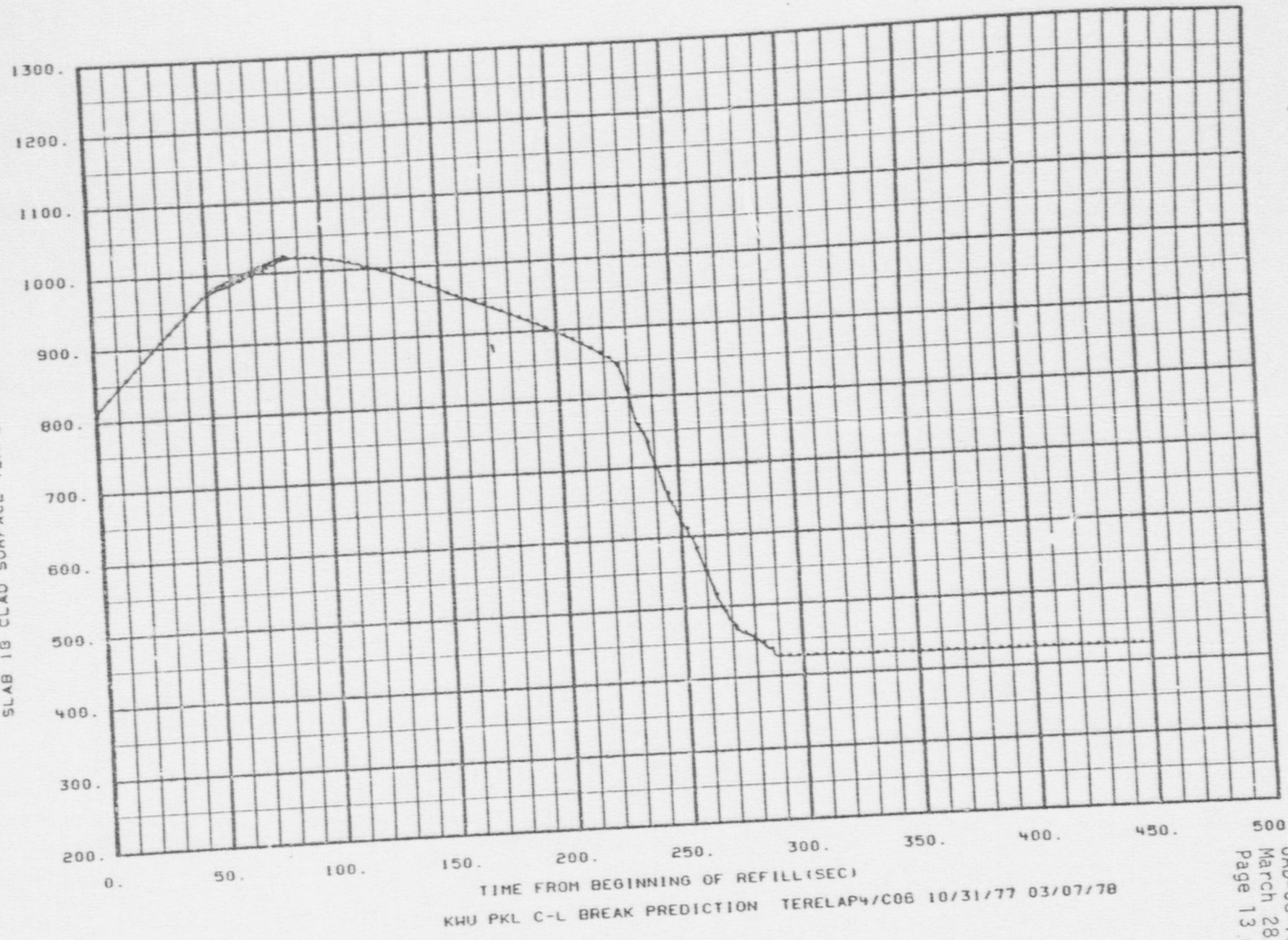

Fig. 11 Average-channel rod surface temperature at $\bar{z}$ = 1.79 m vs. time.

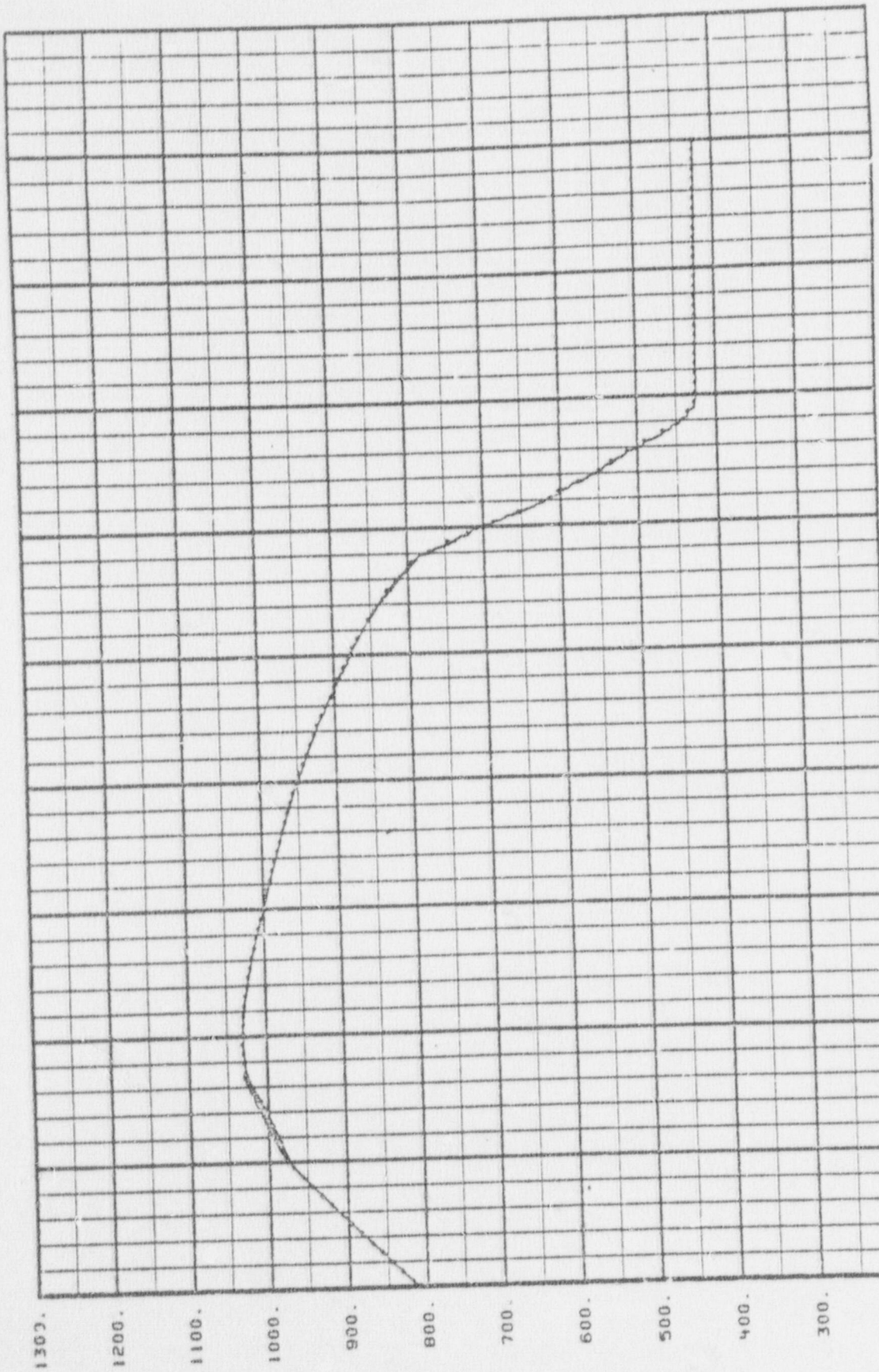

Fig. 12 Average-channel rod surface temperature at Z = 2.11 m vs. time.

Fig. 13 Cool-channel rod surface temperature at Z = 1.79 m vs. time.

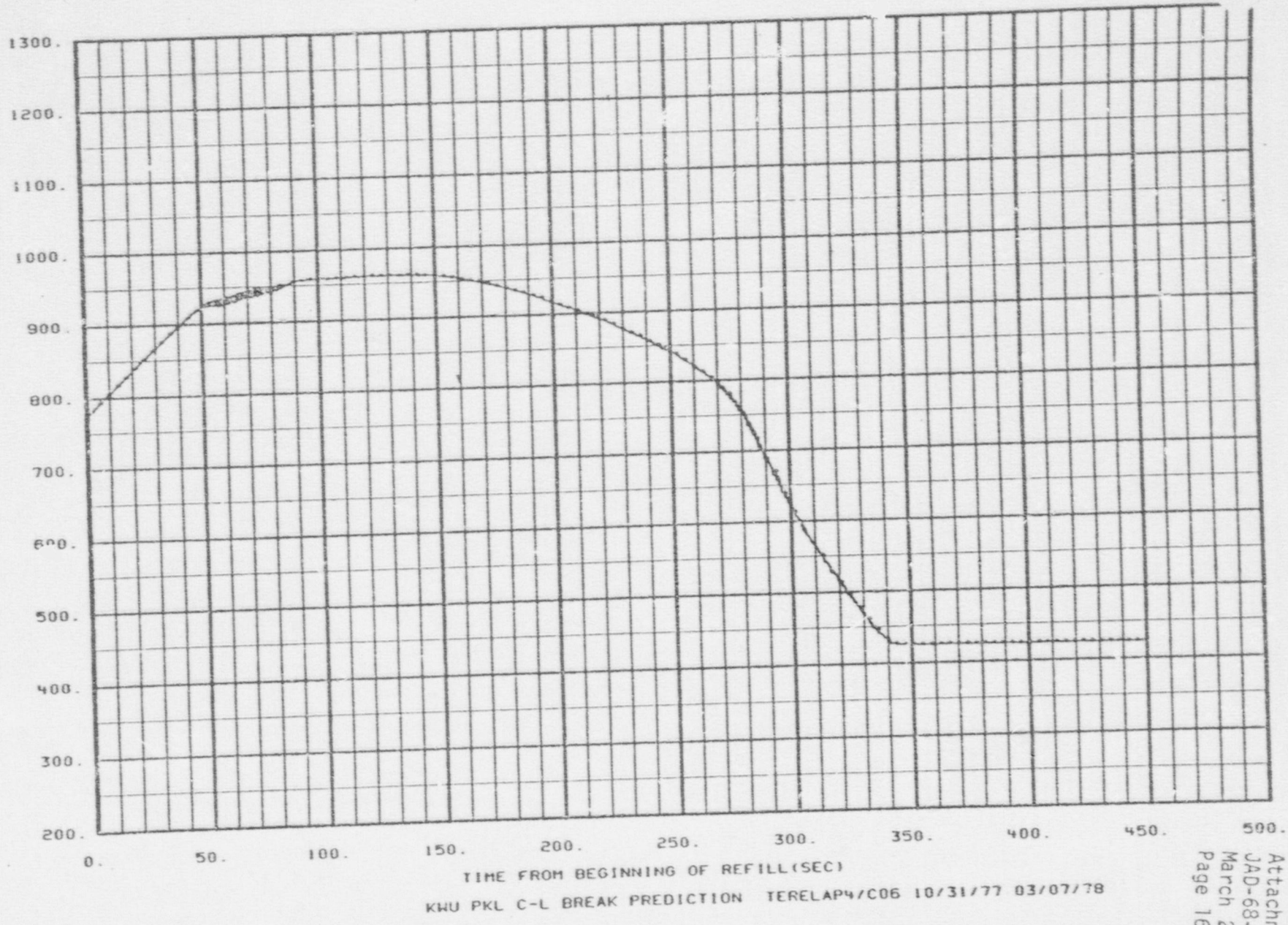

Fig. 14 Cool-channel rod surface temperature at $Z = 2.11$ m vs. time.

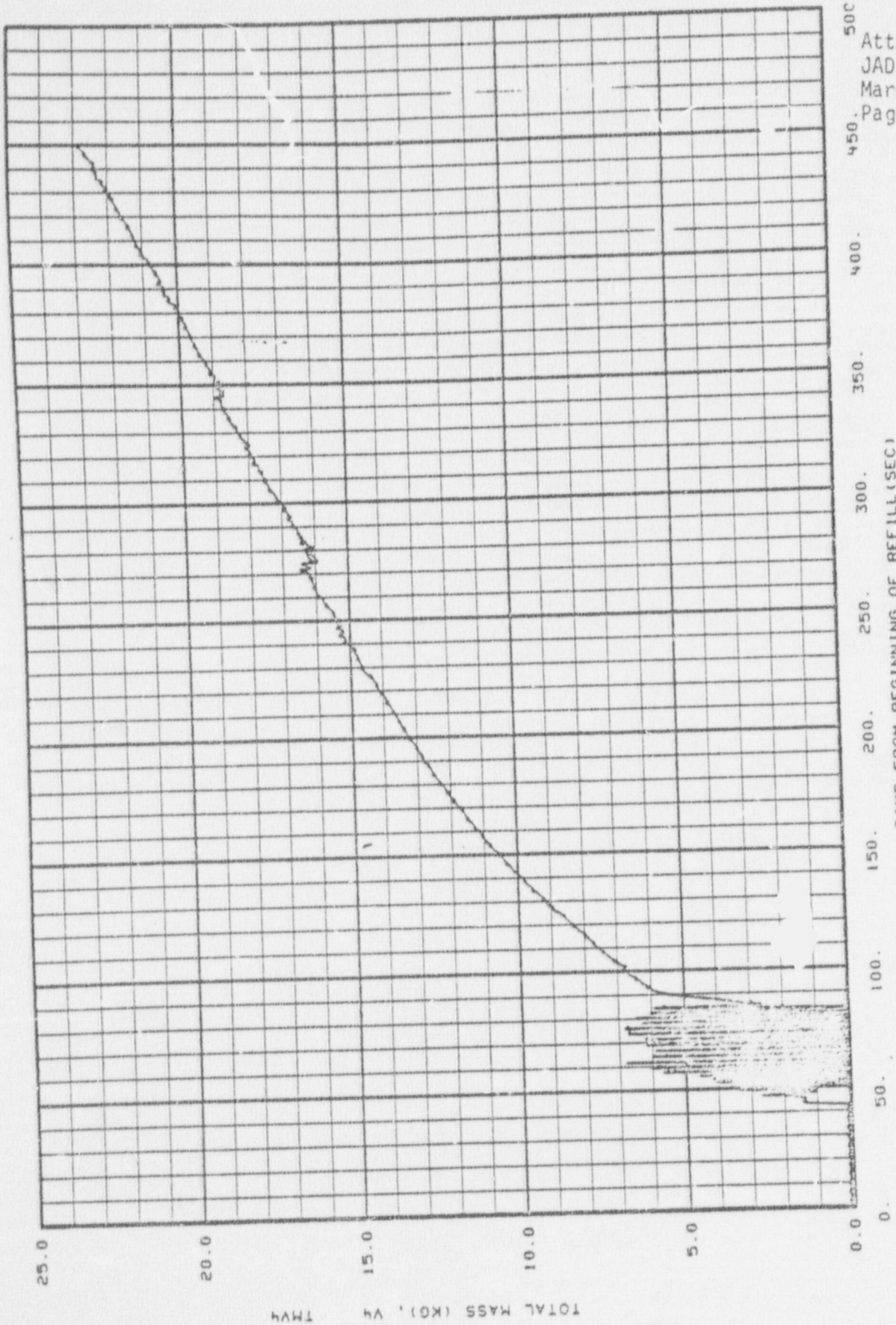

Fig. 15 Total mass in hot channel vs. time.

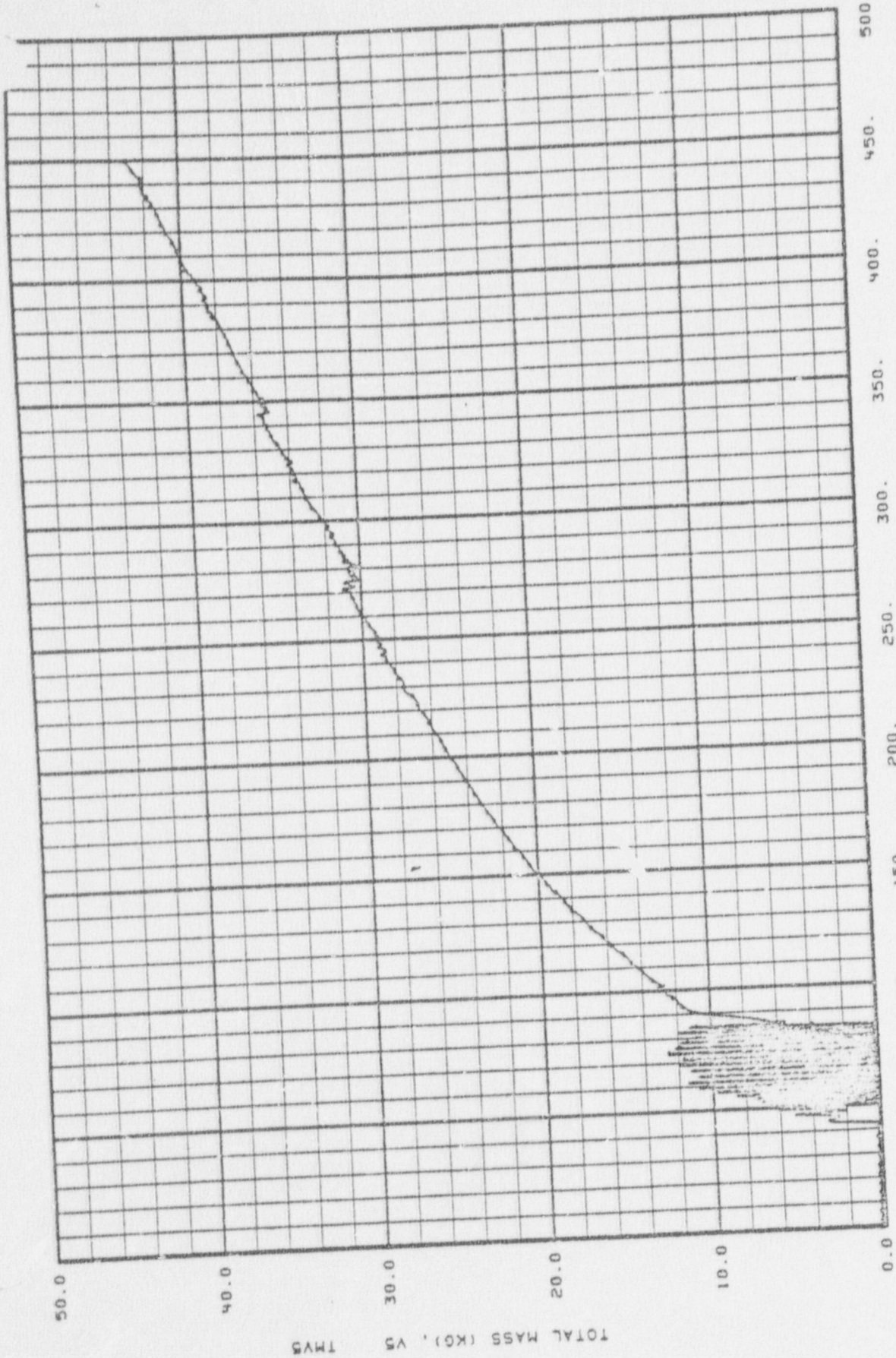

Fig. 16 Total mass in average channel vs. time.

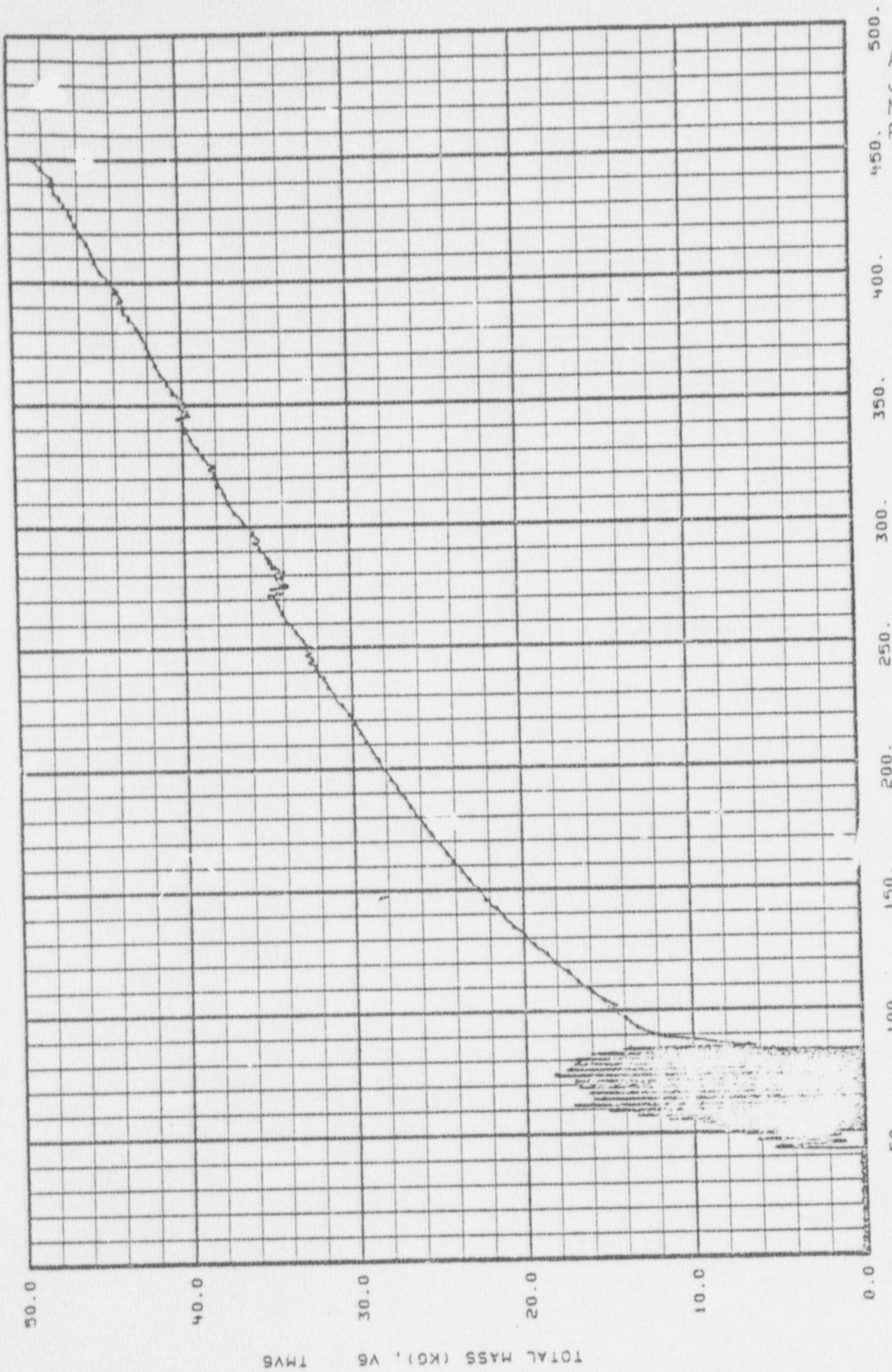

Fig. 17 Total mass in cool channel vs. time.

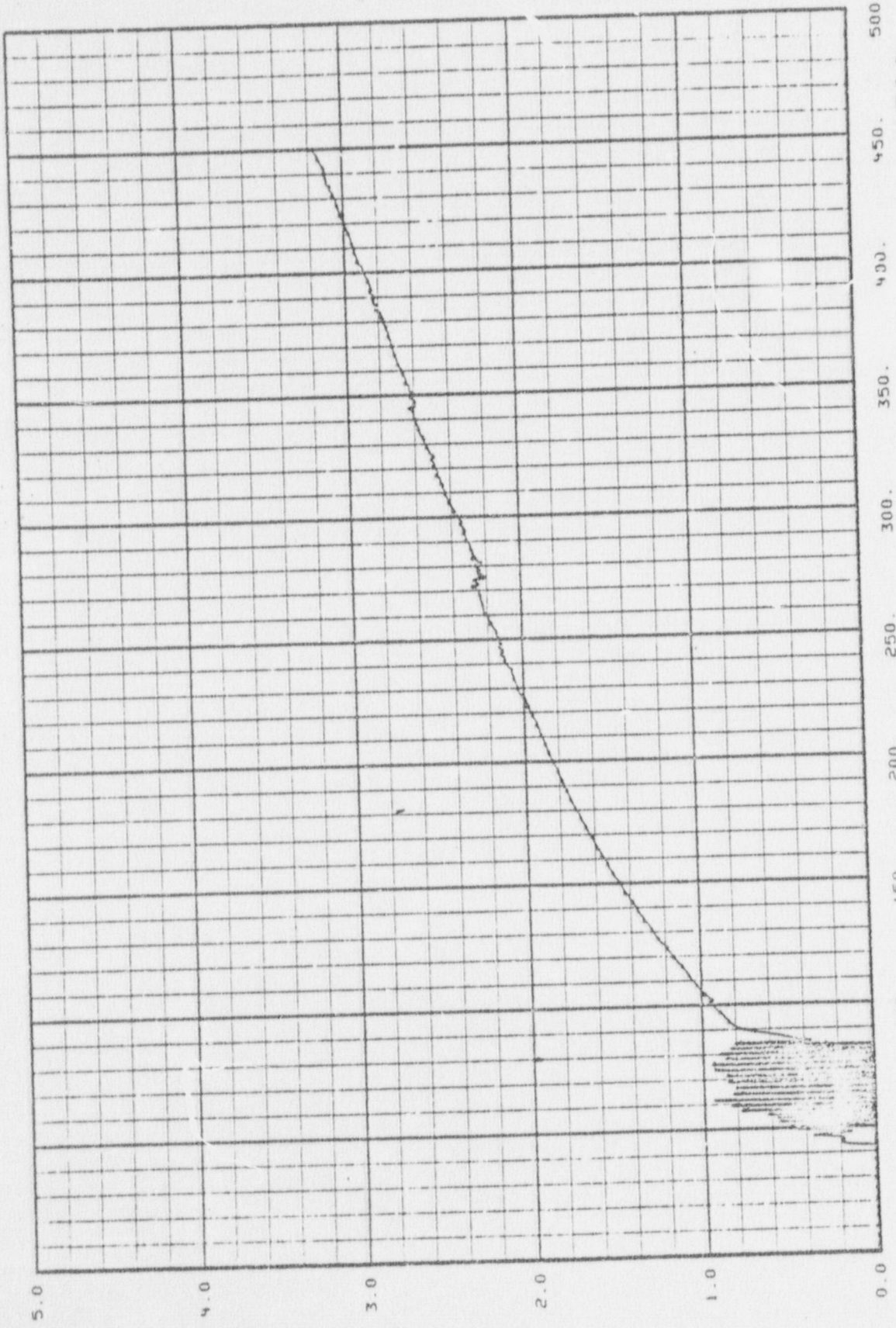

Fig. 18 Hot-channel mixture level vs. time.

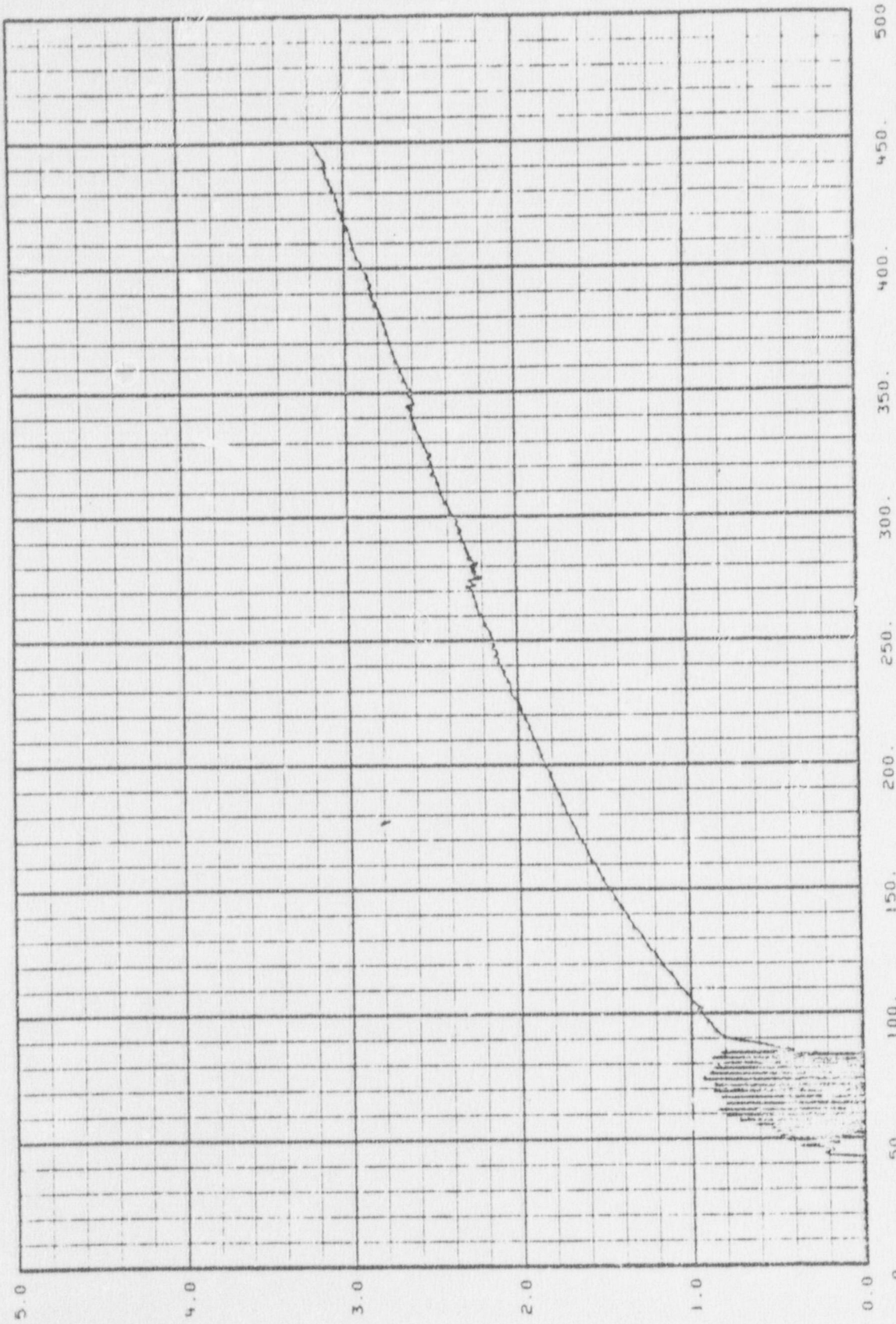

Fig. 19 Average-channel mixture level vs. time.

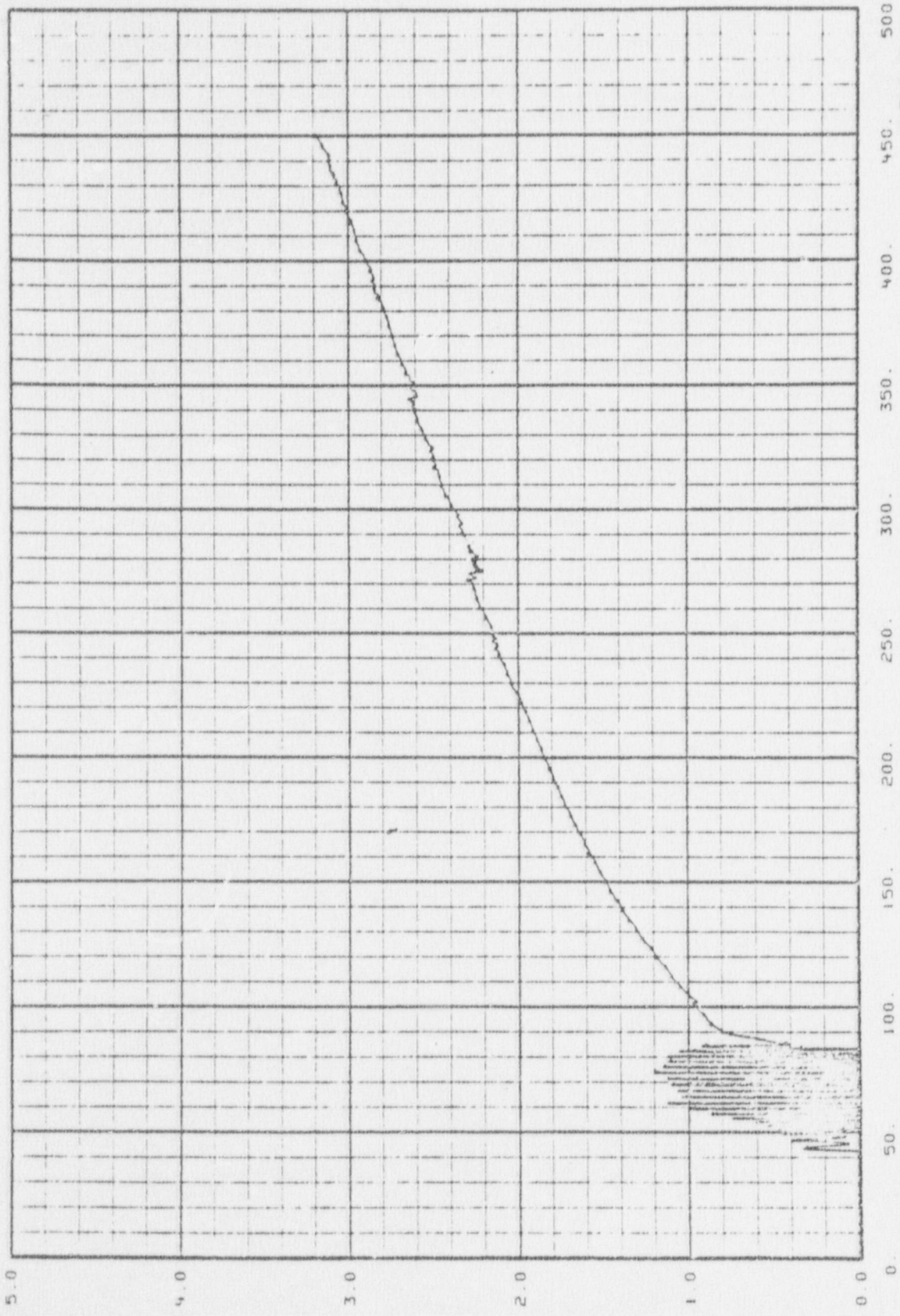

Fig. 20 Cool-channel mixture level vs. time.

11-27-78

INTERIM REPORT

Accession No. _____

Contract Program or Project Title:

Subject of this Document: CVAP-TR-78-011 "Prediction of KWU PKL Experiments K5A and K7A Using RELAP4/MOD6

Type of Document:

Author(s): W. S. Haigh

Date of Document: June 1978

Responsible NRC Individual and NRC Office or Division:

W. Lyon
Reactor Safety Research

This document was prepared primarily for preliminary or internal use. It has not received full review and approval. Since there may be substantive changes, this document should not be considered final.

for H. P. Pearson, Supervisor
Information Management
EG&G Idaho

Prepared for
U.S. Nuclear Regulatory Commission
Washington, D.C. 20555

FIN No. A6047

INTERIM REPORT